Studies on the interaction between *Tobacco Mosaic Virus* Movement Protein and Microtubules

Inauguraldissertation

zur

Erlangung der Würde eines Doktors der Philosophie

vorgelegt der

Philosophisch-Naturwissenschaftlichen Fakultät

der Universität Basel

von

Jamie A. Ashby

aus Großbritannien

Universität Basel

Friedrich Miescher-Institute for Biomedical Research

Basel, September 2003

Genehmigt von der Philosophisch-Naturwissenschaftlichen Fakultät auf Antrag von

Prof. Thomas Boller

Prof. Manfred Heinlein

Prof. Frederick Meins

Basel, 25.09.2003

Prof. Marcel Tanner
Dekan

Table of contents Page

Acknowledgements

Firstly, I would like to thank Prof. Manfred Heinlein for providing me with the opportunity to work in the field of macromolecular trafficking, the freedom to explore my ideas and the guidance to consolidate my findings. I would also like to express my gratitude to Prof. Thomas Boller and Prof. Frederick Meins for their critical appraisal of my work and for their constructive suggestions.

I would like to acknowledge Prof. Andreas Hoenger, Dr. Thomas Wendt and Dr. Vincent Brondani for their invaluable help with experimental matters, and in addition, Prof. Barbara Hohn and Dr. Ortrun Mittelsten-Scheid for their most helpful advice while writing this thesis.

Many thanks to Dean Flanders, Thomas Nyffenegger and Alan Naylor for their excellent I.T. support, and thanks also to Dr. Daniel Hess and Ms. Anne Ulvestad for protein analytical services.

I am grateful to past and present friends from the FMI for making my time an enjoyable one, particularly Dr. Mark Lambermon, Dr. Pawel Pelczar, Ms. Monika Fasler, Alan Naylor and Dr. James Moore.

My warmest thanks must go to my family. Without their sacrifices and constant support, this thesis would not have been written.

Abbreviations

ATP	adenosine 5’-triphosphate
BES	N,N-Bis(2-hydroxyethyl)-2-aminoethanesulfonic acid
BSA	bovine serum albumin
BY-2	bright yellow-2
CC	companion cell
CCB	colloidal coomassie blue
cDNA	complementary DNA
CIAP	calf intestinal alkaline phophatase
CP	coat protein
dpi	days post infection/inoculation
dsDNA	double-stranded DNA
DTT	1,4-Dithio-DL-threitol
EDTA	ethylenediaminetetraacetic acid
EGTA	ethylene glycol-bis(2-aminoethyl)-N,N,N’,N’-tetraacetic acid
FITC	fluorescein-isothiocyanate
GFP5	green fluorescence protein (variant 5)
GST	glutathione-S-transferase
GTP	guanosine 5’-triphosphate
GTP-γ-S	guanosine 5’-[γ-thio]triphosphate
GuHCL	guanidine hydrochloride
hpi	hours post infection/inoculation
HPLC	high performance liquid chromatography
IPTG	isopropyl-β-D-thiogalactoside

MAP	Microtubule-associated protein
MES	2-(N-Morpholino)ethanesulfonic acid
MP	movement protein (TMV P30)
MT	microtubule
MW	molecular weight
$NaBH_4$	sodium boroanhydride
NP-40	nonidet-P40 (Nonylphenylpolyethylene glycol)
nt	nucleotide
OD	optical density
ORF	open reading frame
PBS	phosphate buffered saline
Pd	plasmodesmata
Pipes	1,4-Piperazinediethanesulfonic acid
PTGS	post-transcriptional gene silencing
RT-PCR	reverse transcription polymerase chain reaction
S.E.M.	standard error (of the mean)
SDS-PAGE	dodium dodecyl sulfate-polyacrylamide gel electrophoresis
SE	sieve element
SEL	size exclusion limit
Tris	tris-hydroxymethylaminoethane
TRITC	tetramethylrhodamine-isothiocyanate
vRNA	viral RNA
vRNP	viral ribonucleoprotein complex
WT	wild-type

Abstract

During the invasion of a susceptible host, *Tobacco mosaic virus* (TMV) transports its RNA genome from sites of viral synthesis into neighbouring cells, thus potentiating the spread of infection. In many systems, RNA trafficking is known to be a highly coordinated process, often involving the complex interplay of numerous factors. In plants, however, the mechanisms that govern RNA transport are not well understood. Since viruses have a propensity to exploit pre-existing host machinery for their own purposes, TMV has become a popular model system for the study of RNA trafficking in plants. TMV viral RNA (vRNA) is thought to be transported as a ribonucleoprotein (RNP) with the virally encoded movement protein (MP). Localization studies have demonstrated a temporal redistribution of MP from endoplasmic reticulum (ER)-derived replication bodies onto microtubules (MTs) at mid to late stage of infection. A functional link between the association of MP with microtubules (MT) and RNA trafficking has been established, and furthermore, this association does not require other viral components or plant-specific factors, thereby indicating a direct interaction between MP and MTs. *In vitro*, purified MP interacts directly with preformed, dynamically suppressed MTs and has no requirement for MT polymerization or polymer-specific structural forms. Immunohistochemical studies indicate that MP may interact with the extreme C-termini of α- and β-tubulin, possibly forming a stabilizing sheath. Consistent with the proposal that MP functions as a structural microtubule-associated protein (MAP), MP:MT complexes assembled *in vitro* are highly stable. A possible functional overlap between the putative RNA and MT binding domains of MP has been identified, and although MP:MT complexes are unlikely to support RNA transport directly, such complexes have been implicated to modulate MT-dependent molecular motor activity. Collectively, *in vitro* data are in support of the observation that MP associates with MTs to high amounts, leading to the hypothesis that MP-mediated RNA transport and the MP:MT interaction are related, yet functionally distinguishable processes. Furthermore, based on the similarity of MP to endogenous MAPs, a new model is proposed in which MP-mediated trafficking may occur in the form of a translationally competent ER-vesicle, concurrent with the deployment of MP to the MT surface.

1 Introduction

1.1 Overview of RNA trafficking and localization

In order for multicellular organisms to regulate their biological activities, appropriate information must be communicated in a coordinated manner between tissues, cells and subcellular compartments. The nature of such information varies widely, however, eukaryotes have developed sophisticated strategies which allow them to regulate cellular and developmental events by the selective trafficking and localization of RNA (Chartrand *et al.*, 2001; Jansen, 2001; Palacios and St Johnston, 2001; Kloc *et al.*, 2002; Okita and Choi, 2002). RNA localization is known to occur in a variety of cell types and is thought to be essential for processes such as cell-fate determination, polar cell growth and spatially restricted protein expression. Intracellular RNA localization can occur via several mechanisms, which include random diffusion/cytoplasmic streaming and directional transport on cytoskeleton elements. In both plants and animals, examples of intercellular RNA trafficking have been described, and in addition, certain endogenous plant RNAs have been demonstrated to move systemically, suggesting that RNA trafficking may be involved in non-cell-autonomous signaling. Accumulating evidence suggests that endogenous RNA trafficking is mediated by the interaction of specific *trans*-acting factors with signal elements present within the RNA (Palacios and St Johnston, 2001). A number of localized RNAs are found in large ribonucleoprotein (RNP) complexes (Ferrandon *et al.*, 1994; Knowles *et al.*, 1996; Mouland *et al.*, 2001), and in addition to directing RNAs to their respective destinations, such RNPs may also be involved in translational regulation (Cooperstock and Lipshitz, 2001; Johnstone and Lasko, 2001). RNA trafficking and localization is not only restricted to endogenous RNAs. A number of RNA viruses found in both

animal and plant kingdoms are also known to utilize components of the host transport machinery, presumably in an effort to facilitate the replication and intercellular spread of their genomes.

1.2 Examples of RNA trafficking and localization

1.2.1 *Ash-1* mRNA in *Saccharomyces cerevisiae*

During cell division in budding yeast, mating-type switching (Strathern and Herskowitz, 1979) is repressed by the asymmetric accumulation of transcriptional regulator Ash1p in daughter cell nuclei. (Bobola *et al.*, 1996; Sil and Herskowitz, 1996). Spatial segregation of Ash1p involves the localization of *Ash-1* transcripts at the distal bud tip during late anaphase (Long *et al.*, 1997; Takizawa *et al.*, 1997) and has been demonstrated to require the gene encoding Myo4p, a class V myosin (Haarer *et al.*, 1994; Jansen *et al.*, 1996). By using a yeast mutant in which the myosin binding site on actin is disrupted, it was found that *Ash-1* transcripts no longer localized asymmetrically to the daughter cell (Long *et al.*, 1997), and furthermore, *Ash-1* mRNA appeared to be randomly distributed throughout both mother and daughter cells following treatment with the actin-depolymerizing drug Latrunculin-A (Takizawa *et al.*, 1997), again suggesting the involvement of an actin-dependent mechanism. Compelling evidence to support the role of Myo4p motor transport in *Ash-1* mRNA trafficking was provided by the observation that Myo4p colocalizes with *Ash-1* mRNA-containing particles (Bertrand *et al.*, 1998; Takizawa and Vale, 2000), and in living cells, directly mediates *Ash-1* mRNA movement into the bud tip (Bertrand *et al.*, 1998; Beach *et al.*, 1999). It has emerged that a number of accessory proteins are also required for *Ash-1* translocation, and these are thought to be involved in anchoring *Ash-1* transcripts to Myo4p, stabilizing the actin cytoskeleton and possibly maintaining

translational silence until *Ash-1* mRNA reaches the bud tip (Munchow *et al.*, 1999; Bohl *et al.*, 2000; Long *et al.*, 2000; Takizawa and Vale, 2000).

1.2.2 *MBP* mRNA in oligodendrocytes

Myelin basic protein (MBP) mRNA has been found to localize to the membranes and myelin of oligodendrocyte peripheral processes, up to 50 μm from the site of RNA synthesis (Kristensson *et al.*, 1986; Verity and Campagnoni, 1988). By injecting a fluorescently labeled *MBP* mRNA into cultured mouse oligodendrocytes, it was observed that transcripts formed granular structures within the perykaryon cytoplasm which traveled towards the cellular periphery along narrow processes at an average speed of ~ 0.2 μm/sec (Ainger *et al.*, 1993). A similar distribution of endogenous *MBP* mRNA was also found using *in situ* hybridization techniques, and furthermore, it was observed that upon reaching the cell periphery, the movement of *MBP* mRNA-containing granules was no longer directional, possibly suggesting the existence of a multi-step mechanism. Subcellular fractionation experiments indicated that *MBP* mRNA was associated with cytoskeleton elements within the cellular processes, and interestingly, it was found that treatment with the microtubule destabilizing drug Nocodazole inhibited the translocation of *MBP* mRNA, however, disruption of the actin cytoskeleton had no discernible effect (Carson *et al.*, 1997). By inhibiting kinesin-1 expression using an anti-sense oligonucleotide, it was also found that *MBP* mRNA localization was inhibited. Collectively, these data strongly indicate that anterograde *MBP* mRNA trafficking in oligodendrocytes requires intact microtubules and most likely involves the positive-end directed motor protein kinesin-1.

1.2.3 Pair-rule mRNAs in the *Drosophila* blastoderm embryo

During interphase 14 of *D. melanogaster* embryogenesis, the monolayer of nuclei found at the cortex of the blastoderm embryo subdivides into apical, nuclear and basal compartments (Fullilove and Jacobson, 1971; Rickoll, 1976; Turner and Mahowald, 1976). At this stage, RNA transcripts of the pair-rule genes localize to the apical periplasm in seven transverse stripes along the anteroposterior axis, thereby establishing segmental patterning (Hafen *et al.*, 1984; Edgar *et al.*, 1986). In two independent studies, disruption of the microtubule cytoskeleton with colcemid caused both endogenous pair-rule RNA *fushi tarazu* (*ftz*), and injected *ftz* mRNA to disperse into all three of the blastoderm layers (Edgar *et al.*, 1987; Lall *et al.*, 1999). Furthermore, it was found that when preincubated with human or *Drosophila* embryonic nuclear extract, injected *ftz* mRNAs rapidly localized to the apical periplasm in a microtubule-dependent manner (Lall *et al.*, 1999). Since MTs radiate from apically positioned centrosomes in blastoderms, it was speculated that pair-rule mRNA transport requires the minus-end directed motor protein dynein. It was found that upon coinjection of *ftz* mRNA with anti-dynein heavy chain antibodies, almost complete inhibition of *ftz* localization occurred (Wilkie and Davis, 2001). Moreover, through the use of hypomorphic dynein mutants, or by disrupting the dynein-dynactin complex with an excess of dynamitin (Echeverri *et al.*, 1996), trafficking of *ftz* RNA could be severely impeded, thereby strongly indicating that active motor transport potentiates pair-rule mRNA translocation.

1.2.4 *Vg1* mRNA in *Xenopus* oocytes

In *X. laevis* oocytes, specific maternal RNAs become localized to either the animal or vegetal cortices, thereby leading to cell polarization and formation of the primary

developmental axis in fertilized embryos (Kloc *et al.*, 2001). *Vg1* mRNA is distributed throughout the oocyte early during oogenesis (stages 1 and 2) and localizes to the vegetal cortex from stage 3 onwards (Melton, 1987; Forristall *et al.*, 1995). Using *in situ* hybridization experiments, it was observed that following treatment with the microtubule disrupting drugs colchicine or nocodazole, *Vg1* mRNA no longer localized to the vegetal cortex during embryogenesis stage 3 (Yisraeli *et al.*, 1990). In contrast, *Vg1* mRNA remained localized to the vegetal hemisphere during stages 5 and 6 of oogenesis, regardless of microtubule disruption, although transcripts became mislocalized upon disruption of actin filaments with cytochalasin B. These findings correlated with fractionation experiments demonstrating *Vg1* mRNA release from detergent-insoluble fractions following nocodazole treatment at stage 3, and cytochalasin treatment at stages 5/6, respectively. Furthermore, these data support the notion of a two-step localization mechanism in which *Vg1* mRNA is trafficked to the vegetal hemisphere in a microtubule-dependent manner and anchored proximal to the cortex using an actin-based mechanism. In addition, it was found that *Vg1* association with microtubules requires Vg1RBP/Vera, a protein which specifically recognizes and co-localizes with *Vg1* mRNA at the vegetal cortex (Schwartz *et al.*, 1992; Elisha *et al.*, 1995; Deshler *et al.*, 1997). It has been speculated that *Vg1* mRNA trafficking may require minus-end directed motor trafficking along MTs which have their plus-ends oriented towards the cell interior (Pfeiffer and Gard, 1999). Although such a motor protein has yet to be identified, is has been demonstrated that Vg1RBP/Vera co-fractionates with rough endoplasmic reticulum (RER) and *Vg1* mRNA localizes to a subdomain of the vegetal RER during oogenesis states 2 and 3 (Deshler *et al.*, 1997). It is therefore conceivable that, although localization to the cortex requires the association of both Vg1RBP/Vera and *Vg1* mRNA with intact microtubules, actual translocation in

fact results from a microtubule-based membrane trafficking pathway (Dabora and Scheetz, 1988; Lee and Chen, 1988; Allan and Vale, 1994; Waterman-Storer *et al.*, 1995).

1.2.5 *Bicoid* and *Oskar* RNAs in *Drosophila* oogenesis

Drosophila oocytes develop in an egg chamber consisting of 15 nurse cells and an oocyte, surrounded by a monolayer of follicle cells. The nurse cells are connected to each other, and also to the anterior of the oocyte by large cytoplasmic bridges called ring canals. During stages 1-7 of oogenesis, *bicoid* and *oskar* mRNAs are synthesized in the nurse cells and transported into the oocyte. Later during mid-stages (8/9), anteroposterior patterning is specified in part by the anterior localization of *bicoid* mRNA and posterior localization of *oskar* mRNA, respectively (St Johnston *et al.*, 1989; Wilsch-Brauninger *et al.*, 1997; Riechmann and Ephrussi, 2001; van Eeden *et al.*, 2001). It has been demonstrated that intact microtubules are required for trafficking and localization of these transcripts (Pokrywka and Stephenson, 1991; Clark *et al.*, 1994; Pokrywka and Stephenson, 1995), and in addition, several indirect lines of evidence support the role of molecular motors in *bicoid* and *oskar* mRNA localization (Brendza *et al.*, 2000; Schnorrer *et al.*, 2000; Palacios and St Johnston, 2002). During mid-oogenesis, microtubules are normally oriented with their minus-ends proximal to the anterior pole (Theurkauf *et al.*, 1992). Using a *Drosophila* mutant with a misorganized microtubule cytoskeleton, the presence of microtubule minus-ends could be correlated with *bicoid* mRNA localized to both poles, thereby suggesting a minus-end directed motor transport mechanism (Clark *et al.*, 1997; Schnorrer *et al.*, 2000). Furthermore, disruption of dynein activity by the overexpression of dynamitin led to *bicoid* mRNA mislocalization, apparently without compromising the microtubule

organization (Duncan and Warrior, 2002; Januschke *et al.*, 2002). Similarly, *oskar* mRNA was mislocalized in kinesin deficient mutant *Drosophila* oocytes (Brendza *et al.*, 2000), however, direct observations of motor-dependent RNA trafficking have yet to be described. Interestingly, it has been proposed that kinesin-dependent ooplasmic streaming (Gutzeit, 1986; Bohrmann and Biber, 1994; Palacios and St Johnston, 2002) may contribute to the positioning of *oskar* transcripts during late stages of oogenesis (Glotzer *et al.*, 1997). When injected into oocytes, fluorescent *oskar* RNAs appeared to enter the directional streaming flow and accumulate at the posterior pole, an observation that correlates with the loss of anteroposteriorly organized microtubules during late oogenesis (Theurkauf *et al.*, 1992). Although rather speculative, this theory does highlight the necessity for both trafficking and anchoring machinery during RNA localization, which in the case of *bicoid* and *oskar* mRNA transport, is reflected by the fact that over 20 accessory factors are likely to be involved (Martin *et al.*, 2003).

1.2.6 *Protamine-1* mRNA in mouse spermatids

Independent lines of evidence support the idea that, in order to attain phenotypic equivalency during spermatogenesis, haploid mice spermatids are able to transmit certain mRNAs directly through intercellular crossbridges. Indirect evidence for intercellular RNA transport came from studies using transgenic mice, hemizygous for a chimaeric gene containing the transcriptional regulatory sequences of protamine-1 (*Prm-1*) and the coding region for human growth hormone (*hGH*). It was found that in mice where only half of the germ cells carried the transgene, the *hGH* gene product could be detected in over 90 % of the spermatids, The authors could not, however, differentiate between translocation of the RNA transcript or the protein itself (Braun *et al.*, 1989). By exploiting a karyotype of mice that undergo anomalous meiotic segregation, Caldwell and Handel were able to demonstrate that intercellular *Prm-1*

trafficking was indeed likely to occur. In populations of spermatids that contained individuals nulli- uni- and disomic for the *Prm-1* gene, the distribution of *Prm-1* mRNA in whole testis sections was found to be indistinguishable from that of control mice (Caldwell and Handel, 1991). Interestingly, protamine-1 RNA contains so-called *Y* and *H* sequences (Han *et al.*, 1995), which are known to occur in a number of RNAs associated with mouse testis/brain RNA-binding protein (TB-RBP). Using immunocytochemical and *in situ* labeling techniques, TB-RBP and *AKAP4* (an X-linked RNA containing *Y* and *H* sequences) could be co-localized in the spermatid cytoplasm, and furthermore, within intercellular crossbridges (Morales *et al.*, 2002). Although inconclusive, this might suggest that a ribonucleoprotein (RNP) transport complex is involved in *AKAP4* trafficking between spermatozoa.

1.2.7 Intercellular RNA trafficking in plants

Plant cells are separated from each other by an extensive extracellular matrix or cell wall. Although the cell wall is not totally impervious (Baron-Epel *et al.*, 1988), it is likely to hinder the direct cell-to-cell communication of relatively large molecules such as mRNAs. Furthermore, because plant cells do not migrate, their spatial environment becomes a major determinant of cell fate (Steeves and Sussex, 1989; Van den Berg *et al.*, 1995), and therefore, plants must be able to communicate efficiently between cells and tissues in order to orchestrate their development. To facilitate this, neighbouring plant cells are connected via plasmodesmata (Pd), membrane-contiguous cytoplasmic continuities (Robards and Lucas, 1990). Moreover, due to this symplasmic continuum between groups of cells, it has been proposed that plants behave as supracellular organisms (Lucas and van der Schoot, 1993; Lucas *et al.*, 1995; Jackson and Hake,

1997; Zambryski and Crawford, 2000), with the capacity to regulate gene expression above the single cell level (Lucas *et al.*, 2001; Haywood *et al.*, 2002; Heinlein, 2002a).

1.2.7.1 Long distance RNA trafficking and developmental regulation

The potential role of intercellular RNA trafficking in developmental and physiological processes was highlighted by the finding that mRNA transcripts of phloem-specific leaf sucrose transporter (SUT-1) had the apparent capacity to move cell-to-cell (Kühn *et al.*, 1997). Using *in situ* hybridization techniques, it was possible to localize *Sut-1* mRNA to the companion cells (CC), enucleate sieve elements (SE) and plasmodesmata of potato leaf phloem. Furthermore, since overall SUT-1 expression is repressed by an antisense construct under the control of a CC-specific promoter (Kuhn *et al.*, 1996), it was reasonably speculated that *Sut-1* mRNA is transcribed in the CC before moving through the Pd into the SEs. Intercellular RNA trafficking has also been proposed for Knotted-1 (KN-1), a homeobox transcriptional regulator known to be involved in cell-fate determination in maize vegetative and floral meristems (Sinha, 1999). KN-1 protein has been directly demonstrated to move between cells of the *Arabidopsis* shoot apex (Kim *et al.*, 2002), and furthermore, upon co-injection of tobacco mesophyll cells with *E.coli* produced KN-1 protein, *in vitro* transcribed *Kn-1* sense RNA transcripts were observed to move cell-to-cell (Lucas *et al.*, 1995). Although a direct functional relationship between *Kn-1* RNA movement and cell differentiation was not determined, the authors were able to demonstrate that intercellular RNA movement was sequence-specific in this case. Using a similar microinjection approach, Xoconostle-Cazares *et al*. could show that when *CmPP16* RNA from pumpkin and the corresponding CmPP16 protein were co-injected into mesophyll cells, rapid intercellular RNA movement occurred (Xoconostle-Cazares *et al.*, 1999). Furthermore, using RT-PCR, it

was possible to detect *CmPP16* transcripts in the phloem sap of cucumber scions heterografted onto pumpkin rootstocks, thereby demonstrating long-distance RNA trafficking via the plant vasculature. The role of RNA as a cell-non-autonomous signaling macromolecule is supported by the observation that following long distance transport, RNAs known to be involved in developmental processes can both accumulate in meristematic tissues (Ruiz-Medrano *et al.*, 1999), and apparently influence leaf morphology (Kim *et al.*, 2001). Kim *et al*. exploited a dominant leaf mutant of tomato called *Mouse ears* (*Me*) in which anomalous fusion of the KNOX gene *LeT6* to the 5' coding and promoter region of Pyrophosphate-dependent phosphofructokinase (PFP) results in overexpression of *PFP-LeT6* transcripts in leaves and altered leaf morphology (Chen *et al.*, 1997; Kim *et al.*, 2001). Interestingly, when wild-type scions were heterografted onto *Me* mutant rootstocks, new leaves in the scion developed the *Mouse ears* morphology, suggesting that the *Me* phenotype was graft transmissible. Furthermore, the distribution of *PFP-LeT6* transcript in the shoot apical meristem of heterografted scions was reminiscent of that found in non-grafted *Me* plants, suggesting that spatial patterning of RNA may influence developmental consequences at the shoot apex. Although these data provided strong correlative evidence that *PFP-LeT6* RNA was the signaling molecule responsible for the *Me* phenotype in heterografted scions, it remains plausible that overexpression of this homeotic gene may have led to the misregulation of other developmental signals, such as phytohormones (Ori *et al.*, 1999; Tsiantis, 2001).

1.2.7.2 Systemic RNA trafficking and gene silencing

In addition to plant developmental coordination, intercellular RNA trafficking has also been implicated in the potentiation of systemic post-transcriptional gene silencing

(PTGS), a sequence-specific defense mechanism by which plants target and degrade RNAs that are perceived to be foreign or aberrant (Lucas *et al.*, 2001; Waterhouse *et al.*, 2001; Mlotshwa *et al.*, 2002). Direct evidence for a systemic silencing signal was provided by grafting experiments where spontaneous gene silencing in transgenic tobacco rootstocks was transmitted into isogenic scions that did not display silencing prior to the grafting procedure (Palauqui *et al.*, 1997). In addition, it was found that systemic silencing could be initiated in transgenic tobacco by the introduction of DNA which contained sequences homologous to the transgene (Voinnet and Baulcombe, 1997). The apparent absence of exogenous DNA in systemically silenced tissue supported the concept of a mobile silencing signal, and moreover, since the silencing events appeared to be sequence-specific in both cases, the systemic signal was proposed to be a nucleic acid. Consistent with this hypothesis, short (21-26 nt) double-stranded (ds) RNAs with sequence homology to silenced transcripts have been found to accumulate in silenced tissues (Hamilton and Baulcombe, 1999; Hamilton *et al.*, 2002), and although thought to be the cleavage products of longer dsRNA precursors (Tang *et al.*, 2003), these so-called small interfering RNAs (siRNAs) are sufficient to elicit sequence-specific gene silencing in both mammalian and plant systems (Elbashir *et al.*, 2001; Klahre *et al.*, 2002; Vanitharani *et al.*, 2003). The exact nature of the mobile silencing signal has yet to be elucidated, however, since evidence for systemic trafficking of DNA or long dsRNAs is mostly lacking, it remains a plausible hypothesis that long distance gene silencing is mediated by siRNAs or related RNA species.

1.2.8 Intracellular RNA trafficking in plants

In plants, the mechanisms which govern intracellular trafficking and localization of endogenous RNA remain poorly understood. One of the best studied examples, however, is the localization of storage protein mRNAs to subcompartments of the

rough endoplasmic reticulum (RER) of rice endosperms. During seed development, endosperms accumulate two classes of storage protein, glutelins and prolamines. Following translation on polysomes (Kim *et al.*, 1993; Okita *et al.*, 1994; Okita and Rogers, 1996), glutelin protein is sequestered to a vacuolar compartment via the golgi complex, and prolamine forms so-called protein bodies within the lumen of intracisternal RER (Krishnan *et al.*, 1986; Yamagata *et al.*, 1986). Biochemical studies demonstrated that while *glutelin* mRNA species predominated in cisternal-ER (C-ER) derived vesicles, ER fractions enriched for protein bodies (PB-ER), only contained *prolamine* mRNAs (Yamagata *et al.*, 1986; Yamagata and Tanaka, 1986). The non-random distribution of these transcripts was directly confirmed by *in situ* hydridization experiments (Li *et al.*, 1993), and moreover, by substitution of the *prolamine* 3'-untranslated region (3'-UTR) for that of *glutelin*, it was shown that the *prolamine* chimera was mislocalized to sites reminiscent of endogenous *glutelin* transcripts (Choi *et al.*, 2000). This suggested that sequence-specific signaling elements are involved in mRNA localization during endosperm development, and moreover, disruption of the protamine AUG start codon resulted in severe RNA mislocalization, indicating that *protamine* mRNA may translocate as a ribonucleoprotein (RNP) complex, and possibly requires translation initiation factors for appropriate ER-targeting. Although *prolamine* mRNAs have been shown to associate with detergent-resistant cell fractions containing PBs and cytoskeleton elements (Muench *et al.*, 1998), direct evidence linking *prolamine* mRNA trafficking and active transport is lacking. A putative *trans*-acting factor has been identified, however, and this 120 kDa protein binds the *prolamine* 3'-UTR and co-sediments with the actin cytoskeleton (Sami-Subbu *et al.*, 2001). Nevertheless, due to the fact that both polysomes (Davies *et al.*, 1991) and ER-membranes (Dabora and Scheetz, 1988; Lee and Chen, 1988; Allan and Vale, 1994;

Waterman-Storer *et al.*, 1995) have been described to associate with cytoskeletal filaments, it remains unclear what role the cytoskeleton plays in prolamine localization, and indeed, whether these subcellular compartments are mutually exclusive during endosperm development.

1.3 Tobacco Mosaic Virus (TMV) as a model to study intracellular RNA trafficking in plants

In plants, the molecular mechanisms responsible for intracellular RNA transport remain largely unknown. Evidence from other systems indicates that RNA trafficking and localization is a highly coordinated process, capable of directing transcripts to their respective destinations in an efficient and sequence-specific manner. Although not ubiquitous, cytoskeleton-dependent mechanisms appear to be a common feature of intracellular RNA transport in a variety of cell types. Given the propensity of viruses to exploit pre-existing host machinery, it is not surprising to find that among others, HIV (Kimura *et al.*, 1996; Liu *et al.*, 1999; Mouland *et al.*, 2000; Mouland *et al.*, 2001), Vaccinia (Hollinshead *et al.*, 2001; Mallardo *et al.*, 2001; Rietdorf *et al.*, 2001) and Herpes simplex viruses (Döhner *et al.*, 2002; Mabit *et al.*, 2002; Martin *et al.*, 2002) also utilize cytoskeleton-based transport in order to facilitate the translocation of their viral components through the cytoplasm (Sodeik, 2000; Enquist, 2002). Based on this precept, TMV may also exploit an endogenous transport pathway, and therefore, provide a useful tool for elucidating the host components involved in plant RNA trafficking. TMV is a single stranded positive-sense RNA virus which replicates on ER-derived membranes (Más and Beachy, 1999) before exporting its genome into neighbouring cells via plasmodesmata (Tomenius *et al.*, 1987; Atkins *et al.*, 1991). Since these processes have no requirement for coat protein (CP), it appears that TMV

viral RNA (vRNA) can move both intra- and intercellularly in a non-encapsidated form (Dawson *et al.*, 1988; Heinlein *et al.*, 1998). In addition to modulating the size exclusion limit of Pd (Wolf *et al.*, 1989; Oparka *et al.*, 1997), the 30 kDa movement protein (MP) of TMV is proposed to mediate vRNA transport in the form of a viral ribonucleoprotein complex (Dorokhov *et al.*, 1983; Dorokhov *et al.*, 1984; Citovsky *et al.*, 1990), and therefore, MP may represent an indirect marker for the presence of vRNA during TMV infection. In support of this hypothesis, preliminary studies show that during TMV infection, the distribution of vRNA in living plant cells is very similar to that of MP (Boyko *et. al*, unpublished observation), an observation previously found in TMV-infected BY-2 protoplasts (Más and Beachy, 1999).

1.3.1 Structure and organization of the TMV genome

TMV virions are composed of a 6.4 kb single-stranded, positive-sense RNA which is encapsidated with 2160 helically arranged coat protein (CP) subunits. The genomic RNA is capped with 7-methyl guanosine at the 5’ terminus and forms a histidine-accepting transfer RNA (tRNA)-like structure within the 3’-untranslated region (3’-UTR). Downstream of the 69 nucleotide leader sequence are four open reading frames (ORFs) encoding the 17.5 kDa CP and three non-structural proteins of 126, 183 and 30 kDa, respectively. The 126 kDa and 183 kDa proteins are translated directly from genomic RNA and constitute the replicase function of TMV (Lewandowski and Dawson, 2000). The 126 kDa protein is translated from ORF1 and the 183 kDa protein results from read-through of the amber stop codon which terminates translation of the 126 kDa protein. The CP and 30 kDa movement protein (MP) are translated from subgenomic RNAs that are produced during virus replication.

1.3.2 TMV infection cycle

Following entry of TMV into a host cell (Shaw, 1999), virus infection is thought to initiate through a combination of co-translational and co-replicational disassembly mechanisms. It was shown that *in vitro*, treatment of virions with mild alkali conditions resulted in the rapid exposure of ~ 200 nucleotides from the 5'-end of genomic RNA (Mundry *et al.*, 1991). Furthermore, using a cell-free translation system, it was found that translation of replicase protein was greatly enhanced by pH and ionic conditions similar to those found in the plant cytoplasm, thereby supporting the idea of 5' $\rightarrow$ 3' co-translational disassembly *in vivo* (Wilson, 1984). In addition, it was demonstrated that 3' $\rightarrow$ 5' disassembly of TMV coincided with synthesis of progeny negative-strand RNA and required the presence of the replicase proteins (Wilson, 1985). Therefore, it is likely that the processes of viral disassembly, replicase translation and RNA synthesis are coupled *in vivo*. Replication of TMV RNA proceeds through replicase-dependent synthesis of a complementary negative-strand using the positive-strand as a template. Subsequently, progeny positive strands are synthesized using the negative strand as a template, as are the subgenomic RNAs encoding MP and CP (Buck, 1999). In tobacco protoplasts, negative strand synthesis halts 6-8 hours following inoculation, however, positive strands continue to be synthesized for a further 8-10 hours (Ishikawa *et al.*, 1991). In addition to genomic- and subgenomic-length positive-strand RNAs, replication intermediates isolated from TMV-infected plants appear to include genomic-length double-stranded RNAs and a number of partly double-stranded and partly single-stranded RNAs (Nilsson-Tillgren, 1970; Jackson *et al.*, 1971). It remains unclear, however, whether such double-stranded RNAs (dsRNAs) were formed spontaneously during the RNA extraction procedure, or actually represent RNA species present *in vivo*. Considering that dsRNA can act as a potent elicitor of gene-silencing

(Bass, 2000), one might expect TMV to limit dsRNA formation throughout infection. During early to mid-infection, MP is expressed transiently and accumulates to relatively low levels (Lehto *et al.*, 1990). In contrast, CP accumulates to high amounts later during replication (Siegel *et al.*, 1978; Ooshika *et al.*, 1984; Watanabe *et al.*, 1984; Lehto *et al.*, 1990), and when synthesis of negative-strand RNA has ceased, encapsidates the genomic positive-strand RNA to form virions (Aoki and Takebe, 1975; Palukaitis *et al.*, 1983).

1.3.3 The role of MP during vRNA trafficking

Following infection of tobacco BY-2 protoplasts with a TMV-derivative lacking the genes for MP and CP, it was found that TMV-specific RNAs continued to accumulate, indicating that neither coding sequence contained *cis*-acting elements required for replication (Meshi *et al.*, 1987). Furthermore, analysis of local lesion development in TMV-infected *N. tabacum* demonstrated that cell-to-cell vRNA spread was abolished by mutations in the MP gene, but not the CP gene (Meshi *et al.*, 1987; Dawson *et al.*, 1988). More recent studies have unequivocally proven that the entire CP gene is dispensable for cell-to-cell movement of TMV (Heinlein *et al.*, 1998). The role of MP in vRNA trafficking is further supported by functional complementation studies in which transgenically or virally expressed MPs have the ability to facilitate intercellular spread of TMV-derivatives encoding transport-defective MPs (Deom *et al.*, 1987; Holt and Beachy, 1991). Using a variety of experimental approaches, it was also found that MP has the intrinsic ability to target Pd (Tomenius *et al.*, 1987; Atkins *et al.*, 1991; Ding *et al.*, 1992; Moore *et al.*, 1992) and rapidly increase their size exclusion limit (Wolf *et al.*, 1989; Waigmann *et al.*, 1994). This may indicate that MP directly interacts with putative Pd-targeting factors, however, it was found that MP mutants unable to mediate the cell-to-cell spread of TMV can still target and accumulate at Pd

(Boyko *et al.*, 2000a; Boyko *et al.*, 2000c). Although inconclusive, this would appear to suggest that such loss of movement function corresponds to events preceding Pd targeting of the TMV genome, thereby reaffirming the role of MP during intracellular vRNA transport.

1.3.4 Transport as a ribonucleoprotein complex (RNP)

MP purified from *E.coli* has been demonstrated to bind both ssRNA and ssDNA *in vitro* (Citovsky *et al.*, 1990; Citovsky *et al.*, 1992; Li and Palukaitis, 1996). Such complexes assume an unfolded, elongated structure which is consistent in diameter (~ 2 nm) with dilated Pd (Citovsky *et al.*, 1992; Drygin *et al.*, 1998; Kiselyova *et al.*, 2001). Similar long and elongated RNP complexes have been isolated from tobacco plants infected with wild-type TMV (Dorokhov *et al.*, 1983), but could not be extracted from plants inoculated with virus encoding a temperature-sensitive mutant of MP, and grown at non-permissive temperature (Dorokhov *et al.*, 1984). The fact that MP binds ssRNA in a sequence non-specific manner may also account for the observation that MPs from certain viruses are functionally interchangeable (Deom *et al.*, 1987) and that MP can facilitate the cell-to-cell spread of a number of co-injected nucleic acids (Fujiwara *et al.*, 1993; Noueiry *et al.*, 1994; Waigmann *et al.*, 1994; Ding *et al.*, 1995). MP:vRNA complexes formed *in vitro* are non-translatable when electroporated into tobacco protoplasts or when added to *in vitro* translation reactions (Karpova *et al.*, 1997). Translation repression is abolished when MP is phosphorylated by protein kinase-C or by a plant cell-wall-associated kinase (Karpova *et al.*, 1999), and since *in vitro* assembled vRNPs can also be translated *in planta*, it has been speculated that these complexes are modified during their passage through the Pd (Karpova *et al.*, 1997). Although direct observations of MP-mediated vRNA trafficking have yet to be

made, the collective evidence does support the hypothesis that MP and RNA are co-transported as a vRNP complex.

1.3.5 Subcellular distribution of MP during infection

When fused with the green fluorescent protein (GFP) of *Aequorea victorea*, the spatial distribution of MP in TMV-infected cells can be directly monitored (Heinlein *et al.*, 1995; Epel *et al.*, 1996). Although the visualization of vRNA has been limited to indirect techniques such as *in situ* hybridization (Más and Beachy, 1999), inferences can be made as to the subcellular structures involved in vRNA trafficking by determining the distribution of MP:GFP and vRNA in cells at equivalent stages of TMV-infection. Infection of *N. benthamiana* with a TMV-derivative lacking the CP gene and encoding MP:GFP (TMV-MP:GFP) has demonstrated that the subcellular distribution of MP changes temporally within infected cells (Heinlein *et al.*, 1995; Oparka *et al.*, 1997; Heinlein *et al.*, 1998). Upon initial infection, MP:GFP localizes to Pd, a finding consistent with its role in mediating cell-to-cell vRNA transport (Wolf *et al.*, 1989; Waigmann *et al.*, 1994). As infection progresses, MP:GFP can be observed to form irregular shaped ER-derived cytoplasmic puncta, which increase in size over time (Heinlein *et al.*, 1995). The disappearance of these larger cytoplasmic aggregates (termed inclusion bodies) coincides with the localization of MP:GFP to microtubules (McLean *et al.*, 1995; Boyko *et al.*, 2000b; Gillespie *et al.*, 2002), and late during infection, MP:GFP fluorescence is again localized exclusively to Pd. With the obvious exception of Pd targeting, a very similar pattern of MP:GFP localization has been observed in TMV-MP:GFP infected BY-2 protoplasts (Heinlein *et al.*, 1998; Más and Beachy, 1998). Moreover, vRNA was also shown to localize to the intersections of cortical and cytoplasmic ER strands, larger ER-derived bodies and microtubules in BY-

2 protoplasts, indicating that MP and RNA localization may occur concomitantly (Más and Beachy, 1999).

1.3.5.1 Endomembrane association

In addition to MP and vRNA, the ER-containing inclusion bodies formed during infection with TMV-MP:GFP also contain replicase proteins (Más and Beachy, 1999). It is thought that these bodies are formed by the transient recruitment of membranes from the cortical ER network, coinciding with the accumulation MP (Heinlein *et al.*, 1998; Reichel and Beachy, 1998). Furthermore, the reversion of aggregated ER back to tubular ER occurs concurrently with the apparent redistribution of MP:GFP onto microtubules (Heinlein *et al.*, 1998; Gillespie *et al.*, 2002). Similar changes in the morphology of the ER also occur upon ectopic expression of MP:GFP, indicating that inclusion body formation is replicase-independent (Reichel and Beachy, 1998). Interestingly, infection of BY-2 protoplasts with a TMV-derivative lacking the MP gene did not abolish the association of TMV-specific RNA with perinuclear ER, but did prevent the formation of large replicase-containing inclusion bodies (Más and Beachy, 1999). Furthermore, a deletion mutant of MP lacking 55 amino acids from the C-terminus does not accumulate in aggregated ER-inclusions, but can still facilitate the cell-to-cell movement of vRNA (Boyko *et al.*, 2000c). This is in agreement with previous studies in which an MP-attenuated TMV-derivative was still able to replicate *in planta* (Meshi *et al.*, 1987), and suggests that inclusion body formation is not essential to TMV function. The fact that replicase-containing complexes have been purified from the membrane fractions of infected cells argues that early replication events in fact do take place proximal to membranes (Ralph *et al.*, 1971; Nilsson-Tillgren *et al.*, 1974; Watanabe and Okada, 1986; Young and Zaitlin, 1986; Young *et al.*, 1987; Osman and Buck, 1996). This is supported by electron microscopy studies

illustrating that viral-specific inclusions contain replicase, ER and ribosomes (Martelli and Russo, 1977; Hills *et al.*, 1987; Saito *et al.*, 1987), and may indicate that at time-points when large MP:GFP-containing bodies are observed, viral replication and cell-to-cell spread has already taken place.

1.3.5.2 Microtubule association

In TMV-infected plants and protoplasts, localization of MP to microtubules (MTs) coincides with the reduction in size, and subsequent disappearance of MP-containing ER inclusion bodies (Heinlein *et al.*, 1998). Interestingly, when infected plants are grown at elevated temperatures, the rate of TMV intercellular spread is enhanced (Lebeurier and Hirth, 1966; Dawson *et al.*, 1975). Although the level of MP expression does not increase in plants grown at 32 ^{o}C (compared to 22 ^{o}C), the localization of MP to MTs occurs earlier during infection, indicating that efficiency of intracellular vRNA trafficking is linked to the redistribution of MP from sites of synthesis onto MTs (Boyko *et al.*, 2000b). In BY-2 protoplasts, TMV RNA and MP have been localized to microtubules at equivalent stages during infection (Heinlein *et al.*, 1998; Más and Beachy, 1999). In contrast, vRNA is mislocalized in protoplasts infected with TMV encoding a mutant of MP which does not localize to MTs, but retains RNA binding activity (Kahn *et al.*, 1998). A number of MP deletion mutants have also been characterized *in planta*, and a positive correlation between the localization of MP to MTs and intercellular vRNA movement has been established (Kahn *et al.*, 1998; Boyko *et al.*, 2000c). Compelling evidence to support the role of MTs in vRNA trafficking was provided by the identification of a region within MP that shares sequence-similarity to α-, β- and γ-tubulins (Boyko *et al.*, 2000a). Single amino acid substitutions within this so-called ‘tubulin mimicry domain’ are sufficient to confer temperature-sensitive loss of MT-association and vRNA movement. In α- and β-

tubulins, this region of homology forms an exposed loop structure which is thought to mediate the lateral contacts between microtubule protofilaments (Downing and Nogales, 1998). Whether MP is capable of making equivalent binding contacts with tubulin remains unclear, however, under conditions which typically result in the depolymerization of MTs, such as cold, high molarity salt or Ca^{2+} treatments, MT filaments isolated from infected cells are unusually stable (Boyko *et al.*, 2000a). Biochemical evidence supports the idea that MP can interact directly with MTs (McLean *et al.*, 1995), and as demonstrated by transient expression assays, the ability of MP to associate with MTs is independent of viral replication (Heinlein *et al.*, 1998; Reichel and Beachy, 1998; Kotlizky *et al.*, 2001). Furthermore, MP associates with MTs when ectopically expressed in mammalian cells, thus indicating that plant-specific factors are not required for this interaction (Boyko *et al.*, 2000a).

1.3.5.3 Summary

The collective data provide strong correlative evidence that intracellular trafficking of TMV RNA requires the association of MP with MTs. It is thought that MP mediates vRNA transport in the form of a vRNP complex, however, the direct visualization of actively moving vRNA has yet to be made. Nevertheless, MP associates with MTs when transiently expressed in plant and mammalian cells, and may mediate the stabilization of MT networks by a specialized direct interaction. Whether MP:MT complexes directly engage in vRNA transport is unclear, but given the functional requirement for MP to associate with MTs, further studies of this interaction may provide a broader understanding of the strategies employed by TMV during successful infection of susceptible host plants.

1.3.6 Thesis objectives

The principle aim of this thesis was to elucidate the underlying mechanisms by which MP interacts with MTs. In order to fulfill this objective, it was imperative that we determine whether MP can interact directly with MTs, or whether accessory factors common to both plant and mammalian systems actually mediate the observed MP:MT association. Although direct MP:MT binding was previously demonstrated using purified proteins (McLean *et al.*, 1995), the validity of these results were challenged following the discovery that MP preparations had a propensity to form disordered, non-specific aggregates (Dr. L. Brill, personal communication). Furthermore, due to speculation regarding the involvement of a putative tubulin-mimicry domain present within MP (Boyko *et al.*, 2000a), we hoped to gain an understanding of the dynamic behaviour of such an interaction; i.e. determine whether MP interacts with preformed or actively polymerizing MTs. It was hoped that by studying this interaction using purified proteins *in vitro*, the initial interpretation of data would be somewhat simplified, thereby providing a suitable foundation on which to base further studies involving multi-component complexes. If MP was indeed found to bind MTs directly, we wanted to characterize the interaction in more detail by determining the relative binding affinity and stoichiometry of the reaction. It was believed that under controlled conditions, comparisons could then be drawn between MP and other known microtubule-associated proteins (MAPs), particularly with regard to MT stability. Because the association of MP with MTs correlates with vRNA trafficking, it was crucial that we understood whether both MP and RNA could participate in the interaction with MTs, and whether in principle, a minimal MP:RNA:MT complex would be sufficient to facilitate the translocation of RNA. Several putative models have emerged to explain the mechanism of vRNA transport during infection (Heinlein,

2002b). Of these, it has been proposed that MP acts as a novel type of MAP and is involved in stabilizing the MT network for the purposes of providing a pathway for motor–based trafficking, or perhaps as a counter-defense strategy to evade host defense responses. In an attempt to differentiate between these potential roles, we also thought it important to test the ability of MT-dependent motor proteins to translocate on filaments heavily decorated with MP.

2 Materials and Methods

2.1 Purification of overexpressed MP from E.coli

2.1.1 Purification strategy

2.1.1.1 Subcellular localization of MP expressed in E.coli

Upon overexpression in *E.coli*, MP is known to form 'inclusion bodies' (Citovsky *et al.*, 1990; Brill *et al.*, 2000). These dense protein aggregates are highly insoluble under native conditions, rendering them unsuitable for most common types of preparative biochemistry. Fortunately however, due to their high stability in the presence of salts and non-ionic detergents, inclusion bodies can be readily fractionated from the majority of cellular components by differential centrifugation. Furthermore, inclusion bodies can be fully solubilized under denaturing conditions, and while this results in only semi-pure preparations (80-90 % MP), MP prepared in this manner has been demonstrated to retain biological activity upon renaturation (Citovsky *et al.*, 1990; Waigmann *et al.*, 1994). It was therefore decided that inclusion body fractionation would be used as a starting point in the purification of MP from *E.coli*.

2.1.1.2 Principle of Immobilized Metal Affinity Chromatography (IMAC)

IMAC is a group-specific method for affinity purification of proteins and is based on the reversible interaction of amino acid side groups with divalent metal cations (Porath *et al.*, 1975). Typically, a metal chelator, such as Nitrilotriacetic acid (NTA), is conjugated to a solid matrix where it also occupies 4 of the 6 available binding coordinates of Ni^{2+} or Co^{2+}. The remaining coordinates interact strongly with histidine side groups, particularly when found in tandem repeats of 4–6 residues. Proteins

containing polyhistidine runs (“His-tagged proteins”) are able to interact with metal ions even in the presence of micelle concentrations of non-ionic detergents, high salt concentrations (> 4 M) and chemical denaturants such as 8 M Urea or 6M GuHCl. It was due to these advantageous properties of IMAC resins that we constructed a MP directly fused to 6 consecutive histidine residues, thereby allowing us to further purify MP isolated from inclusion bodies under both denaturing and high stringency conditions.

2.1.1.3 General note about MP purification

Although many His-tagged proteins have been successfully purified from crude cellular extracts (Schmies *et al.*, 2000; Ferguson and Goodrich, 2001; Nunez *et al.*, 2001), a common problem found is that C-terminally tagged proteins often co-purify with truncated, immunologically related products. This is thought to be due to imperfect initiation of translation occurring at methionine codons within the open reading frame, and in the case of MP, the degree to which these truncated products occur appears to vary between preparations. To counter this phenomenon, a number of variations in bacterial growth conditions and purification procedures were applied which included ion exchange-, immuno affinity- and size exclusion-chromatography, respectively. It must be noted, however, that MP purification solely by means of inclusion body isolation and Ni^{2+}-NTA IMAC yielded the most favourable results, and unless otherwise stated in the text, all preparations of MP:$(H)_6$ used for *in vitro* assays were prepared by this method and are thus simply referred to as “MP”.

2.1.2 Construction of plasmids for MP overexpression

2.1.2.1 Overview of the QIAexpress® vector pQE60

The commercial vector pQE60 (Qiagen) is designed for high level expression of proteins in *E.coli* which are fused to a C-terminal $GS(H)_6$ affinity tag. Genes of interest may be cloned into an *NcoI* restriction site, allowing the restoration of an 'in-frame' 5' ATG start codon. Expression is under the control of a strong T5 promoter located upstream of two *Lac* operator regions and a Shine-Dalgarno sequence. During normal growth, expression is repressed by high levels of the $LacI^q$ gene product which is constitutively supplied in *trans* from the pREP4 repressor plasmid present in commercial *E.coli* strain M15 (Qiagen; derived from *E.coli* strain K12). A stop codon and two transcription terminator sequences directly downstream of the multiple cloning site facilitate precise termination of protein translation and prevent read-through of transcription. Plasmids pQE60 and pREP4 confer ampicillin and kanamycin resistance, respectively, and efficient induction of expression is achieved by applying IPTG to the growth media.

2.1.2.2 Cloning procedures

Standard molecular biology techniques were employed during the production of MP-expression constructs and are essentially as described (Sambrook and Russell, 2001). Plasmid pTf5-NX2 (Boyko *et al.*, 2002) was utilized as a template for PCR-amplification of the MP gene. Primers containing specific sequence mismatches (see Appendix II) were used to introduce unique 5' *Eco47III* and 3' *BamHI* restriction sites into the MP sequence during PCR. Resulting products were digested with *Eco47III* followed by *BamHI* and full-length products were purified from 1 % agarose gels (QIAquick gel extraction kit, Qiagen) and quantified by measuring the absorbance at

260 nm. Expression vector pQE60 was digested with *NcoI* and treated with Klenow fragment, thereby filling in the 5'-overhang and creating a blunt end compatible with the *Eco47III* digested PCR product. The vector was further digested with *BamHI*, gel purified and quantified. Insert was ligated to vector (at a molar ratio of 3:1) using T4 DNA ligase, according to the manufacturers recommendations and competent *E.coli* strain M15 (Qiagen) was directly transformed with ligation mixture and grown overnight at 37 ^{o}C on LB-Agar containing 50 μg/mL of carbenicillin and 25 μg/mL of kanamycin. The integrity of the resulting expression vector (designated pQTf5-WT) was determined by plasmid DNA extraction and DNA sequence analysis. Positive expression clones contained a restored 5' ATG start codon and coding sequence of MP, with a 3'-proximal sequence coding for -GS$(H)_6$ directly adjacent to a downstream TAA stop codon.

2.1.3 Overexpression of MP

A single bacterial colony was used to inoculate 20 mL of 2X YT media containing 50 μg/mL of carbenicillin and 25 μg/mL of kanamycin. Overnight cultures were subsequently grown at 37 ^{o}C with agitation (230 rpm). Large-scale cultures were prepared by inoculating 400 mL of the above media with 10 mL of overnight culture and were grown under the described conditions until OD_{600} reached ~ 0.8 (typically 3 hours). MP overexpression was initiated by the addition of 2 mM of IPTG and cultures were further grown for 3 hours as described, after which, cells were harvested by centrifugation at 10,000 x g in a Sorvall GSA rotor for 10 mins at 4 ^{o}C.

2.1.4 Isolation of MP-containing inclusion bodies

Cell pellets were resuspended in 15 mL of ice cold *lysis buffer* (20 mM Tris-CL [pH 8.0], 30 U DNase I, 10 μg/mL RNase A and protease inhibitor cocktail [Promega]),

frozen in liquid nitrogen and thawed on water-slush. Lysates were repeatedly sonicated (50 W) on ice (Labsonic 2000; B. Braun, Melsungen, Germany) and insoluble inclusion bodies were collected by centrifugation at 13,000 x g in a Sorvall SS34 rotor for 15 minutes at 4 ^{o}C. Inclusion bodies containing MP were washed by sonication in 10 mL of ice cold *inclusion body wash buffer* (20 mM Tris-CL [pH 8.0], 2 M Urea, 500 mM NaCl, 10 μg/mL RNase A, 2 % (v/v) Triton X-100 and protease inhibitor cocktail) followed by resedimentation at 25,000 x g in a Sorvall SS34 rotor for 10 minutes at 4 ^{o}C. Inclusion bodies were repeatedly washed in this manner until a sediment of consistent colour was obtained (typically 3 times). Inclusion bodies were then solubilized by sonication in 5 mL of ice cold *solubilization buffer* (100 mM NaH_2PO_4 [pH 7.5], 1 M NaCl, 10 mM Tris base, 8 M Urea and 10 % [v/v] Glycerol) containing 5 mM Imidazole (*SB5*), followed by incubation on a rotary mixer overnight at 4 ^{o}C. Protein suspensions were cleared of insoluble material by centrifugation at 15,000 x g in a Sorvall SS34 rotor at 4 ^{o}C prior to further purification steps.

2.1.5 Ni $^{2+}$-NTA Affinity Chromatography

The cleared protein suspensions were combined with 2.5 mL of Ni^{2+}-NTA sepharose (Qiagen) by platform shaking for 30 minutes at 4 ^{o}C, after which time, the resin and lysates were packed into disposable 1 cm diameter plastic columns (Bio-Rad Laboratories) and the resin allowed to settle. Columns were drained by gravity flow and the Flow-through fractions were collected for later analysis. Non-specifically bound proteins were subsequently removed by washing the columns twice with 5 column volumes of *SB5* (Wash Fractions I and II) followed by twice with 8 column volumes of *SB20* (Wash fractions III and IV). Elution was achieved by gently layering 10 volumes of *SB500* onto the top of the resin bed and allowing the buffer to drain through by gravity flow, while collecting 500 μL fractions (Elution fractions I–VIII).

As determined by SDS-PAGE and Colloidal Coomassie Blue (CCB) staining, residual non-specifically bound proteins co-eluted with MP in the early elution fractions (EI-IV*)*, while highly purified MP eluted in subsequent fractions, albeit in lower quantities.

2.1.6 Renaturation of purified MP

Elution fractions containing the highest apparent MP purity were renatured by direct dialysis against 50 mL of deionized water (dH_2O) for 30 minutes at room temperature and then twice against 4 L of dH_20 for several hours at 4 ^oC. Proteins were cleared of aggregated material by centrifugation at 20,000 x g for 30 min (4°C) in a desktop microcentrifuge, followed by centrifugation at 100,000 x g for 1 hour in a Beckman TLA-100.3 rotor at 4°C. A protein concentration assay was performed (Bradford, 1976) and solutions were diluted to 0.1 – 0.5 mg/mL (~ 3–15 μM) with dH_2O before being rapidly frozen in liquid nitrogen and stored at –80 ^oC. When specific buffering was required, MP was rapidly thawed at 30 ^oC and immediately placed on ice before the appropriate buffer components were added to the desired concentration. To control for variations in buffer-induced aggregation, MP was then incubated for at least 30 minutes on ice and centrifuged for 15 minutes at 100,000 x g in a Beckman TLA-100 ultracentrifuge at 4°C before being assayed for protein concentration as above. This procedure was performed after every aliquot thaw/buffer addition.

2.1.7 Determination of final MP purity by Mass Spectrometry

MP was purified and renatured as above and 10 μg of protein was visually analyzed by 12 % SDS-PAGE and CCB staining. Under sterile conditions, the 30 kDa MP band was excised from the gel, reduced with 2 % (w/v) DTT, alkylated with 5 % (w/v) iodoacetamide before the protein was digested overnight at 37 ^oC with protease Lys-C in 50 mM ammonium bicarbonate buffer, pH 8.0 (Shevchenko *et al.*, 1996). The

extracted peptides were analyzed by capillary liquid chromatography tandem mass spectrometry (LC-MSMS) using a Magic C18 100 µm x 10 cm HPLC column (Spectronex, Switzerland) connected online to a Finnigan DecaXP iontrap (ThermoFinnigan, CA). A linear gradient from 5% to 50% (v/v) of buffer *B* (0.1% Formic Acid, 80% Acetonitril in H_2O; diluted with 0.1% Formic Acid, 2% Acetonitril in H_2O) was delivered with a Rheos 2000 HPLC system (Flux, Switzerland) at 100 µl/min over 60 minutes. A precolumn flow splitter reduced the flow to approximately 300 nl/min and the peptides were manually loaded with a 10 µl Hamilton syringe on a peptide captrap (Michrom BioResources, Inc, CA) mounted in the injection loop of the Mass Spectrometer (MS). The eluting peptides were ionized by electrospray ionization, detected, and the individual ionized peptides were automatically selected and fragmented further in the iontrap. Subsequent MSMS spectra, containing sequence information for the corresponding single peptides, were analyzed *in silico* using the program TurboSequest versus a customized database containing the known sequence of MP (Goelet *et al.*, 1982). Peptide sequences that were not automatically attributable to MP were manually analyzed, taking into account variations in amino acid oxidation and/or acetylation. Peptide sequences not assigned by this method were considered to be non-lysine cleavage products, the result of alternative chemical modifications or of foreign origin.

2.2 In vitro RNA binding assays

2.2.1 RNA band-shift assay using a short ^{32}P-labeled probe

This method was established to verify the RNA binding activity of our MP preparations using a method comparable to those previously described for MP in the literature. A 123 nucleotide [$^{\gamma\text{-}32}$P]UTP-labeled RNA was produced by *in vitro*

transcription (MAXIscript T7 kit; Ambion Inc.) using a PCR-derived DNA template corresponding to the 5'-terminal region of the GFP gene containing a synthetic 5'-proximal T7 promoter sequence. Transcripts were purified by 6% denaturing PAGE (Stern and Gruissem, 1987) and resuspended in dH_2O (specific activity, 1.1 x 10^7 cpm/μg of RNA). The *in vitro* RNA-binding assay was performed by incubation of 10 nM (~ 4.4 ng) of RNA probe with increasing amounts of MP (pre-equilibrated with 10 mM Tris-Cl [pH 7.5]) for 30 min at 4 °C in a 10 μL reaction mixture containing 10 mM Tris-Cl, pH 7.5, and 0.1% (v/v) Triton X-100. Samples were then loaded onto 1% non-denaturing agarose gels (in 45 mM Tris-borate [pH 8.0] and 0.1% [vol/vol] Triton X-100) and electrophoresed for 2 hours at 6.5 V/cm. Gels were dried at 80 °C and exposed to X-ray film for 3 hours at -75°C.

2.2.2 Modified conditions suitable for TMV-derived RNA

A 6.7 kb TMV-derived RNA was produced by *in vitro* transcription (MEGAscript T7 kit, Ambion Inc.) using *Acc65I*-linearized plasmid pTf5-WT as a template. Following transcription, template DNA was digested with 2U of DNase I for 15 minutes at 37 ^oC and RNA was purified by extraction with a mixture of acid-buffered Phenol (pH 5.5), Chloroform and Isoamylalchohol (25:24:1 v/v) followed by gel filtration (Microspin™ G-25 column, Amersham Biosciences) into RNase-free H_2O. RNA was quantified by measuring the absorbance at 260 nm and binding assays were performed by incubating 10 nM (625 ng) of RNA with increasing amounts of MP for 15 minutes at 4 ^oC in a reaction mixture (20 μL) containing 10 mM Tris-Cl (pH 7.5) and 1 mM DTT. In control reactions, BSA (in 10 mM Tris-Cl, pH 7.5) was substituted for MP. Samples were loaded onto a 1% non-denaturing agarose gel (in 40 mM Tris-acetate and 1 mM EDTA) containing 0.1 μg/mL ethidium bromide and were electrophoresed at 12.5

V/cm for 45 minutes. Gels were recorded using an EagleEye II UV transluminator (Stratagene, Ca).

2.3 Infection of BY-2 protoplasts and Nicotiana benthamiana with mutant TMV-derivatives encoding –$(H)_6$ affinity tags

It was reasonably suggested that the presence of a –$(H)_6$ affinity tag might be detrimental to MP function during viral infection. To address this question, TMV derivatives were produced that lacked the coat protein (CP) ORF and encoded either MP:GFP, MP:$(H)_6$:GFP or MP:GFP:$(H)_6$. Tobacco BY-2 protoplasts and *Nicotiana benthamiana* leaf epidermal cells were subsequently infected with *in vitro* transcribed infectious RNA derived from these viral constructs.

2.3.1 Construction of TMV derivatives

2.3.1.1 TMV-MP:$(H)_6$:GFP

Plasmid pTf5-NX2 (Boyko *et al.*, 2002) was digested with *BlnI* for 3 hours at 37 ^{o}C, and linearized DNA was purified (QIAquick PCR purification kit, Qiagen) and subsequently digested with *SalI* for 3 hours at 37 ^{o}C. To prevent self-ligation of the linearized plasmid DNA, the 5'-phosphate groups were removed with 10 units of calf intestinal alkaline phosphatase (CIAP) directly added to the restriction reaction for 15 minutes at 37 ^{o}C. The resulting 9.5 kb plasmid DNA was excised from a 1 % agarose gel, purified (QIAquick gel extraction kit, Qiagen) and quantified by measuring absorbance at 260 nm. To produce the DNA insert coding for -GS$(H)_6$, two complementary oligonucleotides (see Appendix II), were synthesized (Microsynth, Switzerland), desalted (Microspin™ G-25 column, Amersham Biosciences) and the oligonucleotides (6 μM) were individually phosphorylated with 10 units of T4

Polynucleotide Kinase (PNK) in the supplied reaction buffer for 30 minutes at 37 ^{o}C. The combined oligonucleotides were annealed by heating to 75 ^{o}C and slowly cooling to room temperature. The resulting dsDNA insert containing 5' *SalI* and 3' *BlnI* compatible cohesive ends, was ligated to the prepared plasmid DNA at a molar ratio of 10:1, respectively, using T4 DNA ligase. Cells of the *E.coli* strain DH5α were transformed with 10 µL of ligation mixture and constructs containing the desired insert were verified by DNA sequence analysis. Positive constructs were modified (red) within the hinge region between MP and GFP (blue) to encode the following protein sequence: **MP**-PVVDGS(H)$_6$LGPGIS(G)$_5$ILDLK-**GFP**.

2.3.1.2 TMV-MP:GFP:(H)$_6$

Using a similar approach, a dsDNA (see Appendix) coding for -R(H)$_6$ and containing cohesive ends compatible with *NotI*/*XhoI* digested Tf5-NX2 was prepared and ligated to vector as described. Positive constructs were identified by DNA sequence analysis and encoded: **MP**:**GFP**-(H)$_6$, with a single amino acid deletion from the C-terminus of GFP.

2.3.2 Preparation of BY-2 protoplasts and transfection with viral RNA derived from "His-tagged" TMV constructs

RNA transcripts corresponding to TMV (+) sense strands were produced by *in vitro* transcription (MEGAscript T7 kit, Ambion Inc.), using *Acc65I* digested plasmids pTf5-MP:GFP (NSPAX), pTf5-MP:(H)$_6$:GFP or pTf5-MP:GFP:(H)$_6$ as templates, in reactions containing CAP analogue (m^{7}G(5')ppp(5')G, Ambion Inc.). No further RNA purification was required prior to protoplast transfections. To produce BY-2 protoplasts, 50 mL of tobacco BY-2 suspension cell culture was centrifuged in a Sigma 3K10 swing-bucket centrifuge for 1 minute at 600 rpm (~ 65 x g) at 20 ^{o}C and cells

were resuspended in 40 mL 0.4 M D-mannitol and allowed to plasmolyse for 10 minutes at room temperature. Cells were sedimented for an additional minute as above and were resuspended in 15 mL of enzyme solution (1 % w/v cellulase Onozuka RS and 0.1 % w/v pectolyase Y23, in 0.4 M D-mannitol) and incubated in a petri dish for 3 hours at 28 ^{o}C with occasional agitation. Following digestion, cells were washed twice with 40 mL 0.4 M D-mannitol and aliquots containing approximately 2 x 10^{6} protoplasts (1-2 ml) were transferred into sterile 10 mL tubes and pelleted as above. Pellets were resuspended in 600 µL *electroporation buffer* (0.3 M D-mannitol, 70 mM KCl, 5 mM MES pH 5.8) and were mixed with viral RNA transcripts (~ 40 µg in 200 µL *electroporation buffer*) in a 0.4 cm gap electroporation cuvette (Bio-Rad Laboratories). Protoplasts were transfected by electroporation using the Bio-Rad gene pulser II, applying infinite resistance (∞) at a capacity of 125 µF, and a pulse of 0.3 kV for ideally 4.5-5.2 ms. The protoplasts were immediately transferred to 10 mL tubes and incubated on ice for 30 minutes, and subsequently, room temperature for 5 minutes. Then, 10 mL of protoplast culture medium (2.2 mg/mL MS salts, 1 µg/mL Thiamine-CL, 0.1 µg/mL myoinositol, 10 µg/mL sucrose, 0.2 µg/mL 2,4-dichlorophenol acetic acid [pH 5.8] and 400 mM D-mannitol) was added. Aliquots of protoplasts (1 mL) were cultured at 28 ^{o}C in the presence of 10 µg/mL actinomycin-D for 18 hours.

2.3.3 Infection of *Nicotiana benthamiana* with viral RNA transcripts derived from "His-tagged" TMV constructs

N. benthamiana plants were grown from seed under conditions of 70 % humidity and temperature of 22 ^{o}C during the 16 hour photoperiod and 20 ^{o}C during the dark period. Expanded leaves of 5 week old plants were mechanically inoculated (in the presence of

carborundum) with RNA transcripts prepared as described (Materials and Methods section 2.3.3) and plants were grown for a further 3 days according to the above growth regime.

2.3.4 Analysis of infection sites

Infected leaves were illuminated with a BLAK RAY B-100AP UV lamp (UVP Inc., Upland, Ca) and images were captured using a Canon EOS-D30 digital camera equipped with Canon EF 100 mm 1:2.8 macro lens. Images were imported into Adobe Photoshop 6.0.1 software (Adobe Systems Incorp.) before the total number of pixels and mean pixel intensity within each respective infection site were determined using the built-in histogram function. Values obtained from at least two infected leaves were averaged and pixel intensities corresponding to non-infected leaf tissue (30 readings per leaf) were used for background corrections. Equivalent metric units for area were calculated according to the known pixel:area ratio obtained from a calibration image.

2.3.5 Subcellular localization of MP

Following culturing at 28 ^{o}C for 18 hours, transfected protoplasts (0.5-1 mL) were chemically fixed with an equal volume of protoplast fixative (6 % [w/v] paraformaldehyde and 10 mM EGTA in PBS [pH 7.4]) for 30 minutes at room temperature. Cells were pelleted by centrifugation at 800 rpm in a Sigma 3K10 swing-bucket centrifuge for 4 minutes at room temperature and resuspended in 150 µL of the resulting supernatant. Samples were spun onto Poly-L-Lysine coated glass slides in a Shandon Cytospin 3 for 2 minutes at 2000 x g and dried overnight at 4 ^{o}C in the dark. For immunohistochemical labeling of tubulin, samples were washed with PBS (pH 7.4) containing 0.5 % (v/v) Tween-20 and 10 mM EGTA (PBST-E) for 10 minutes at room temperature, and the cells were then permeabilized with cold methanol (-20 ^{o}C) for 10

minutes followed by two washing steps with PBST, each for 10 minutes. Monoclonal anti-α-tubulin antibody (DM1A; EMD Biosciences Inc., Germany) was applied to samples (1:500 dilution) under humid conditions for 1.5 hours at room temperature. Slides were washed six times at room temperature with a large volume of PBS before tetra-rhodamine isothiocyanate TRITC-conjugated secondary anti-mouse IgG antibody (1:100; Pierce Biotechnology) was applied and the samples were incubated for 1 hour at room temperature in a darkened humid chamber. After samples were washed as above and briefly rinsed with dH_2O, glass coverslips were mounted onto a drop of Mowiol (Calbiochem) containing 2.5 % 1,4-diazobicyclo-[2.2.2.]-octane (DABCO) as an antifade agent. Detached *N. benthamiana* leaves containing fluorescent infection sites were directly placed on glass slides and viewed under oil using a 60 X objective lens. Fluorescence microscopy was carried out on a Nikon Eclipse E800 microscope equipped with Plan Apochromat objective lenses (Nikon). For specific visualization of GFP and TRITC fluorescence, DM505 (Nikon) and G-2A (Nikon) filter sets were used, respectively. Images were acquired and processed using an ORCA-100 progressive scan interline charge-coupled-device camera (Hamamatsu Photonics, Hamamatsu City, Japan) and Openlab 3.1 software (Improvision, Coventry, England).

2.4 In vitro Microtubule-associated protein (MAP) assay

2.4.1 Principle of the MAP assay

A relatively simple *in vitro* method to test whether a protein can interact with microtubules is cosedimentation (Ackmann *et al.*, 2000). This approach relies on the fact that purified tubulin dimers can be polymerized *in vitro* to form true microtubules with typically 12-15 protofilaments (Bohm *et al.*, 1984; Chretien *et al.*, 1992) and lengths varying between 2-40 μm (Farrell *et al.*, 1987). Due to the large size of these

structures (at least 400 MDa/μm), MTs and associated proteins can be sedimented by centrifugation, leaving soluble non-binding proteins and unpolymerized tubulin in the supernatant. The protein content of each fraction can then be quantified by SDS-PAGE and scanning gel densitometry. If one allows a steady-state in the binding reaction to be achieved and also assumes independent binding sites on the MT surface, this interaction can be viewed as classical receptor-ligand equilibrium binding (Klotz, 1946; Scatchard, 1949; Hulme and Birdsall, 1991). Therefore, when the concentration of polymerized tubulin (receptor) is kept constant and the binding protein (ligand) is titrated over 3 orders of magnitude, $[ligand]_{bound}$ can be plotted versus. $[ligand]_{free}$, yielding a saturation hyberbole according to the Langmuir equation (see Appendix III for derivation of this, and related equations). The binding stoichiometry (n) and dissociation constant (K_d) of the ligand can then be solved by non-linear regression analysis.

2.4.2 Determination of appropriate reaction conditions

Initial attempts to perform the MAP assay demonstrated that MP non-specifically aggregated in the standard published reaction buffer BRB80 (80 mM Pipes-OH [pH 6.8], 1 mM $MgCl_2$ and 1 mM EGTA) containing 1 mM GTP. To overcome this problem, the solubility of MP was systematically tested in the presence of each of the buffer constituents and combinations thereof. Since a fixed MT concentration is also a requisite for quantitative analysis of binding, conditions that support MT stability were tested in a similar manner.

2.4.2.1 MP solubility assay

Frozen aliquots of MP in dH_2O were rapidly thawed at 30 ^oC and immediately centrifuged at 20,800 x g for 20 minutes (4 ^oC) in an Eppendorf 5417C desktop

microcentrifuge and placed on ice. Respective buffer components (summarized in Table 2) were mixed in 1.5 mL eppendorf tubes at room temperature. Approximately 7 μg of MP was then added to the buffer mixtures (final volume 30 μL), briefly vortexed and incubated at room temperature for 1 hour. Mixtures were centrifuged for 30 minutes at 20,800 x g in a Sorvall 5404 microcentrifuge (room temperature) and the supernatants were transferred to fresh eppendorf tubes. Pellets were resuspended in 30 μL of 10 mM Tris-Cl (pH 6.8) and both fractions were analyzed by SDS-PAGE and CCB staining. When 95 % or more of the MP remained in the supernatant, the protein was considered soluble. In all cases where MP was insoluble, no MP could be detected in the supernatant fraction.

2.4.2.2 Microtubule stability assay

Tubulin heterodimers (5 mg/mL) purified from bovine brain (Cytoskeleton Inc.) were thawed on ice and polymerized in buffer BRB80 containing 1 mM GTP for 45 minutes at 37 ^{o}C in a 10 μL reaction. To suppress the microtubule dynamics, taxol (Paclitaxel, Sigma) dissolved in anhydrous DMSO was added to a final concentration of 50 μM in three steps with 10 minute incubations at 37 ^{o}C in-between additions. Microtubules were further stabilized by incubation at room temperature for at least 12 hours. To remove unpolymerized tubulin, 90 μL of BRB80 containing 25 μM Taxol was added and the microtubules were sedimented at 20,800 x g in an Eppendorf 5417C microcentrifuge at room temperature. Aspirated supernatants were discarded and microtubules were resuspended in 60 μL of the test buffer without GTP, by gentle pipetting, and were incubated for 30 minutes at room temperature. Polymerized and depolymerized tubulin was separated by centrifugation at 20,800 x g for 30 minutes at room temperature and supernatants were transferred to fresh tubes. Pellets were

resuspended in 60 μL of 10 mM Tris-Cl (pH 6.8) and both fractions were analyzed by SDS-PAGE and CCB staining.

2.4.3 MAP assay

Microtubules were polymerized as above with the following modifications. To ensure the removal of free GTP from the buffer, stabilized MTs were washed twice by sedimentation and resuspension in BRB80 containing 25 μM Taxol as described. Final pellets were resuspended in 25 μL of *MAP binding buffer* (12 mM Pipes-OH [pH 6.85], 0.5 mM $MgCl_2$, 10 % [v/v] Glycerol, 0.01 % [v/v] Tween-20 and 10 μM Taxol) and a 5 μL aliquot was removed, heat-denatured at 80 ^{o}C for 5 minutes and measured for protein concentration by the method of Bradford (Bradford, 1976). MP in dH_2O was rapidly thawed at 30 ^{o}C, incubated on ice for 30 minutes and cleared of non-specific aggregates by centrifugation at 100,000 x g for 15 minutes in a Beckman TLA-100 ultracentrifuge at 4°C. An aliquot of the MP was removed and measured for protein concentration. Binding reactions (25 μL) were performed by incubating 1-3 μM polymerized tubulin with up to 10 μM MP in *MAP binding buffer* for 10 minutes at room temperature. MTs and associated MP were pelleted by centrifugation at 20,800 x g for 10 minutes in an Eppendorf 5417C centrifuge at room temperature and supernatants were transferred to fresh tubes. Pellets were resuspended in 25 μL of 10 mM Tris-Cl (pH 6.8) and both fractions were analyzed by SDS-PAGE and CCB staining. To control for non-specific aggregation effects, aliquots of the MP stock (0.1-10 μM) were treated in the same manner without MTs, and analyzed by SDS-PAGE and CCB staining. Each binding reaction was performed at least three times, and for the lowest concentrations of MP (0.1-3 μM), reactions volumes were scaled-up to

better facilitate protein detection on CCB stained gels. For downstream quantification, 0.1-20 μM MP was analyzed directly by SDS-PAGE and CCB staining.

2.4.4 Control reactions to determine the effect of $-(H)_6$ on MT binding *in vitro*

MP and MTs were prepared as described for the MAP assay. Binding reactions (50 μL) were assembled in *MAP binding buffer* containing 1.5 μM of either; GST-$(H)_6$ (kindly donated by A. Furmanek, FMI, Basel), recombinant $(H)_6$-Tau 441 (Panvera), BSA (Pierce Biotechnology) or MP, respectively. Samples were incubated in the presence or absence of 6 μM polymerized tubulin at room temperature for 30 minutes and MTs together with associated proteins were sedimented by centrifugation at 20,800 x g in an Eppendorf 5417C centrifuge for 10 minutes at room temperature. Supernatants were discarded and the pellets were resuspended in 30 μL of 10 mM Tris-Cl (pH 6.8) and analyzed by SDS-PAGE and CCB staining. To visually compare the protein amounts, 1.5 μM of each respective protein was analyzed on the same SDS-PAGE gel without prior treatment.

2.4.5 Analysis of Microtubule binding by MP *in vitro*

CCB stained SDS-PAGE gels were digitized using a Typhoon 9400 variable mode imager (Amersham Biosciences) and images were imported into Scion Image beta 4.01 densitometry software (Scion corporation). A standard curve of known MP amounts was produced by measuring the average pixel intensity (arbitrary units) within a fixed area containing protein bands of MP (0.1-20 μM). The mean pixel intensity of at least 10 background readings was subtracted from these values which were subsequently plotted against the corresponding original MP concentration, yielding a straight line (r^2

= 0.995). MP amounts on sample gels were estimated by measuring the mean pixel intensity (minus gel background) and reading the μM equivalent from the standard curve. It should be noted that differences in gel staining resulted in variable values for [MP], therefore, to validate these data, the apparent $[MP]_{bound}$ and $[MP]_{free}$ concentrations were summed and plotted against the theoretical starting concentration. Only data sets producing a straight line relationship (termed 'internal standard') were considered for further analysis. From control gels, the amount of non-specifically pelleted MP was quantified using the above approach and final values for $[MP]_{bound}$ and $[MP]_{free}$ were adjusted accordingly (typically < 5% difference). Binding data where were produced by plotting values for $[MP]_{bound}$ versus $[MP]_{free}$ and fitting a curve to these data according to either a one-site (Appendix III eq. 11) or two-site (Appendix III eq. 12) equilibrium binding model, as detailed below:

One-site model:
$$\bar{v} = \frac{n[L]}{K_d + [L]}$$

Two-site model:
$$\bar{v} = \frac{n_1[L]}{K_{d1} + [L]} + \frac{n_2[L]}{K_{d2} + [L]}$$

Where $\bar{v}$ is the fraction of all MP binding sites on tubulin, n is the total number equivalent MP binding sites, [L] is the relative concentration of unbound MP and K_d is the binding dissociation constant of MP

Values for binding stoichiometry (n), dissociation constant (K_d) and relative strength of curve fitting (r^2) were calculated using the built-in non-linear regression analysis function. To discriminate between the most appropriate binding model, the fits of each respective curve were compared by one-way analysis of variance (ANOVA), assuming a null hypothesis that a one-site model is correct (Motulsky and Christopoulos, 2003).

For outputs of the regression analyses and ANOVA calculations, please refer to Appendix III. Scatchard-Rosenthal plots (Scatchard, 1949; Rosenthal, 1967) were produced by plotting $[MP]_{bound}/[MP]_{free}$ versus $[MP]_{bound}$ and fitting a 3 parameter rational term to the data ($y = a+b/1+cx$) using a best-fit trial and error approach.

2.5 Visualization of MP:MT complexes formed in vitro

Initial attempts to visualize MP:MT complexes formed *in vitro* by antibody labeling and fluorescence microscopy demonstrated that without fixation, such complexes were unstable over the course of the labeling procedure. Additionally, when the complexes were chemically fixed in free solution prior to labeling, extensive MT-bundling and artefactual MP-aggregation became readily apparent. Therefore, a perfusion chamber system was established which allowed MTs to be immobilized on glass slides by virtue of the molecular motor protein kinesin. Complexes formed in the perfusion chamber could then be manipulated in such a way as to preclude formation of the aforementioned artefacts while still facilitating immunohistochemical labeling and fluorescence microscopy.

2.5.1 Immobilization of MTs in kinesin coated perfusion chambers

Perfusion chambers were produced by placing two 50 mm strips of scotch tape lengthways along a plain glass slide with a gap of 6 mm between each strip. An 18 mm square glass coverslip was then attached to the tape strips using transparent nail varnish. The resulting chambers had a volume capacity of 8 ± 2 μL, and buffers could be perfused through the chamber by pipetting buffer into one side and simultaneously removing buffer from the other using Whatman paper as an absorbent wick. Rates of buffer exchange were typically in the range of 5-10 μL per second, however, pilot experiments using an aqueous dye (bromophenol blue) showed that buffer flow was not

laminar along the edges, and therefore, subsequent microscopic analyses were made at the centre of the chamber in order to attain experimental consistency. Human (recombinant) GST-conjugated kinesin-1 heavy chain (amino acids 1-379; Cytoskeleton Inc.) was applied to the chamber (1.7 μg/mL [12 nM]) in *kinesin binding buffer* (BRB80 containing 1 mM DTT, 10 μM Taxol and 0.25 mg/mL casein) and incubated at room temperature for 5 minutes. Unbound proteins were washed out with approximately 5 chamber volumes (50 μL) of *kinesin wash buffer* (BRB80 containing 1 mM DTT, 10 μM Taxol and 0.1% BSA) at room temperature. Prepared chambers could then be stored under humid, darkened conditions for at least a week (4 ^{o}C) without significant loss of MT binding activity. Tubulin was polymerized as described in Materials and Methods section 2.4.2.2 and diluted with *kinesin wash buffer* (~ 90 nM tubulin dimer) before 5 volumes were perfused through the chamber and incubated for 5 minutes at room temperature. Unabsorbed MTs were washed out with 7.5 volumes of *MAP binding buffer* (12 mM Pipes-OH [pH 6.85], 0.5 mM $MgCl_2$, 10 % [v/v] Glycerol, 0.01 % [v/v] Tween-20 and 10 μM Taxol). At this stage the chambers could be stored under darkened, humid conditions at room temperature for up to an hour.

2.5.2 Formation and visualization of MP:MT complexes

MP in dH_2O was rapidly thawed and diluted to 0.1-5 μM with *MAP binding buffer* (12 mM Pipes-OH [pH 6.85], 0.5 mM $MgCl_2$, 10 % [v/v] Glycerol, 0.01 % [v/v] Tween-20 and 10 μM Taxol) before being cleared of aggregated material for 15 minutes at 100,000 x g in a Beckman TLA 100.3 rotor at 4 ^{o}C. Five chamber volumes of MP solution (10 nM – 5 μM) were perfused into the chamber and incubated at room temperature for between 1 and 30 minutes. Unbound MP was removed with 10

volumes of *MAP binding buffer* before proteins were fixed for 10 minutes at room temperature with 1% (v/v) gluteraldehyde in *MAP binding buffer*. Intact chambers were immediately immersed in PBS containing 0.5 % (v/v) Tween-20 (PBS-T). The chambers were disassembled and the slides containing bound proteins were dried for 1 hour at room temperature. All subsequent steps were performed at room temperature. Free aldehydes were quenched twice for 10 minutes with a large volume of 0.1 % (w/v) $NaBH_4$ in PBS-T and samples were further washed for 10 minutes with PBS-T. For immunohistochemical labeling, either rat monoclonal anti-α-tubulin antibody (YOL-1/34; Camon Labor Service, Wiesbaden, Germany) was used in combination with a rabbit polyclonal antibody reactive against the N-terminus of MP (anti-MP-N; residues 6-22), or mouse monoclonal anti-α-tubulin antibody (DM1A; EMD Biosciences Inc., Darmstadt, Germany) was used in combination with anti-MP-C (MP residues 209-222), respectively. Primary antibodies were applied to samples (1:200 dilution in PBS-T) and incubated for 1.5 hours before the slides were washed three times with a large volume of PBS-T. FITC-conjugated secondary anti-rabbit IgG antibody (1:100; Pierce Biotechnology) and either TRITC-conjugated secondary anti-rat IgG antibody (1:100; Jackson Immuno Research laboratories) or TRITC-conjugated secondary anti-mouse IgG antibody (1:100; Pierce Biotechnology) were applied to the samples and incubated for 1 hour under darkened conditions. Samples were washed five times with a large volume of PBS-T before glass coverslips were mounted onto a drop of Mowiol (Calbiochem), containing 2.5 % 1,4-diazobicyclo-[2.2.2.]-octane (DABCO) as an antifade agent. Fluorescence microscopy was carried out as previously described (Materials and Methods section 2.3.4) and final images were prepared using Adobe Photoshop 6.0.1 software (Adobe Systems Incorp.)

2.6 Co-precipitation experiments in vitro using immobilized MP as an affinity bait

In an attempt to determine whether MP interacts specifically with binding contacts present on the surface of *polymerized* tubulin or can interact with unpolymerized tubulin dimers, a system was established whereby MP was immobilized on Ni^{2+}-NTA-conjugated sepharose beads and used as an affinity bait to co-precipitate free tubulin α/β heterodimers or polymerized tubulin *in vitro*. The effect of RNA on MP:tubulin binding was also investigated using a similar approach.

2.6.1 Co-precipitation of MTs and tubulin heterodimers *in vitro*

In order to reduce the likelihood of buffer induced MP-aggregation, 10 µL of bovine brain tubulin dimers (10 mg/mL; Cytoskeleton Inc.) and bovine serum albumin (BSA; 2 mg/mL; Pierce Biotechnology) were dialysed overnight at 4 ^{o}C against 400 mL of *pulldown buffer* (40 mM Pipes-OH [pH 6.85], 0.5 mM $MgCl_2$, 10 % [v/v] Glycerol, 0.01 % [v/v] Tween-20 and 5 mM Imidazole). Microtubules were polymerized *in vitro* and exchanged into *pulldown buffer* containing 10 µM Taxol as described (Materials and Methods section 2.4.2.2) To ensure that MP bound the Ni^{2+}-NTA affinity matrix by virtue of the $-(H)_6$ tag, 100 µL of MP (0.5 mg/mL in dH_2O) was denatured with 1.4 mL of *solubilization buffer* (SB) without imidazole (100 mM NaH_2PO_4, [pH 7.5], 1 M NaCl, 10 mM Tris base, 8 M Urea and 10 % (v/v) Glycerol) and was incubated overnight at 4 ^{o}C. Ni^{2+}-NTA beads (30 µL of 50 % slurry; Qiagen) were equilibrated with 500 µL of SB, sedimented briefly at 20,800 x g (room temperature) using an Eppendorf 5417C desktop microcentrifuge and resuspended in 200 µL (~ 5 µg) of denatured MP solution. MP was allowed to bind the beads for 30 minutes at room temperature with gentle shaking before unbound protein was removed by sedimenting

the beads and aspirating the resulting supernatants. MP was refolded on the beads by resuspending the pellets in 500 μL of *pulldown buffer* and incubating for at least 1 hour at 4 ^{o}C, with gentle shaking. Beads were again pelleted and the supernatants discarded before binding reactions were set-up in the following way. To block non-specific binding sites, the beads were resuspended in 40 μL of BSA solution (8 μg in *pulldown buffer*) and incubated for 10 minutes at 4 ^{o}C. Tubulin (5 μg tubulin dimers or MTs in *pulldown buffer* containing 50 μM Taxol) was added to a final volume of 50 μL and incubated at 4 ^{o}C for 15 minutes before the beads were pelleted by centrifugation at 20,800 x g for 1 minute in an Eppendorf 5417C desktop microcentrifuge at room temperature. Supernatants containing unbound material were carefully transferred to fresh 1.5 mL eppendorf tubes and the pellets containing bound proteins were washed five times by repeatedly pelleting/resuspending the beads in fresh *pulldown buffer* containing 10 μM Taxol (750 μL), with 10 minute incubations at 4 ^{o}C between each centrifugation. Bound proteins were eluted by incubating the beads for 30 minutes at 4 ^{o}C in 50 μL of SB containing 500 mM Imidazole before fractions containing bound and unbound proteins (10 μL) were separated by 12 % SDS-PAGE and transferred to polyvinylidene diflouride membrane (Bio-Rad Laboratories). Membranes were probed with either anti-MP-C (reactive against MP residues 209-222) or anti-α-tubulin (DM1A) followed by peroxidase-conjugated secondary antibody (Pierce Biotechnology), and the presence of either protein was indirectly detected with Supersignal™ West Dura substrate (Pierce Biotechnology) by exposure to X-ray film. To control for non-specific binding of tubulin to the sepharose beads, the above procedure was also performed using beads that were not conjugated to MP.

2.6.2 Co-precipitation of RNA and tubulin heterodimers *in vitro*

A 6.7 kb TMV-derived RNA was produced by *in vitro* transcription (MEGAscript T7 kit, Ambion Inc.) using *Acc65I*-linearized plasmid pTf5-MP:GFP:$(H)_6$ as a template. Following transcription, template DNA was digested with 2U of DNase I for 15 minutes at 37 ^{o}C and RNA was purified by extraction with a mixture of acid-buffered Phenol (pH 5.5), Chloroform and Isoamylalchohol (25:24:1 v/v) followed by gel filtration (Microspin™ G-25 column, Amersham Biosciences) into RNase-free H_2O. RNA was quantified by measuring the absorbance at 260 nm and verified by 1 % non-denaturing agarose gel electrophoresis. All other reaction components were prepared as described in the preceding section. Following the conjugation and refolding of MP on Ni^{2+}-NTA beads (5 μg MP or 3.25 μM final concentration), non-specific binding sites were blocked by incubating the beads for 10 minutes at 4 ^{o}C in 30 μL of *pulldown buffer* containing 10 μg of BSA. As summarized in Table 1, binding reactions (50 μL final volume) were then set-up using a two-step approach whereby equal volumes of either tubulin heterodimers (1.63 μM final concentration) or RNA (5 μg or 0.05 μM final concentration) were first added to the beads and incubated for 15 minutes at 4 ^{o}C. Following this, equal volumes of either tubulin, RNA or *pulldown buffer* were then added and incubated for a further 15 minutes at 4 ^{o}C. MP was omitted in reactions 5 and 6 in order to control for non-specific binding of either tubulin or RNA to the sepharose beads. The beads were subsequently pelleted by centrifugation at 20,800 x g for 1 minute in an Eppendorf 5417C desktop microcentrifuge at 4 ^{o}C and the supernatants were collected. Pelleted beads were washed five times by repeatedly pelleting/resuspending the beads in ice-cold *pulldown buffer* containing 10 μM Taxol (400 μL), with 10 minute incubations on ice between each centrifugation. Bound components were eluted for 30 minutes at 4 ^{o}C with 70 μL of *solubilization buffer*

containing 500 mM Imidazole and 10 μL aliquots of each pellet fraction were analyzed by SDS-PAGE and Western blotting using antibodies specific against MP and α-tubulin, respectively. RNA within the remaining eluents was repurified by gel filtration (Microspin™ G-25 column, Amersham Biosciences) into RNase-free H_2O and analyzed by 1 % non-denaturing agarose gel electrophoresis and UV-translumination.

Reaction	1	2	3	4	5*	6*
First incubation						
Tubulin	10 µL	10 µL	X	X	10 µL	10 µL
RNA	X	X	10 µL	10 µL	X	X
Second incubation						
Tubulin	X	X	10 µL	X	X	X
RNA	X	10 µL	X	X	X	10 µL
pulldown buffer	10 µL	X	X	10 µL	10 µL	X

(*) MP was omitted from these reactions.

Table 1 Co-precipitation of RNA and tubulin heterodimers *in vitro* using immobilized MP as an affinity bait: summary of binding reactions performed

2.7 In vitro kinesin motility assays

Perfusion chambers were fabricated as described in Materials and Methods section 2.5.1 and were coated for 3 minutes at room temperature with 10 μL of casein (0.25 mg/mL) and human GST-conjugated kinesin-1 heavy chain (50 μg/mL; Cytoskeleton Inc.) in *motility buffer* (50 mM Pipes-OH [pH 6.85], 1 mM EGTA, 2 mM $MgCl_2$, 2 mM ATP, 10 μM Taxol, 10 % [v/v] Glycerol and 150 mM KCl). In order to reduce oxidative damage to proteins, unbound material was removed with 50 μL of *motility buffer* containing an oxygen scavenger system (*motility buffer*$^{+OS}$) consisting of 18 μg/mL catalase, 0.1 mg/mL glucose oxidase, 2.25 mg/mL D-glucose and 10 mM DTT. An equal mixture of TRITC-labeled and unlabeled bovine brain tubulin (Cytoskeleton Inc.) was polymerized as described in Materials and Methods section 2.4.2.2 and 50 μL of polymer solution (12.5 μg/mL or 110 nM polymerized dimers in *motility buffer*$^{+OS}$) was perfused through the chamber and incubated for 2 minutes at room temperature. Unbound MTs were removed with 50 μL of *motility buffer*$^{+OS}$ followed by 100 μL of *minimal buffer* (50 mM Pipes-OH [pH 6.85], 2 mM $MgCl_2$ and 10 μM Taxol) before various concentrations of MP (pre-equilibrated in *minimal buffer*) were perfused through the chamber (50 μL) and incubated for 30 seconds at room temperature. Perfusion chambers were washed with a further 50 μL of *minimal buffer*, placed on the stage of a Nikon Eclipse E800 microscope and fluorescent microtubules on the upper surface of the chamber were visualized using a G-2A (Nikon) filter set. To initiate kinesin motor activity, 100 μL of *motility buffer*$^{+OS}$ (without KCl) was perfused through the chamber and images of microtubules were recorded every 1.25 seconds using an ORCA-100 progressive scan interline charge-coupled-device (CCD) camera (Hamamatsu Photonics, Japan) and Openlab 3.1 software (Improvision, England). For

each experimental condition, the mean velocity of at least 30 MTs were manually calculated by comparing the relative position of each respective MT end at known time intervals for 2-3 minutes. The statistical difference between mean microtubule velocities following the various treatments were determined using a two-tailed unpaired *t*-test, and the percentage of MTs undergoing any discernible translocation was also calculated for each respective MP concentration.

3 Results

3.1 Purification of MP from E.coli

The MP gene was PCR amplified from a plasmid vector harbouring a cDNA of the TMV genome and was subcloned into *E.coli* expression vector pQE60. Upon expression in *E.coli*, the resulting movement proteins contained a C-terminal -GS$(H)_6$ affinity tag and was purified by isolation of MP-containing inclusion bodies and Ni^{2+}-NTA Immobilized Metal Affinity Chromatography (IMAC). Following IMAC, aliquots of the Flow-through, Wash and Elution fractions were analyzed by SDS-PAGE and CCB-staining (Fig. 1). As apparent from the Flow-through fraction, MP isolated from inclusion bodies was only partially purified (< 80 % by visual estimation) and contained a significant amount of protein that did not interact with the column matrix (Fig. 1, lane 1). Notably however, not all of the 30 kDa MP was able to bind the matrix, indicating that either the affinity tag was absent from these particular moieties, or that the binding capacity of the Ni^{2+}-NTA resin had been exceeded. Wash fraction I (Fig. 1, lane 2) contained a relatively low amount of MP (taking a 2 X dilution factor into account) and also detectable levels of contaminating protein. The contaminating material appeared to diminish in Wash fractions II-IV (Fig. 1, lanes 3-5), although low amounts of apparently non-specifically bound MP continued to be present. Initially it was presumed that effective MP elution could be achieved by using a step-wise Imidazole concentration gradient. This however, proved to be incorrect when a four-step elution (100–500 mM Imidazole) was performed, since the concentration range within which residual contaminants were removed broadly overlapped with the elution profile of MP (not shown). The result was unacceptable losses of MP in early contaminated eluents and was concomitant with a high dilution (< 0.1 mg/mL) of

apparently pure MP in subsequent elution fractions. Further compounding this fact, a range of methods intended to concentrate MP (including; Centricon™ protein concentration [Millipore], microspin-gel filtration [Amersham Biosciences] and hypertonic-dialysis), proved largely ineffective. A number of washing regimes were performed in an attempt to overcome this problem, and a compromise was reached using a single, high concentration of Imidazole (500 mM) and collecting lower fraction volumes (Materials and Methods section 2.1.5). High amounts of MP (~ 1 mg/mL) were indeed observable in the most immediate Elution fractions (EI-IV; Fig. 1, lanes 6-9), but also contained contaminating proteins. However, in Elution fractions V-VIII (Fig. 1, lanes 10-13), highly purified MP could be obtained in quantities still sufficient for the intended downstream applications. It was speculated that as the Imidazole concentration initially increased within the matrix, proteins making nominal binding contacts with Ni^{2+} were preferentially eluted early (i.e. *E.coli* proteins with accessible histidines or MP interacting via < 6 histidines), whereas MP interacting by virtue of the entire His-tag eluted when the Imidazole concentration reached the necessary threshold.

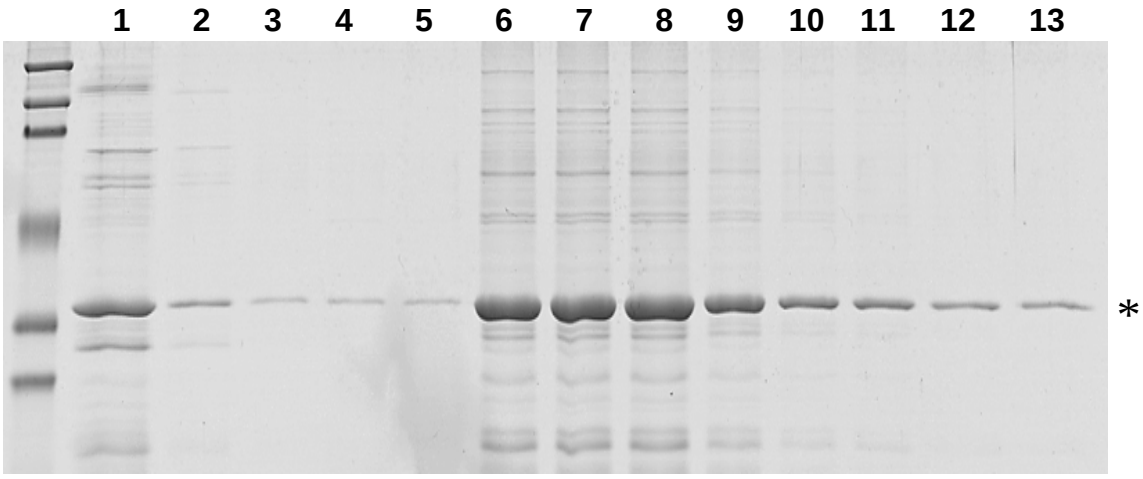

Figure 1 Purification of MP from *E.coli* by Ni^{2+}-NTA affinity chromatography. MP was expressed in *E.coli* and inclusion body proteins were solubilized with *solubilization buffer* containing 5 mM Imidazole (*SB5*). Following IMAC (Materials and Methods section 2.1.5) 10 µL aliquots of each resulting fraction were analyzed by SDS-PAGE and CCB-staining. Both contaminating *E.coli* proteins and MP can be seen in the Flow-through fraction (lane **1**) and after further washing with *SB5* (lanes **2** and **3**) and *SB20* (lanes **4** and **5**), only non-specifically bound MP is detectable. Elution with *SB500* led to fractions containing both MP and *E.coli* proteins (lanes **6**-**9**), however, purified MP began to elute in subsequent fractions (lanes **10**-**13**). MP (30 kDa) is indicated by the star (*).

3.1.1 Determination of MP purity

Following renaturation (Materials and Methods section 2.1.6), 10 μg of MP was analyzed by SDS-PAGE and CCB-staining. As was typical for most preparations, the purity of 30 kDa MP was estimated to be above 95 % (Fig. 2b). Western blots probed with a polyclonal antibody reactive against the C-terminus of MP confirmed that the 30 kDa protein was indeed MP (not shown). According to the SwissProt protein database, the *E.coli*. genome encodes nearly 200 proteins with molecular weights ranging between 29 and 31 kDa. To determine whether any contaminating proteins within this range were being masked by the presence of 30 kDa MP on SDS-PAGE gels, the protein content of this band was analyzed by in-gel Lys-C digestion and LC-MSMS (Materials and Methods section 2.1.7.). Using this highly sensitive method (fmol detection) it was possible to assign 19 different peptides to MP, confirming 78.7% of the total amino acid sequence (Fig. 2a and c). Oxidized and acetylated amino acids within the peptides were taken into account and although the entire sequence of MP was not covered, the number, and relative abundance of non-assignable peptides was sufficiently low that the 30 kDa band could be considered pure MP.

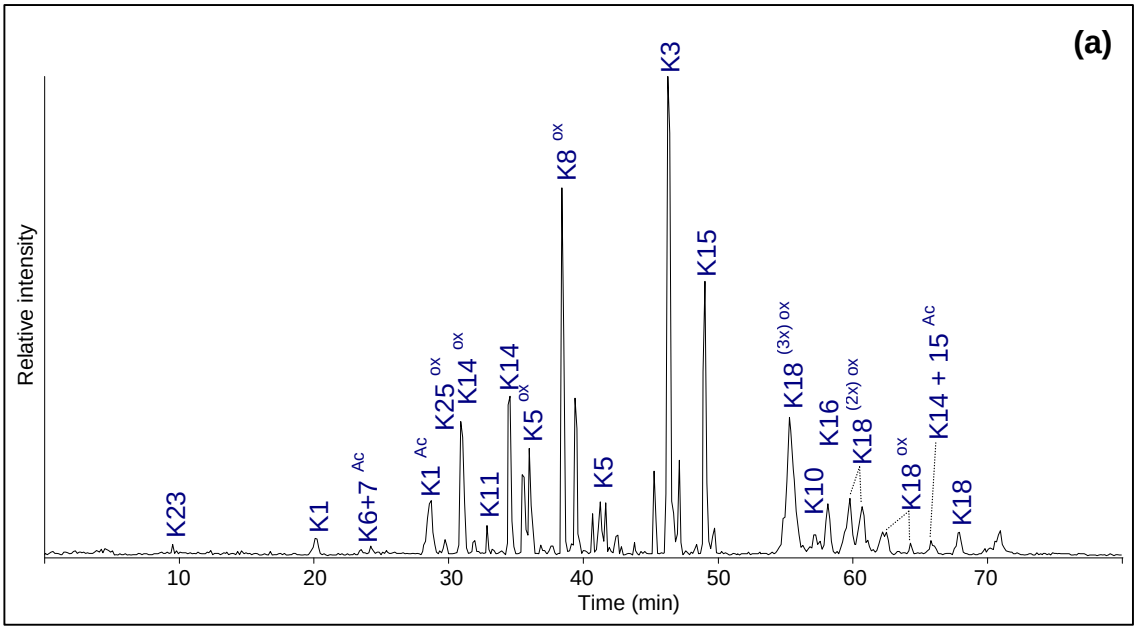

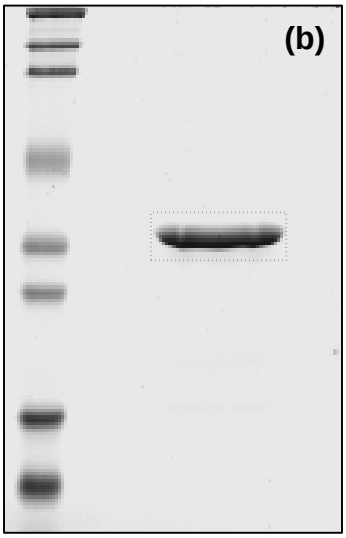

Peptide	Sequence
K1	ALVVK
K1^{Ac}	^{Ac}ALVVK
K3	VNINEFIDLTK
K5^{ox}	ILPSM^{Ox}FTPVK
K5	ILPSMFTPVK
K6+7^{Ac}	SVMCSK^{Ac}VDK
K8	IMVHENESLSEVNLLK
K10	LIDSGYVCLAGLVVTGEWNLPDNCRGGVSVCLVDK
K11	RMERADEATLGSYYTAAAK
K14^{Ox}	VVPNYAITTQDAM^{Ox}K
K14	VVPNYAITTQDAMK
K15	NVWQVLVNIRNVK
K14 +15^{Ac}	VVPNYAITTQDAMK^{Ac}NVWQVLVNIRNVK
K16	MSAGFCPLSLEFVSVCIVYRNNIK
K18 $^{(3x) Ox}$	ITNVRDGGPM^{Ox}ELTEEVVDEFM^{Ox}EDVPM^{Ox}SIRLAK
K18	ITNVRDGGPMELTEEVVDEFMEDVPMSIRLAK
K23	NSSNDRSVPNK
K25	DFGGMSFK

Fig 2 Determination of MP purity. (**a**) Base peak LCMS chromatogram of Lys-C digested MP (10 µg). The peaks represent the most intense ionized peptides eluting from the HPLC matrix prior to MSMS sequence determination. Oxidized or acetylated amino acids are indicated as K_n^{ox} and K_n^{Ac}, respectively. (**b**) CCB-stained SDS-PAGE gel containing 10 µg of MP following renaturation. The box indicates the area of gel excised for Lys-C in-gel digestion. (**c**) Peptide sequences attributable to MP, as determined by LC-MSMS analysis.

3.2 In vitro RNA binding by MP

Although it is has been documented that tobamovirus MPs bind RNA sequence non-specifically *in vitro* (Citovsky *et al.*, 1990), it was imperative that we determined whether our renatured MP had retained such an activity. One of our principle aims was to investigate the potential influence that RNA may exert on interactions between MP and MTs *in vitro*, and furthermore, by comparing the RNA binding activities of MP mutants *in vitro* to the infection phenotypes of corresponding mutant viruses, inferences might be made as to the mechanism of TMV dysfunction *in planta* (Boyko *et al.*, 2002).

3.2.1 RNA binding behaviour of MP *in vitro*

As demonstrated by the standard RNA band-shift assay (Fig. 3a), MP purified from *E.coli* still had the capacity to interact with RNA *in vitro*. At stoichiometries between 1-2 MP per RNA, MP formed a migratory complex with RNA, which remained apparent until high concentrations of MP were applied (> 5 MP per RNA). Above this protein:RNA ratio, there appeared to be a transition from the migratory complex to a non-migratory form which was retained in the well. Although inconclusive, it is unlikely that this retarded complex was solely the result of buffer-induced MP aggregation, since MP treated under almost identical conditions (minus RNA) and subjected to ultracentrifugation at 100,000 x g, remained soluble in the supernatant (not shown). As shown in Fig, 3b, reaction conditions were modified to accommodate TMV genomic RNA and the band-shift assay was repeated. Even at apparently high MP:RNA stoichiometries (≤ 50 MP per RNA), no discernible shift in RNA migration was observed, however, when a greater amount of MP was used, a total retention of RNA in the well again became apparent. Interestingly, when the stoichiometries were

expressed in terms of MP per nucleotide (nt), it was found that this retardation had occurred at between 1 MP per 68–136 nt which was comparable with the stoichiometry sufficient to cause a migratory band-shift using the smaller probe (1 MP per 75-150 nucleotides). The fact that the genomic RNA was retained in the well may simply reflect the sheer theoretical size of the protein-RNA complex (> 5 MDa). It remains unclear whether the MP-RNA complexes formed by each respective method are equivalent, although to a certain extent, these results support the commonly held notion that MP binds RNA in a cooperative manner (Citovsky *et al.*, 1992; Boyko *et al.*, 2002).

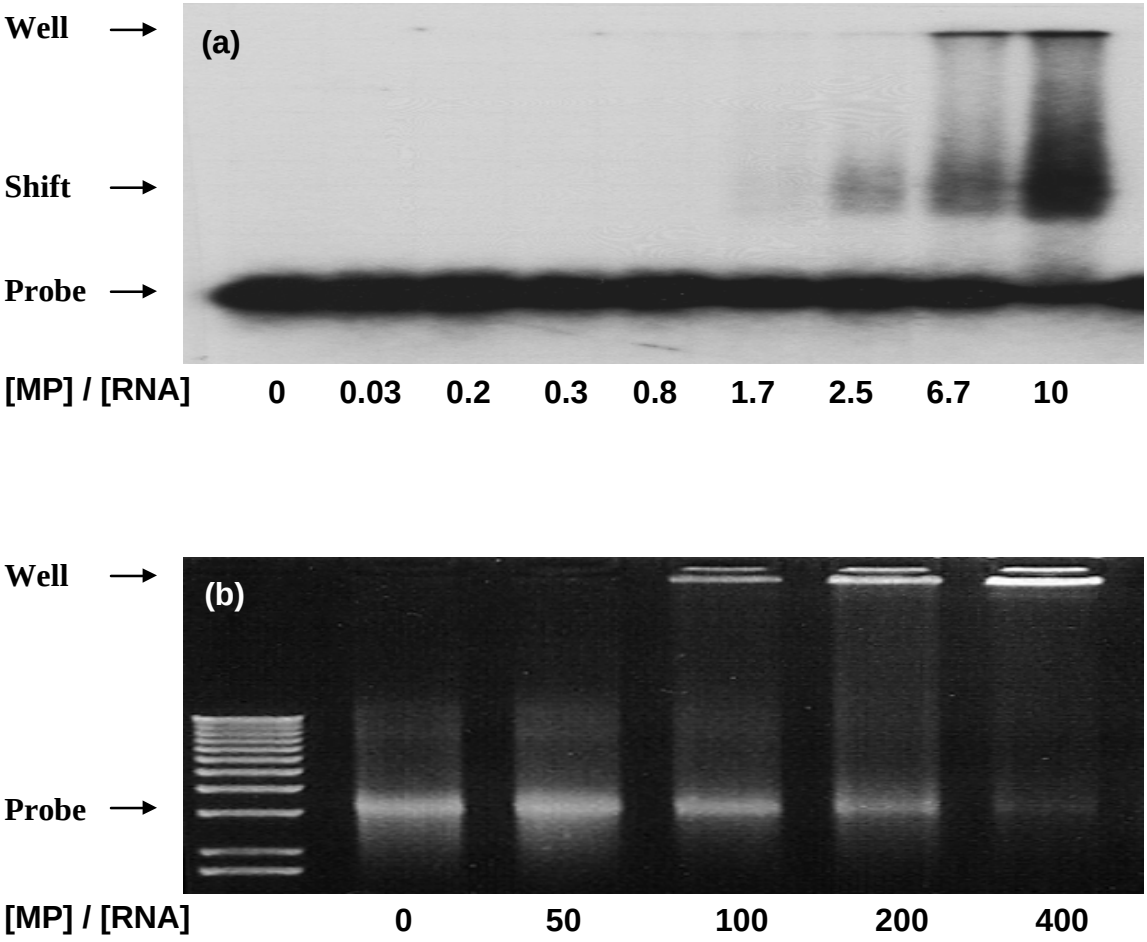

Figure 3 RNA binding activity of MP *in vitro*

Increasing amounts of purified MP were incubated with 10 nM of a short (123 nt) ^{32}P-labeled RNA (**a**) or a 6.7 kb TMV-derived RNA (**b**) and resulting complexes were separated by non-denaturing agarose gel electrophoresis and visualized as described in Materials and Methods section 2.2. At a ratio of between 1-2 MP per RNA (corresponding to 1 MP per 75-150 nt), a clear migratory shift of the short RNA is observed (**a**). This migratory complex increases in intensity at higher MP concentrations, concomitant with the appearance of more extensively retarded RNA-protein complexes. Similarly, the TMV-derived RNA (**b**) was shifted at a molar ratio of between 50-100 MP per RNA (1 MP per 68-136 nt), although the resulting complexes were of all of a non-migratory nature. In control reactions, TMV-derived RNA was not shifted by BSA at a protein:RNA ratio of 400:1.

3.3 Infection of Nicotiana benthamiana and BY-2 protoplasts with TMV encoding MP fused to –$(H)_6$ affinity tags

In order to investigate whether TMV harbouring an MP-$(H)_6$ fusion protein remained infectious or indeed, whether the presence of polyhistidine *per se* interfered with the known subcellular localization of MP:GFP, we transfected BY-2 protoplasts with TMV-derived RNA encoding MP:GFP, MP:$(H)_6$:GFP or MP:GFP:$(H)_6$. Although the correct localization of MP in BY-2 protoplasts is indicative of MP-mediated cell-to-cell movement function *in planta* (Heinlein *et al.*, 1998), this activity was directly determined by inoculating intact leaves of *N. benthamiana* plants with the above RNA transcripts and visualizing infection sites by fluorescence microscopy.

3.3.1 Infection of BY-2 protoplasts

At 18 hours post transfection (hpt), TMV-MP:GFP had clearly replicated and GFP fluorescence could be localized to MTs (Fig. 4a-c), an observation consistent with the cell-to-cell movement function of MP *in planta*. Similarly, both TMV-MP:$(H)_6$:GFP and TMV-MP:GFP:$(H)_6$ were able to produce an infection phenotype comparable to TMV-MP:GFP at 18 hpt and localization of –$(H)_6$ tagged MP:GFP with microtubules could be observed in both cases (Fig. 4f and i). Although not directly demonstrative of MP cell-to-cell movement function, these data do illustrate that six consecutive histidine residues do not interfere with MP localization. Expression of free GFP from a MP and CP attenuated TMV construct results in the diffuse, cytoplasmic localization of GFP fluorescence (Heinlein *et al.*, 1995). For reasons not fully understood, the degree of MP:GFP fluorescence found in association with MTs appeared to vary, with some MTs apparently more heavily decorated with MP:GFP than others. Although the relative amount of MP:GFP in association with MTs was comparable for the viruses

tested (not shown), on microtubules displaying heavy MP:GFP association, there was a corresponding weak immunohistochemical labeling of tubulin. Although inconclusive, this observation indicated that along stretches of MTs where tubulin was poorly labeled, MP was in the proximity of the MT surface in large amounts, or that at least some of the MP was occupying the antigenic site via a direct interaction, resulting in steric hindrance of the antibody-tubulin interaction.

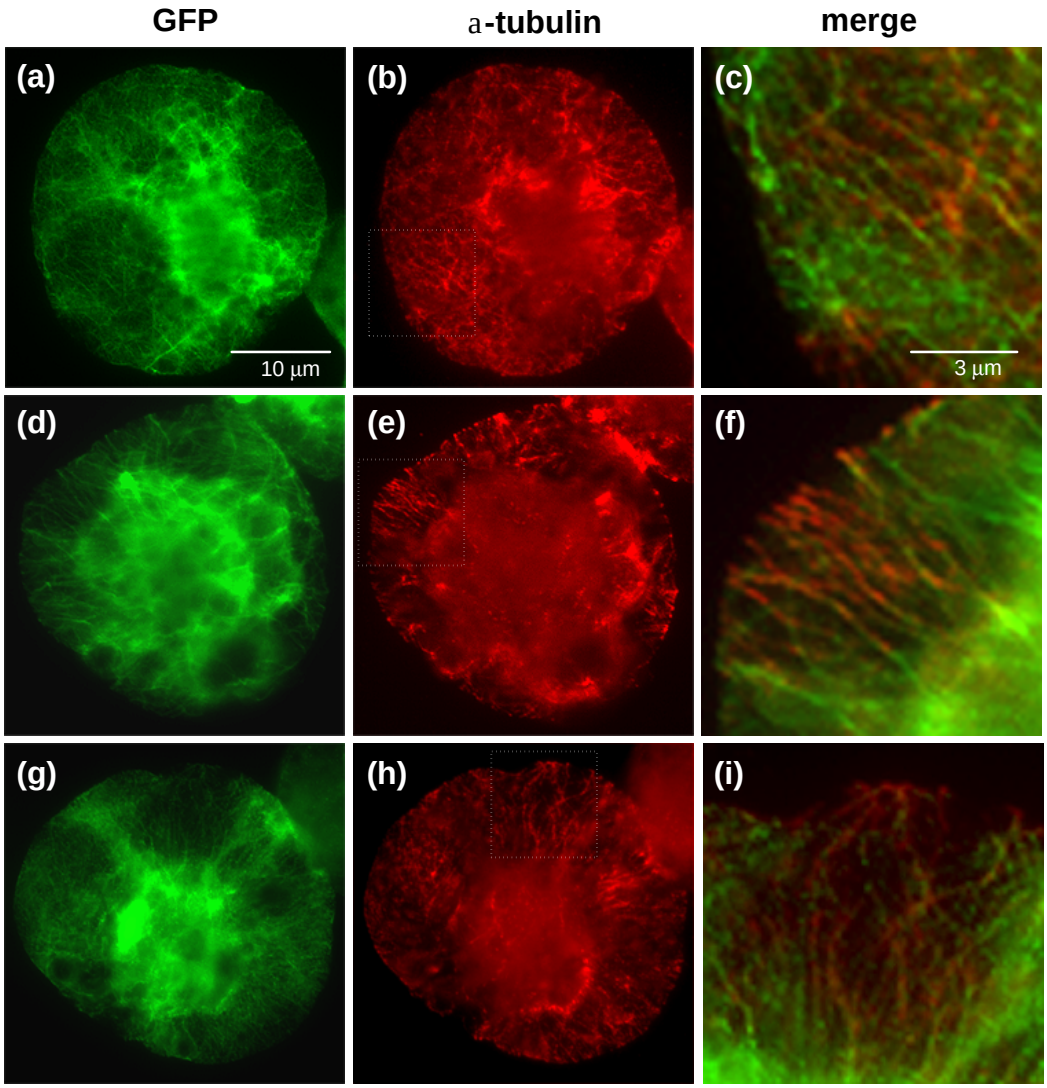

Figure 4 Infection of BY-2 protoplasts with TMV-derivatives encoding –$(H)_6$ affinity tags. Tobacco BY-2 protoplasts were transfected with RNA derived from TMV-MP:GFP (**a**, **b** and **c**), TMV-MP:$(H)_6$:GFP (**d**, **e** and **f**) and TMV-MP:GFP:$(H)_6$ (**g**, **h** and **i**), respectively. At 18 hpt, cells were chemically fixed and immuno-labeled with anti-α-tubulin antibody. As determined by the onset of GFP fluorescence, all three viruses were considered infectious in protoplasts, and the respective MP:GFP chimaeras could be clearly associated with filamentous structures (**a**, **d** and **g**). Antibody labelling of α-tubulin (**b**, **e** and **h**) and analysis of the merged composite images (**c**, **f** and **i**) confirmed that MP:GFP was localized to microtubules in all three cases, an observation consistent with the cell-to-cell movement function of MP.

3.3.2 Infection of *N. benthamiana*

As a test for viral infectivity and MP-mediated intercellular trafficking of vRNA, infectious RNA *in vitro* transcribed from pTf5-MP:GFP (NSPAX), pTf5-MP:$(H)_6$:GFP and pTf5-MP:GFP:$(H)_6$ (Materials and Methods section 2.3.1) were used to inoculate leaves of *N.benthamiana* plants. At 3 days post inoculation (dpi), infected leaves were detached, illuminated with UV light and photographed using a digital camera (Fig. 5a, c and e). In all three cases, fluorescent infection sites were clearly visible, indicating that each respective TMV-derived virus retained both the capacity to replicate, and also to move cell-to-cell. In the case of TMV-MP:$(H)_6$:GFP, the resulting infection sites were brighter than those caused by either TMV-MP:GFP or TMV-MP:GFP:$(H)_6$ (Fig. 5b), however, this increase in fluorescence did not correlate with an increase in the average infection site area (Fig. 5a) In contrast, both the average size and relative brightness of infection sites caused by TMV-MP:GFP:$(H)_6$ were lower than those of TMV-MP:GFP or TMV-MP:$(H)_6$:GFP (Fig. 5a and b). In order to determine whether –$(H)_6$ interferes with the known subcellular localization of MP:GFP *in planta*, infection sites produced by each respective TMV-derivative were compared by fluorescence microscopy (Fig. 6b, d and f). The subcellular distribution of TMV-MP:GFP in cells throughout the infection site were found to be consistent with previous reports of a coat protein attenuated TMV-derivative virus expressing an MP:GFP fusion protein (Heinlein *et al.*, 1998). Briefly, in cells adjacent to the leading (outer) edge of infection, MP:GFP was localized to cell wall sites. As one observed cells progressively closer to the centre of infection, MP:GFP could be first seen to associate with cytoplasmic inclusion bodies, then both smaller inclusion bodies and filamentous structures, filamentous structures only, and in cells closest to the centre, again cell wall proximal sites. This characteristic range of MP:GFP subcellular distributions throughout the

infection site was also observed for MP:GFP expressed from TMV-MP:$(H)_6$:GFP and TMV-MP:GFP:$(H)_6$, respectively. It should be noted that in almost all cells infected with TMV-MP:$(H)_6$:GFP, significantly higher amounts of MP:GFP could be detected in sites adjacent to the cell wall. Although this may account for the overall brightness of the resulting infection sites, the presence of –$(H)_6$ appeared to have little apparent effect on the ability of MP:$(H)_6$:GFP or MP:GFP:$(H)_6$ to associate with MTs (Fig. 6b, d and f). This result also highlights that the reduced rate of TMV-MP:GFP:$(H)_6$ spread was probably not due to aberrant localization of MP:GFP:$(H)_6$. Although it is apparent that MP:GFP:$(H)_6$ accumulated to lower levels than the other MP:GFP fusion proteins, the precise mechanisms governing the level of MP and rate of vRNA movement remain unclear.

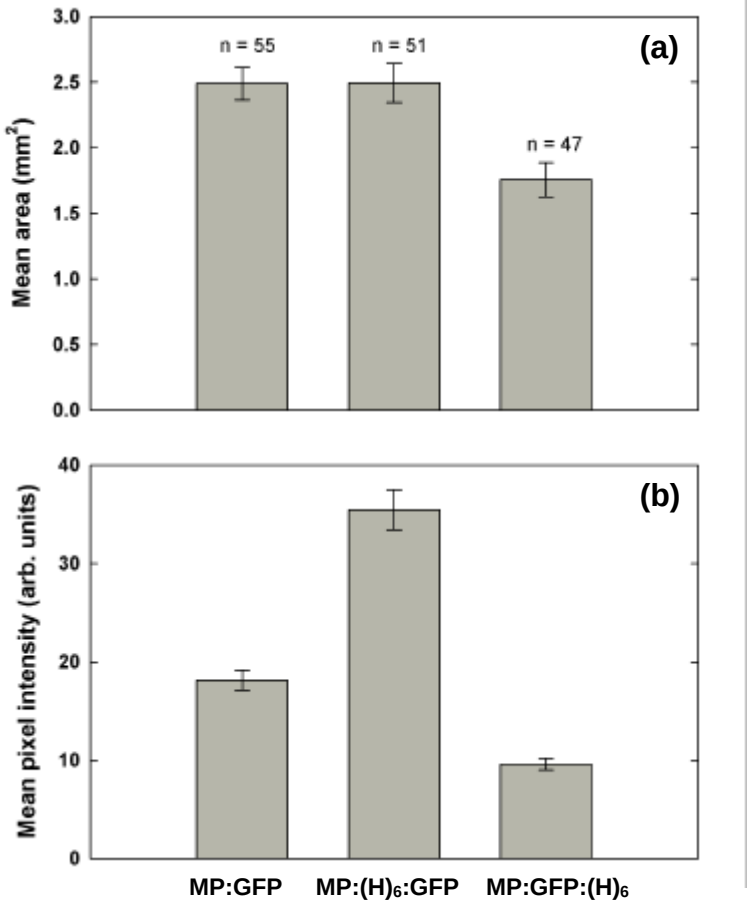

Figure 5 Analysis of infection sites on *Nicotiana benthamiana* leaves caused by TMV-derivatives encoding –$(H)_6$ affinity tags. Leaves infected with TMV-MP:GFP, TMV-MP:$(H)_6$:GFP or TMV-MP:GFP:$(H)_6$ were detached 3 days post infection and recorded under UV illumination by digital photography. The area and average pixel intensity within resulting infection sites were determined densitometrically, and as shown in (**a**), infection sites caused by both TMV-MP:GFP and TMV-MP:$(H)_6$:GFP were comparable in size (2.48 ± 0.13 and 2.49 ± 0.15 mm^2, respectively). In contrast, infection with TMV-MP:GFP:$(H)_6$ led to an average infection site area of 1.76 ± 0.13 mm^2, indicating a reduced rate of vRNA cell-to-cell movement. Relative to MP:GFP fluorescence (18.1 ± 1.0 arbitrary units), MP:$(H)_6$:GFP appeared to overaccumulate (35.4 ± 2.1 arb. units), although a corresponding increase in infection site area was not apparent (**b**). The depreciated level of MP:GFP:$(H)_6$ fluorescence (9.6 ± 0.6 arb. units) did correlate with a reduced infection site area, however, the possibility that –$(H)_6$ caused MP to mislocalize could not be discounted without further microscopic analyses. Error bars represent the standard error of the mean.

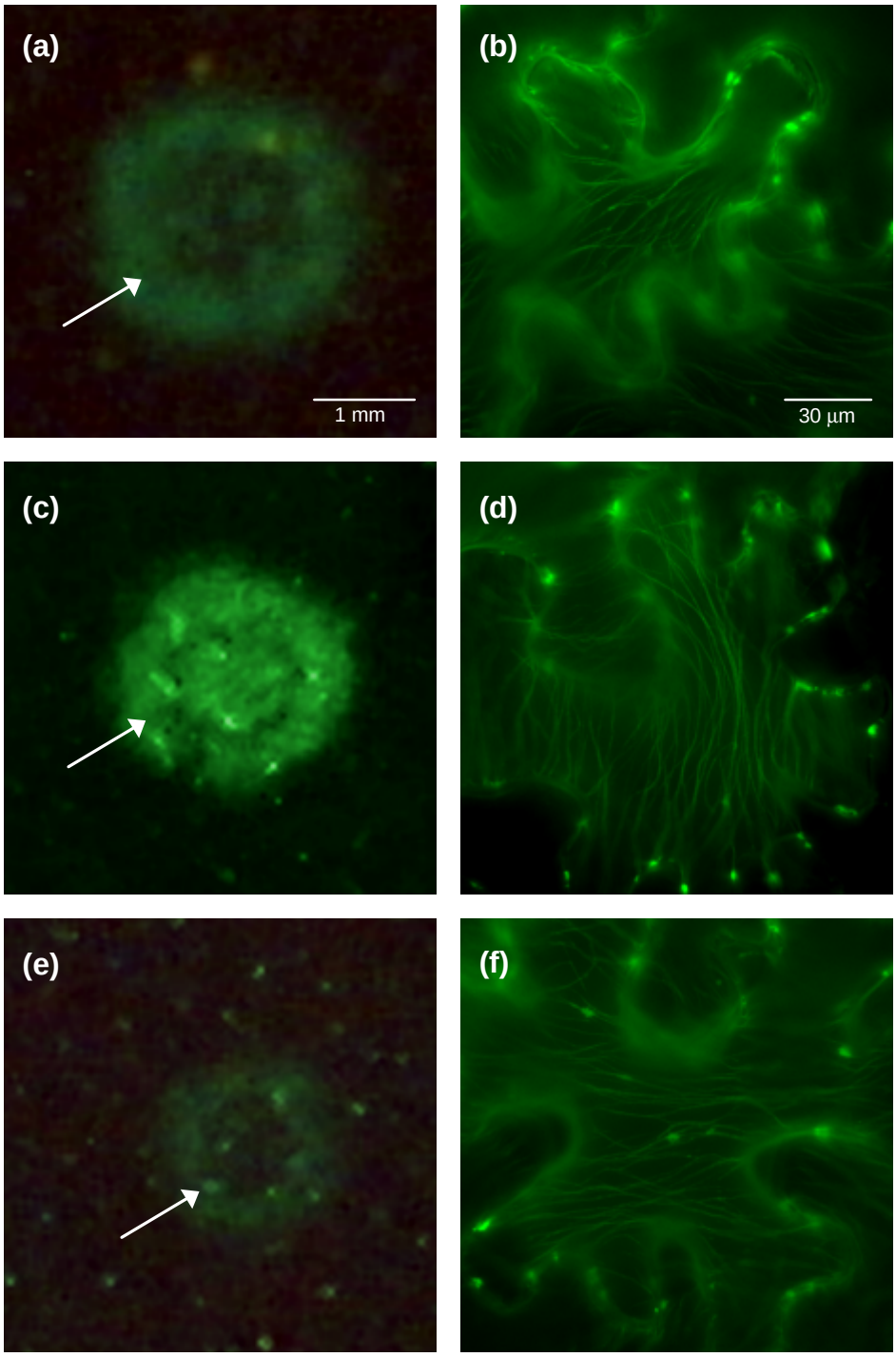

Figure 6 Infection of *Nicotiana benthamiana* leaf epidermal cells with TMV-derivatives encoding –$(H)_6$ affinity tags. Expanded leaves of *N. benthamiana* plants were mechanically inoculated with RNA derived from TMV-MP:GFP (**a** and **b**), TMV-MP:$(H)_6$:GFP (**c** and **d**) and TMV-MP:GFP:$(H)_6$ (**e** and **f**), respectively. At 3 days post infection, detached leaves were visualized by UV-digital photography (**a**, **c** and **e**) and fluorescence microscopy (**b**, **d** and **f**). As determined by the appearance of expanding

fluorescent infection sites, all three viruses were considered infectious with regard to viral replication and intercellular trafficking of vRNA. Although of a similar size, infection sites caused by TMV-MP:$(H)_6$:GFP (**c**) appeared to be brighter than those due to TMV-MP:GFP (**a**), possibly reflecting enhanced MP:$(H)_6$:GFP expression. In contrast, the infection sites caused by TMV-MP:GFP:$(H)_6$ (**e**) appeared to be both smaller, and less fluorescent than TMV-MP:GFP induced sites, however, microscopic analysis revealed that for each respective virus, the subcellular distribution of MP:GFP fluorescence was largely consistent with previous reports (Heinlein *et al*., 1998). Although inconclusive, MP:$(H)_6$:GFP accumulation in cell wall proximal sites (**d**) appeared to account for the relatively high fluorescence of infection sites caused by TMV-MP:$(H)_6$:GFP. Nevertheless, in cells behind the leading edge (LE) of infection (arrow), MP:GFP, MP:$(H)_6$:GFP and MP:GFP:$(H)_6$ could be localized to filamentous structures characteristic of microtubules (**b**, **d** and **f**; Boyko *et al*., 2000a), thereby indicating that all three fusion proteins were indistinguishable with regard to MT association. Although the presence of –$(H)_6$ had subtle effects on the level of MP accumulation and rate of vRNA trafficking, these data do collectively demonstrate that viral replication, cell-to-cell trafficking and MP:MT association are not inhibited by –$(H)_6$ to the point of rendering the TMV-derivative viruses non-viable.

3.4 Biochemical analysis of MP:MT binding in vitro

3.4.1 Optimization of reaction conditions

The reaction buffer BRB80 (80 mM Pipes-OH [pH 6.8], 1 mM $MgCl_2$, 1 mM EGTA) containing GTP is commonly used for MT-based biochemical assays (Ackmann *et al.*, 2000). Attempts to directly perform the MAP assay (Materials and Methods section 2.4.3) with MP using this buffer system resulted in an apparent non-saturable and linear binding relationship (not shown). Direct visualization of these 'complexes' by immunohistochemical labeling of α-tubulin and MP followed by fluorescence microscopy demonstrated that MP had formed large, irregular-shaped aggregates on and around extensively bundled MTs (not shown). Regardless of the evident MP-MT interaction, non-specific aggregation could not discounted as the sole determining factor. Due to this experimental constraint, interpretations of the binding reaction remained unreliable. To improve the stability of MP, a systematic approach was established whereby MP solubility was tested in a range of buffers empirically known to support MT polymerization (Lee and Timasheff, 1977; Waxman *et al.*, 1981; Pedrotti *et al.*, 1993). Briefly, MP was incubated in premixed buffer, centrifuged and the pellet and supernatant fractions were analyzed by SDS-PAGE and CCB staining. Table 2 summarizes a number of MT-compatible conditions within which MP solubility was tested. As mentioned, buffer BRB80 (+ GTP) induced the otherwise soluble MP to aggregate. Solubility in this buffer could not be improved by the presence of 10 % (v/v) glycerol or by non-ionic detergents in micelle concentrations (Table 2, 2-8). Testing the BRB80 components individually showed that GTP was the causal agent of MP insolubility when present at 1 mM (Table 2), a concentration typically used to facilitate net MT stability *in vitro*. As a possible substitute for GTP,

the non-hydrolyzable analogue, Guanosine 5'-[γ-thio]-triphosphate (GTP-γ-S) was also tested and found to produce a similar level of MP aggregation. Although not shown, it was also found that a number of salts (e.g. $H_2PO_4^-$, Na^+ and K^+) at concentrations below 50 mM effectively "salted-out" MP from solution. This observation was not entirely unsurprising given that MP has been shown by subcellular fractionation experiments to behave as an integral-membrane protein (Reichel *et al.*, 1999), and that many such proteins have a general propensity to aggregate in low concentrations of salt (Prof. M. Spiess, personal communication). Additionally, it was found that buffers containing 80 mM Pipes-OH (pH 6.8) induced a less pronounced, yet detectable decrease in MP solubility (Table 2, 4-5). Although considered to be minor (< 5 % loss of MP in pellets), it was speculated that the effects of ~ 150 mM ionic strength (Seitz *et al.*, 2002), may still lead to extraneous non-specific binding and thus, overestimation of the MP:MT binding stoichiometry (Timasheff, 2002). MP was therefore tested in more dilute buffer (12 mM Pipes-OH [pH 6.8]) and was indeed found to remain soluble even when stored for a period of days at 4 ^oC. It should be noted that a hydrophobic component to the MP-MT interaction during infection cannot be ruled out, however, it was hoped that by reducing the ionic strength of the buffer to a minimum, the biochemical analysis *in vitro* could be somewhat simplified. Since GTP was now known to induce MP aggregation, both GTP and unpolymerized tubulin dimers were removed from the MT polymer fraction by repeatedly pelleting and resuspending MTs into GTP-free buffer. *In vitro*, MTs spontaneously convert between phases of elongation and shortening, and since MTs require GTP for the elongation phase of their dynamics, the absence of exogenous GTP results in a net breakdown of MTs over time (Caplow and Fee, 2003). To counteract this fact, pelleted MTs were resuspended in GTP-free buffer containing the drug taxol, a strong suppressant of MT dynamics

(Wilson *et al.*, 1985; Derry *et al.*, 1995). Glycerol was also included in the *MAP binding buffer* to additionally enhance MT stability (Prof. A. Hoenger, personal communication). Providing the polymerized MTs were allowed to equilibrate in the presence of taxol and GTP (≥ 12 hours) before being resuspended in *MAP binding buffer* (12 mM Pipes-OH [pH 6.85], 0.5 mM $MgCl_2$, 10 % [v/v] Glycerol, 0.01 % [v/v] Tween-20 and 10 μM Taxol), MTs remained almost totally stabilized in the absence of GTP for at least 30 minutes following buffer exchange (Fig. 7b).

Component	Buffer compositions															
80 mM Pipes-OH, pH 6.8	+	+	+	+	+	+	+	+	+	+	+					
12 mM Pipes-OH, pH 6.8												+	+	+	+	+
1 mM Mg Cl_2	+	+	+	+	+	+	+	+	+				+	+	+	+
1 mM EGTA	+	+	+	+	+	+	+	+	+		+					
1 mM GTP	+	+	+	+	+	+	+	+	+						+	
1 mM GTP-γ-S																+
25 µM Taxol														+	+	+
10 % (v/v) Glycerol	+	+	+	+	+					+	+	+	+	+	+	+
1 % (v/v) Nonidet-P40		+				+										
0.1 % (v/v) Nonidet-P40			+				+									
1 % (v/v) Triton X-100				+				+								
0.1 % (v/v) Triton X-100					+				+							
0.01 % (v/v) Tween-20														+	+	+
Soluble (yes/no)	N	N	N	N	N	N	N	N	N	Y	Y	Y	Y	Y	N	N

Table 2 Solubility of MP in microtubule-compatible buffers. In order to determine which component of the reaction buffer BRB80 (80 mM Pipes-OH [pH 6.8], 1 mM $MgCl_2$, 1 mM EGTA [+ 1mM GTP]) was responsible for MP aggregation, MP was incubated in the above buffer compositions, incubated for 1 hour and subjected to high-speed centrifugation as described in Materials and Methods section 2.4.2.1. The resulting pellet and supernatant fractions were analyzed by SDS-PAGE and CCB staining and if 95% or more of MP remained in the supernatant, the protein was considered to be soluble in that particular buffer (as indicated). Using this approach it was possible to identify GTP as the causal agent of MP aggregation (highlighted in red). All other standard components of BRB80 had no significant effect on the solubility of MP. As a potential substitute for GTP, the structural analogue GTP-γ-S was tested and also found to induce comprehensive MP aggregation. Neither micelle concentrations of non-ionic detergents nor glycerol appeared to have any positive effect on the solubility of MP.

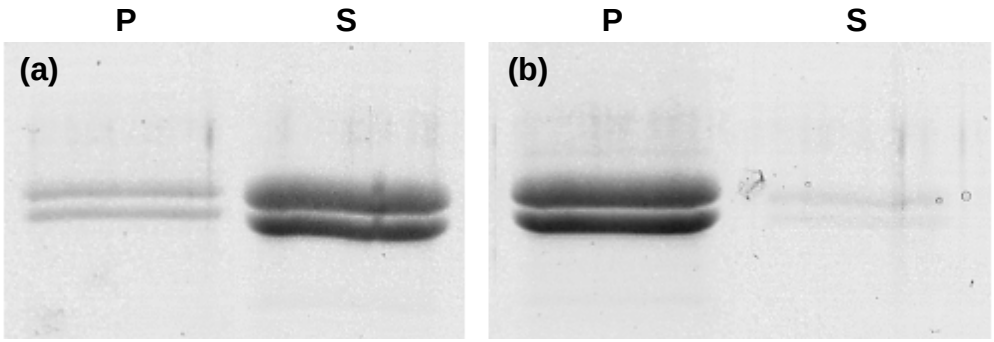

Figure 7 Examples of the microtubule stability assay. MTs were polymerized as described in Materials and Methods section 2.4.2.2 and were resuspended in 60 µL of either 10 mM Tris-Cl (pH 7.5), 1 mM $MgCl_2$ and 25 µM Taxol (**a**), or MAP binding buffer (12 mM Pipes-OH [pH 6.85], 0.5 mM $MgCl_2$, 10 % [v/v] Glycerol, 0.01 % [v/v] Tween-20 and 10 µM Taxol), as shown in panel (**b**). Samples were incubated for 30 minutes and polymerized tubulin was sedimented by centrifugation. Pellet (**P**) and supernatant (**S**) fractions were analyzed on separate SDS-PAGE gels by CCB staining. MTs were highly unstable in Tris-based buffers (pH 6.8 or pH 7.5), regardless of the presence of Taxol. It was found that even upon dilution, and in the absence of GTP, stable MTs could be maintained when Pipes (pH 6.8-7.0) was employed as the buffering agent in the presence of Taxol.

3.4.2 MAP assay

The microtubule binding activity of MP was tested using the optimized *MAP binding buffer* (Materials and Methods section 2.4.3). In order to fulfill the criteria for saturation binding analysis, increasing amounts of MP was titrated over 3 orders of magnitude (sub-supramolar) against a fixed concentration (1.1 μM) of polymerized tubulin dimers. Following incubation, MTs and associated MP were sedimented and both the pellet and supernatant fractions were analyzed by SDS-PAGE and CCB staining. As can be seen in Fig. 8, an absence of tubulin in the supernatant fractions indicated that the MTs remained dynamically stable throughout the course of the reaction. Saturable binding was apparent as determined by the appearance of MP in supernatant fractions at a 3:1 molar ratio of MP to tubulin and above. Replicate experiments using freshly prepared MTs and MP produced directly comparable results. However, due to the detection threshold of CCB, it was speculated that saturation of MT binding sites by MP might not be seen at MP concentrations below 3 μM. Reaction volumes were therefore increased 3-fold for reactions containing between 0.1 and 3 μM MP (not shown). Although more MP could be seen in the supernatant fraction in this case, the ratio at which MP became visible remained the same at approximately 3:1. To control for buffer-induced aggregation of MP, reactions were repeated in the absence of tubulin. In some cases very low amounts of MP could be detected in the pellet fractions and where applicable, these amounts were accounted for when calculating the amount of MP per lane.

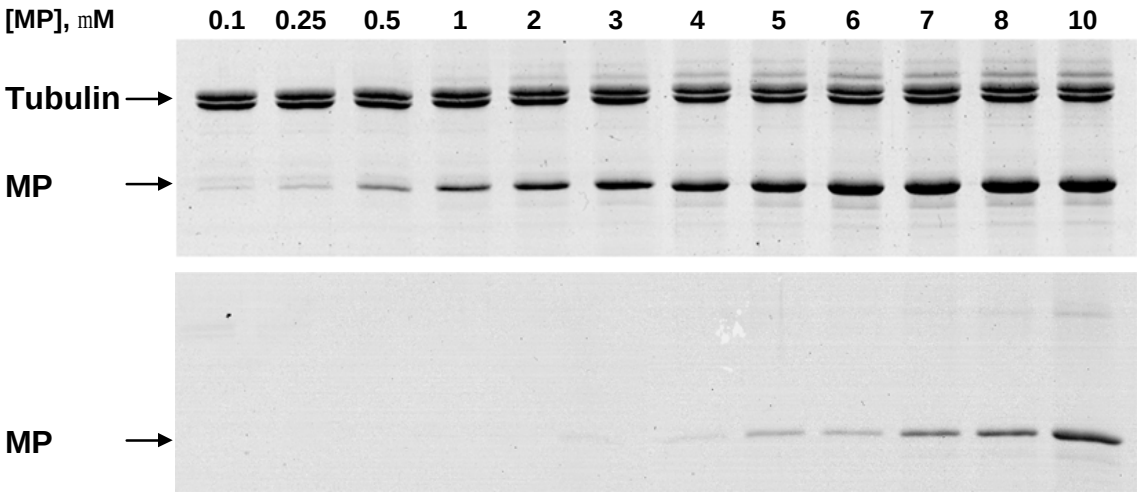

Figure 8 Microtubule binding by MP *in vitro.* Increasing amounts of MP were incubated with 1.1 μM of polymerized tubulin dimers in *MAP binding buffer* and MTs together with associated MP were sedimented by centrifugation. Pellet (top panel) and supernatant (bottom panel) fractions were analyzed by SDS-PAGE and CCB staining. Detectable levels of tubulin are exclusively found in the pellet fractions, indicating that the MTs remained stable under the reaction conditions used. In addition, the presence of MP in the pellet fractions demonstrates that MP had the capacity to interact directly with pure MTs. This interaction was saturable as determined by the increasing presence of MP in the supernatants at an MP:tubulin ratio of 3:1 and above. Although not shown, when reaction volumes were increased 3-fold, the ratio at which MP was detectable in the supernatant remained about 3:1, suggesting that the detection threshold of CCB (~ 50 ng MP) was not a limiting factor.

3.4.3 Determining the effect of –$(H)_6$ on MT binding

The association of MAPs with MTs is thought to arise predominantly via ionic interactions (Cassimeris and Spittle, 2001). At a pH of 7.0 (reaction pH = 6.8) the predicted charge of –$(H)_6$ is + 1.42 (ProtParam, IK@N Bioinformatics), therefore, using a similar approach to the MAP assay, we tested whether –$(H)_6$ is sufficient to directly mediate MT binding contacts. Test proteins GST-$(H)_6$, $(H)_6$-Tau 441 or MP-$(H)_6$ (all at 1.5 μM) were incubated with (+) or without (-) a molar excess of polymerized tubulin (6 μM) and pelleted material was analyzed by SDS-PAGE and CCB staining. As expected, approximately all of the MP cosedimented with MTs (Fig. 9, lane 11), as compared to the starting amount of material (Fig. 9, lane 10). In the absence of tubulin, soluble MP remained exclusively in the supernatant (Fig. 9, lane 12). A similar result was obtained using recombinant $(H)_6$-Tau, a well characterized neuronal MAP (Fig. 9 lanes, 4-6). In contrast, neither soluble GST-$(H)_6$ (Fig. 9, lanes 1-3) or BSA (Fig. 9, lanes 7-9) appeared to cosediment with tubulin to any significant degree, taking into account the molar excess of MTs. Although these results demonstrate that a -$(H)_6$ affinity tag is insufficient to produce stoichiometric MT binding *in vitro*, low amounts of GST-$(H)_6$ and BSA did cosediment with tubulin. The amount of non-specific binding was comparable in both cases, however, the degree to which –$(H)_6$ contributed to this interaction, and whether a similar non-specific component is involved in the MP-MT interaction remains unclear.

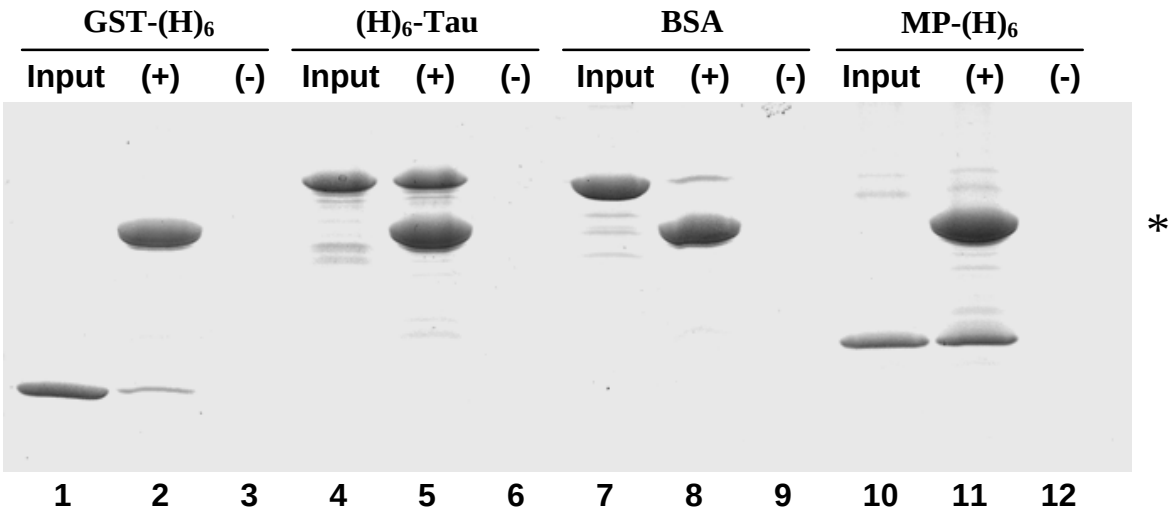

Figure 9 MAP assay control reactions to determine the effect of –$(H)_6$ on microtubule binding *in vitro.* Test proteins (1.5 μM) were incubated either with (+) or without (-) 6 μM polymerized tubulin in *MAP binding buffer* and subjected to centrifugation. Pellet fractions were analyzed by SDS-PAGE and CCB staining. The position of tubulin is denoted by (∗) and for visual comparison, 1.5 μM of each test protein was directly loaded on the gel without prior centrifugation (**input**). In the absence of tubulin (lanes **3,6,9** and **12**), the apparent lack of protein in the pellets indicated that all four test proteins remained soluble under the conditions used. A small amount of GST-$(H)_6$ was observed to cosediment with MTs (lane **2**), however, compared to the starting amount of material (lane **1**) this degree of binding appeared to be neglible, possibly reflecting a weak non-specific interaction. Similarly, BSA also did not bind MTs to any significant amount (lane **8**), as compared to the starting amount of protein (lane **7**). Conversely, with a molar excess of tubulin, almost complete binding of $(H)_6$-Tau (lane **5**) and MP (lane **11**) could be observed. Although a non-specific component to this binding could not be ruled out, the collective data suggested that a –$(H)_6$ moiety alone was insufficient to mediate strong interactions with MTs *in vitro*.

3.4.4 Analysis of the MT binding properties of MP *in vitro*

Following the MAP assay, the amount of MP in the pellet ($[MP]_{bound}$) and supernatant ($[MP]_{free}$) fractions was quantified by densitometry of the digitized gels. The amount of MP in each respective fraction was corrected for non-specifically pelleted MP and, subsequently, values for $[MP]_{bound}$ were plotted versus $[MP]_{free}$, yielding a saturation hyperbole. In an attempt to characterize the equilibrium binding reaction, a curve was fit to these data according to a simple model describing a receptor:ligand binding reaction where only one type of ligand binding site exists, and all binding sites of this type are independent and do not display an allosteric influence on subsequent ligand binding (Appendix III eq. 11). It must also be assumed when using this model that there is a single type of monovalent ligand, when values for the binding stoichiometry and K_d are required. As can be seen in Fig. 10, a curve fit using the one-site model did not pass smoothly through all data points, a fact reflected in the relatively low value of $r^2 = 0.967$ (an indicator that actual data deviate from the model-dependent predicted curve). Nonetheless, non-linear regression analysis of this curve yielded apparent values of $K_d = 71.6 \pm 14.5$ nM with a stoichiometry of 2.8 ± 0.12 MP/$tubulin_{monomer}$. The K_d value determined by this method was within the range commonly found for other MAPs (Ackmann *et al.*, 2000), although it should be noted that since a low ionic strength buffer was employed, and MAP binding is thought to result largely via ionic interactions, the apparent affinity of MP for MTs may be slightly enhanced. The value for stoichiometry was considered to be high, therefore, in order to determine whether the one-site model was indeed appropriate, Scatchard-Rosenthal plots were produced by plotting $[MP]_{bound}/[MP]_{free}$ versus $[MP]_{bound}$ according to the Scatchard equation (Appendix III eq. 13; Fig. 11, inset). In theory, adherence to the above criteria would result in a straight line with a slope of $-1/K_d$ and stoichiometry found at the x-intercept.

Manually fitting a curve to these data illustrated a clear deviation from the predicted straight line relationship (Fig. 11) and in fact resulted in a line of upward curvature. Scatchard curves of this type can be interpreted in a number of ways (Norby *et al.*, 1980; Zierler, 1989). For instance, the existence of more than one type of ligand binding site on a receptor can account for apparently biphasic curves, and are usually attributable to sites with differing affinities for the same ligand. In this case, independence is assumed both within and between types of binding site. Alternatively, one may infer that ligand binding undergoes homotropic allosterism, that is, initial binding of ligand to a single type of binding site has a negative influence on subsequent ligand binding to the same type of site. In an attempt to differentiate between the underlying binding mechanisms, a curve was fit to plots of $[MP]_{bound}$ versus $[MP]_{free}$ according to a two-site model (Appendix III eq. 12), where binding site independence was again assumed. In this case, non-linear regression yielded two values for K_d and stoichiometry (K_{d1} = 31.3 ± 16.6 nM; n_1 = 1.81 ± 0.55; K_{d2} = 1.56 ± 1.34 μM; n_2 = 1.56 ± 0.436), indicating both a high and low affinity MP-binding site on tubulin. The overall fit of the line was improved (Fig. 12; r^2 = 0.986) as compared to the one-site model, and comparison of the two curves by one-way analysis of variance (Fig. 13; F = 4.72, P = 0.026) indicated that statistically, a two-site model was indeed the more appropriate. It should be noted that absolute values obtained from Scatchard plots are rendered unreliable due a deviation from the Gaussian distribution during data transformation. Taken together with the statistically strong fit of a two-site model, it is tempting to conclude that MP binds alternative sites on tubulin, however, whether the second site actually resides on the surface of tubulin, or occurs via a tubulin:MP:MP ternary complex remains a matter of conjecture. Additional complexities arise due to insufficient knowledge regarding the homogeneity of MP. Since it is possible that

multivalent or alternative folded states of renatured MP exist, and indeed, the low affinity site may represent a non-specific binding site, further experimentation is clearly required in order to make a categorical conclusion about the mechanistic nature of the MP:MT interaction *in vitro*.

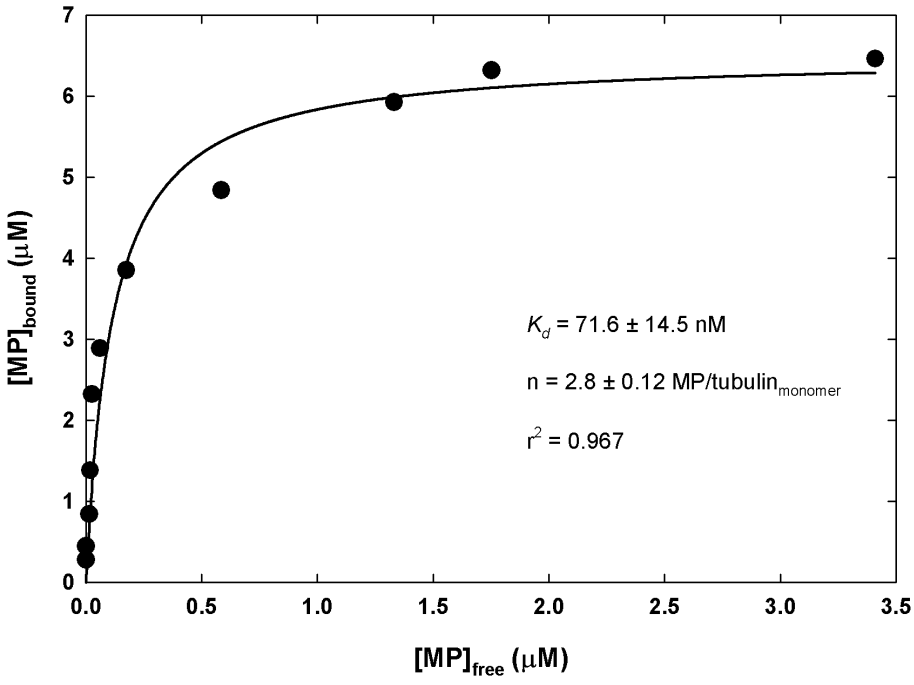

Figure 10 Equilibrium binding of MP to MTs *in vitro*: one-site model. Equilibrium binding experiments were performed by incubating purified MP (0.1-10 μM) with *in vitro* polymerized tubulin (2.2 μM monomer) before bound and unbound MP was separated by centrifugation and analyzed by SDS-PAGE and CCB staining. Values for $[MP]_{bound}$ and $[MP]_{free}$ were determined by densitometry as described in Materials and Methods section 2.4.5. Plotting $[MP]_{bound}$ versus $[MP]_{free}$ gave a saturation hyperbole and a curve was fit to these data according to the binding model describing a single type of non-interacting binding site on tubulin (Materials and Methods section 2.4.5). The fit curve was analyzed by non-linear regression and yielded an apparent K_d of 71.6 ± 14.5 nM, a value comparable to other characterized MAPs. The curve saturated at an apparent stoichiometry of 2.8 ± 0.12 equivalent binding sites per tubulin monomer. Because the curve did not pass smoothly through all of the data points (r^2 = 0.967; where 1 indicates a perfect fit), it remains feasible that a one-site model does not adequately describe these data.

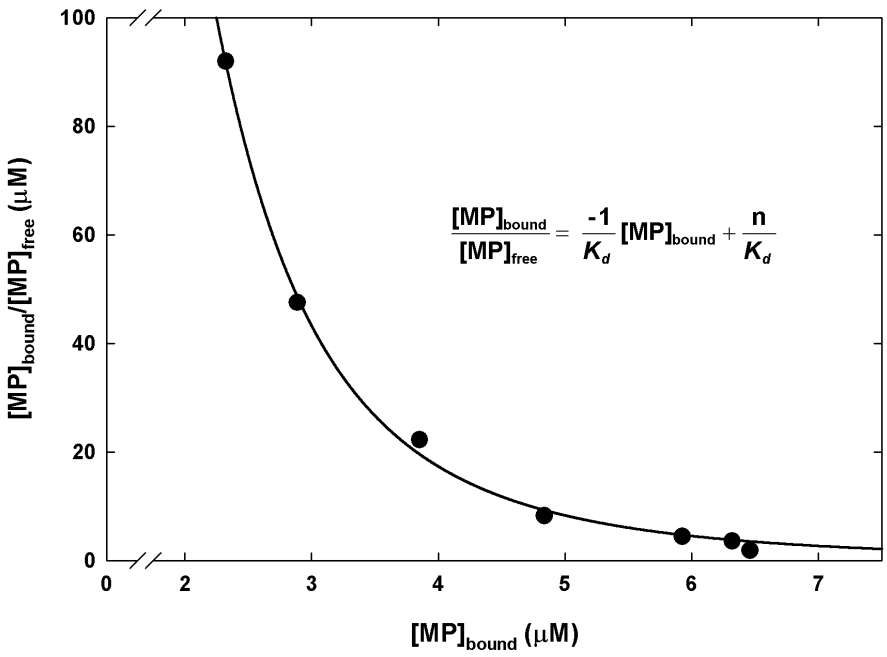

Figure 11 "Linearization" of equilibrium binding data: Scatchard-Rosenthal plot. Equilibrium binding experiments were performed as described in Materials and Methods section 2.4.3 and values of $[MP]_{bound}/[MP]_{free}$ were plotted versus $[MP]_{bound}$. According to the Scatchard equation (**inset**), equilibrium binding data plotted in this manner should result in a straight line when the criteria for a single type of independent, non-interacting ligand binding site are met. These data clearly deviate from the predicted straight line, and therefore, a curve was fit (y = a+b/1+cx) using a best-fit trial and error approach (r^2 = 0.98). The upwards curvature and apparent biphasic nature of this line can indicate the following; negative cooperativity (homotropic steric hindrance) in a one-binding site system, the existence of two or more independent MP-binding sites per tubulin or a non-specific binding component to the reaction (Norby *et al.*, 1980). Care should be taken when interpreting Scatchard plots, since following transformation, data no longer adhere to the assumed Gaussian distribution.

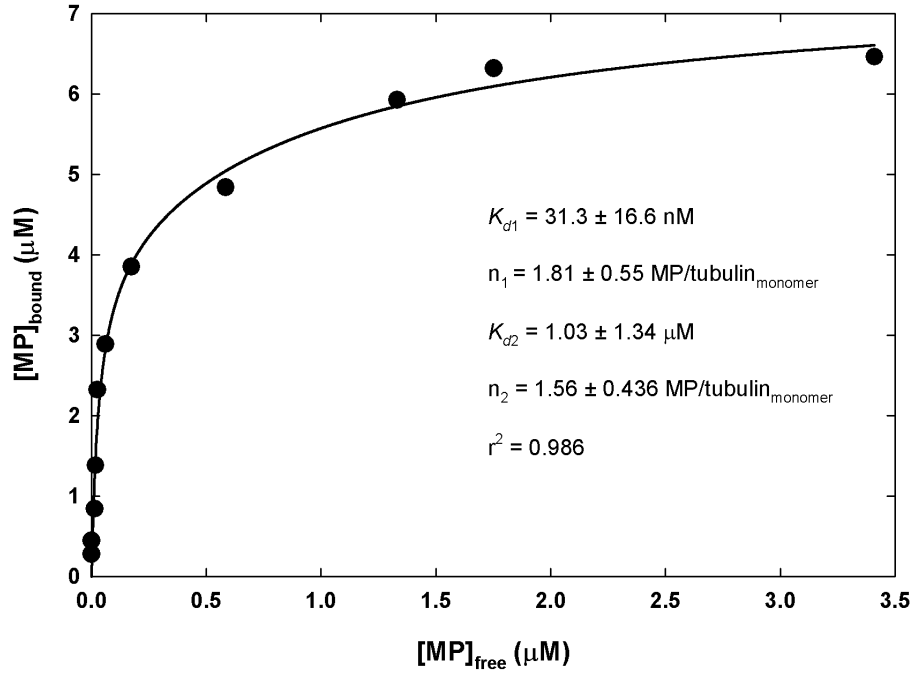

Figure 12 Equilibrium binding of MP to MTs *in vitro*: two-site model. Equilibrium binding experiments were performed as described in Materials and Methods section 2.4.3 and in this case, a curve was fit to the plot of $[MP]_{bound}$ versus $[MP]_{free}$ according to a model describing two types of independent, non-interacting binding sites on tubulin (Materials and Methods section 2.4.5). Non-linear regression analysis indicated the existence of a high affinity (K_{d1} = 31.3 ± 16.6 nM; n_1 = 1.81 ± 0.55) and a low affinity (K_{d2} = 1.56 ± 1.34 μM; n_2 = 1.56 ± 0.436, respectively) MP-binding site on tubulin. The curve appeared to fit the data relatively well (r^2 = 0.986), as compared to using a one-site model (Fig. 10). The possibility that the improved fit resulted from an increased number of parameters, and therefore inflexion points, could not be discounted using this analysis alone.

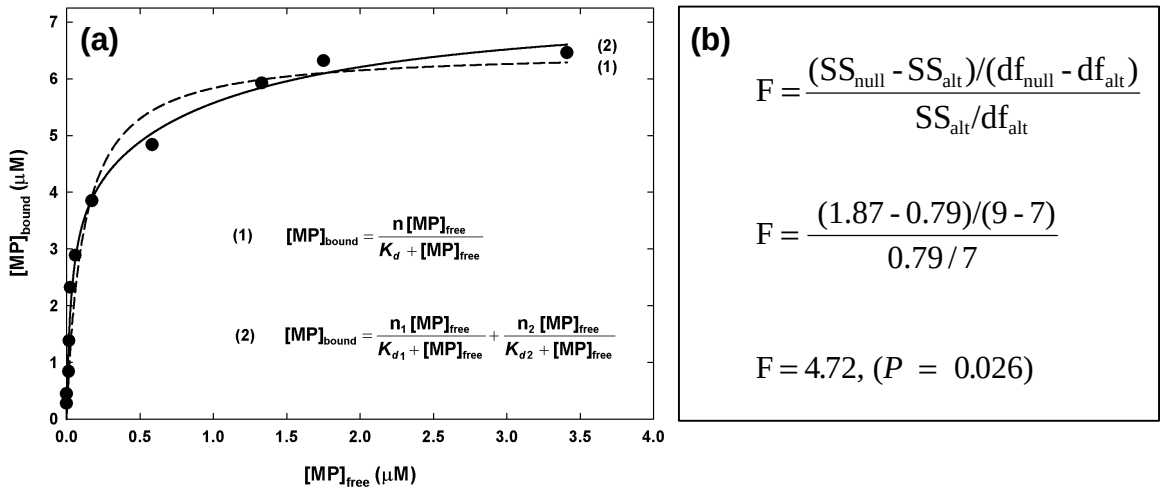

Figure 13 Analysis of MP equilibrium binding to MTs *in vitro*: comparison of binding data fit to a one-site or two-site model. Equilibrium binding experiments were performed as described in Materials and Methods section 2.4.3 and curves were fit to a plot of $[MP]_{bound}$ versus $[MP]_{free}$ according to models describing a single type of independent binding site (**a1**) or two different independent binding sites (**a2**). The fit of these curves were compared by one-way ANOVA of the non-linear regression data obtained for each respective curve fit. The F *ratio* was calculated (**b**) assuming a null hypothesis (null) that the one-site model fits the data better, and an alternative hypothesis (alt) that the two-site model is more appropriate. SS is the sum of the squares and df is degrees of freedom. Since the F *ratio* was found to be greater than one, the null hypothesis could be rejected, which was confirmed by the calculated *P*-value of 0.026. It could therefore be statistically inferred that *in vitro*, MP binding to MTs is a biphasic reaction involving more than one MP-binding site on tubulin or possibly resulting due to multivalent/isotypic forms of MP.

3.5 Visualization of MP:MT complexes formed in vitro by fluorescence microscopy

3.5.1 Establishment of the perfusion chamber system

MTs are highly sensitive to their immediate buffer environment, making the direct immunolabeling of MAP:MT complexes technically unfeasible without prior fixation. Initial attempts to fix MP:MT complexes in free solution resulted in extensive and irregular bundling of MTs (not shown). Although MP appeared to colocalize with MTs in this case, the presence of large MP aggregates suggested that the interaction may have occurred largely through non-specific crosslinking, particularly when MP was in molar excess. A system was therefore established whereby immobilized MTs could be incubated with MP and unbound protein removed before fixation. Briefly, a simple perfusion chamber was coated with a mixture of casein and the molecular motor kinesin. *In vitro* polymerized MTs were anchored to the kinesin in the absence of ATP, in order to inhibit motor activity before MP was introduced and allowed to bind MTs. Unbound protein was washed out and the resulting complexes were rapidly fixed with glutaraldehyde before α-tubulin and MP were immunohistochemically labeled. One major drawback to using the perfusion chamber method is that one has no accurate knowledge of the actual amount of MTs within the chamber, since this is dependent on both the concentration of kinesin and tubulin, and also the time that each respective component is absorbed to the chamber. Assuming that every MT was immobilized, the maximum theoretical tubulin concentration within the chamber would have increased to 0.5 μM, due to a concentration of the original 90 nM solution. As determined by visual inspection of rhodamine-labeled MTs before and after absorption, the realistic concentration was significantly lower than this figure. Therefore, MP was applied at a

wide range of concentrations in an attempt to emulate the MP:Tubulin stoichiometries used during the MAP assay. To test for crossreactivity leading to false MP signals, a variety of anti-tubulin, anti-MP and secondary antibody combinations were used to label MTs undecorated with MP. The following combinations were considered suitable; anti-α-tubulin YOL1/34 (α-tubulin residues 414-422) in combination with anti-MP-N (MP residues 6-22), or anti-α-tubulin DM1A (α-tubulin residues 426-450) in combination with anti-MP-C (MP residues 209-222), respectively. Due to poor labeling efficiency, anti-β-tubulin antibodies were not used.

3.5.2 Fluorescence microscopy

Using either of the above antibody combinations, it was not possible to observe any significant MP colocalization with MTs at MP concentrations below 200 nM (not shown). Since estimates of the tubulin concentration were wholly unreliable, it could only be speculated that the apparent lack of MP co labeling was either due to insufficient amounts of MP, and consequently a fluorescence signal below the microscope detection limit, or alternatively, a low signal to noise ratio resulting from non-specific binding of MP to the chamber surface. In either case, the tubulin staining produced a smooth, consistent fluorescence signal along the length of the MTs. In contrast to this, incubations with higher concentrations of MP (0.75-2.5 μM) resulted in a noticeably punctate tubulin labeling when either YOL1/34 or DM1A anti-tubulin antibody was employed alone, and in extreme cases, an almost total absence of tubulin labeling (for examples see Fig. 14, row a). This observation suggested that MP may have been present at or near the antigenic sites for either antibody (collectively mapping to α-tubulin residues 414-450), and indeed, immunolabeling of MP:MT complexes (MP > 0.75 μM) with the antibody combinations described above resulted

in apparent MP colocalization along the entire length of the MTs. The distribution of MP along the MTs was not uniform, however, and along certain stretches of the MTs, the MP labeling appeared to be particularly strong (Fig. 14, row b). Although the overall tubulin-specific signal was higher than that of MP, these areas where the MP signal was stronger clearly correlated with a largely reduced tubulin-specific signal (Fig. 14, row c and d). Although inconclusive, this result indicated that at least in part, MP had the capacity to obscure the antigenic site recognised by either anti-tubulin antibody, and that residues found at either termini of MP were accessible to anti-MP antibodies, possibly suggesting that these regions of MP were not directly involved in the MP:MT interaction. Further experimentation, such as the use of truncated or mutagenized MP would be required in order to test this hypothesis. It should be noted that upon TMV infection of BY-2 protoplasts, MTs heavily decorated with MP:GFP are also stained poorly by anti-α-tubulin antibody DM1A, although care should be taken when drawing conclusions from such dissimilar experimental systems. Biochemical analysis of the MP:MT interaction strongly suggests that equilibrium binding deviates from a single ligand, single receptor mechanism. In principle, the observed non-uniform distribution of MP along MTs *in vitro* supports this hypothesis, although it must be conceded that due to extensive washing, the above conditions do not fully reflect equilibrium binding. Nonetheless, MP complexed with MTs is recognized by anti-MP antibodies reactive against both N- and C-termini. Considering the possible interpretations of a ‘two-site’ binding model (Results section 3.4.4), the above observations favour a binding mechanism whereby MP can interact directly with tubulin, although, a less ordered binding reaction may occur, possibly resulting in a tubulin:MP:MP ternary complex. Due to the similar predicted binding stoichiometries for either mechanism ($n_1 = 1.81 \pm 0.55$ and $n_2 = 1.56 \pm 0.436$ MP:tubulin dimer), it is

not possible using this method to make firm conclusions regarding the relative abundance of MP on the MT and the corresponding binding mechanism. Similarly, it remains unclear whether non-uniform MP distributions reflect structural differences within the MT itself, or indeed, whether MP can interact with β-tubulin.

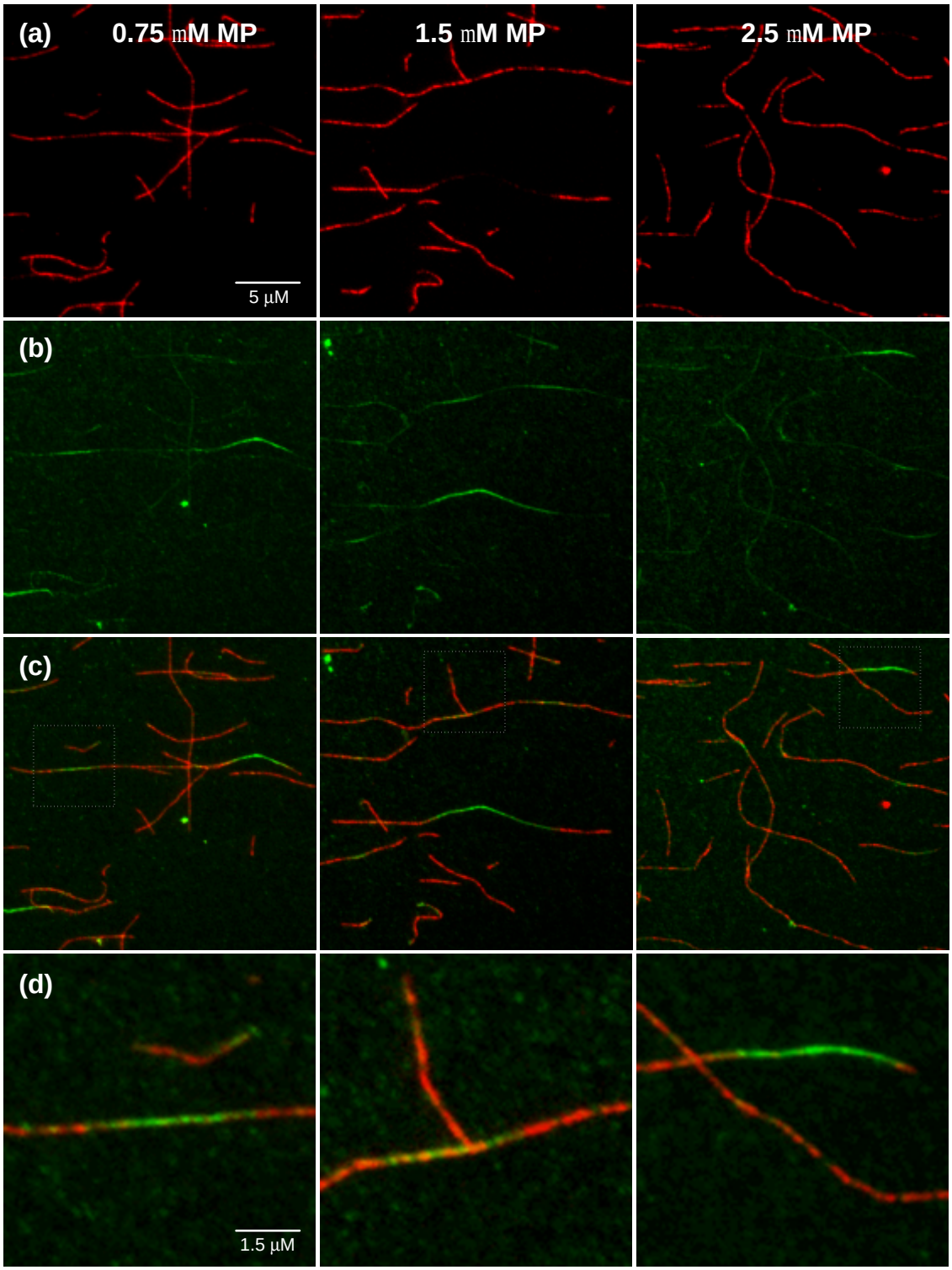

Figure 14 Visualization of MP:MT complexes formed *in vitro* by immunohistochemical labeling and fluorescence microscopy. MTs were polymerized *in vitro* (~ 90 nM tubulin) and immobilized in perfusion chambers precoated with kinesin. A molar excess of MP was introduced as indicated, incubated for 2 minutes at room temperature and unbound MP was removed with 10 volumes of

MAP binding buffer. Resulting MP:MT complexes were fixed and labeled with antibodies specific for α-tubulin (YOL1/34; row a) and MP (anti-N-term; row b), respectively. Under the conditions used, MP could be clearly observed to colocalize with the MTs at a level above that of background fluorescence (row a and b). Although the overall MP-specific fluorescence was less than the corresponding tubulin signal (row c and d), the presence of MP could be correlated with a mere punctate labeling of tubulin,. in contrast to MTs or stretches of MTs undecorated by MP that showed strong and smooth tubulin labeling (not shown). Moreover, in areas where MP fluorescence was particularly strong, an almost complete absence of tubulin staining was observed. Although these data do not strictly reflect equilibrium binding (due to excessive washing), the non-uniformity of the MP:MT colocalization is in support of biochemical evidence that suggests *in vitro*, MP binds MTs via a bi- or possibly multiphasic mechanism. The precise manner by which MP impedes the anti-tubulin:antigen interaction remains unclear, although in principle, these data are consistent with observations of TMV-infected BY-2 protoplasts in which heavy MP:MT colocalization corresponds to a diminished tubulin immunolabeling.

3.6 Co-precipitation experiments in vitro using immobilized MP as an affinity bait

3.6.1 Co-precipitation of MTs and tubulin heterodimers *in vitro*

It has been described in the literature that certain 'tubulin' binding proteins preferentially interact with specific structural forms of tubulin such as tubulin dimers (Spittle and Cassimeris, 1996; Fukata *et al.*, 2002) or microtubules ends (Carvalho *et al.*, 2003; Howard and Hyman, 2003). Therefore, in order to determine whether MP can interact with binding contacts found on tubulin dimers or specifically interacts only with polymerized tubulin, purified MP was immobilized on Ni^{2+}-NTA sepharose beads and used as an affinity bait for the co-precipitation of either *in vitro* polymerized MTs or tubulin dimers. Pellet and supernatant fractions were separated by centrifugation and were analysed by SDS-PAGE and Western blotting, and to control for non-specific binding of tubulin to sepharose, the same procedure was followed in the absence of MP. Western blots probed with anti-MP-C antibody showed that throughout the course of the binding reaction, MP remained coupled to the affinity matrix in amounts that were comparable between reactions (Fig. 15a). Probing equivalent Western blots with anti-α-tubulin antibody showed that even after extensive washing, detectable levels of tubulin could be found in pellet fractions containing MP (Fig. 15b). In pellet fractions without MP, no tubulin was detected, thereby indicating that precipitation of tubulin had occurred via an interaction with MP, and not by virtue of non-specific contacts with the sepharose beads. Tubulin did not co-precipitate with Ni^{2+}-NTA sepharose beads in the absence of BSA (not shown), again suggesting that an MP:tubulin complex had formed, as opposed to an MP:BSA:tubulin ternary complex. Repeating the experiment confirmed that under the conditions used, MP interacted more

favourably with tubulin dimers than MTs, although the reason for this is not fully understood. Also, it cannot be ruled out that what appeared to be an MP:MT interaction was actually the result of MT depolymerization and the interaction of MP with tubulin dimers or short tubulin oligomers. Nevertheless, the fact that soluble tubulin dimers were able to bind MP *in vitro* suggests that polymer-specific structural forms of tubulin are not a prerequisite to MP binding. Furthermore, considering that the $–(H)_6$ tag was in close proximity to the affinity matrix, it is likely that residues found at the extreme C-terminus of MP were inaccessible for tubulin binding, suggesting that the MP:tubulin interaction was not mediated solely by this region of MP, an observation in agreement with previous reports (Boyko *et al.*, 2000a; Boyko *et al.*, 2000c). Repeating the experiment confirmed that under the conditions used, MP interacted more favourably with tubulin dimers than MTs, although the reason for this is not fully understood. It could be envisaged, however, that while the physical distribution of MP on Ni^{2+}-NTA beads may have had a nominal effect on the correct orientation and binding of free tubulin dimers to MP, a net reduction in the number of available MP binding sites per equivalent (polymerized) tubulin dimer may have occurred, thus resulting in weaker overall binding. Also, it cannot be ruled out that what appeared to be an MP:MT interaction was actually the result of MT depolymerization and the interaction of MP with tubulin dimers or short tubulin oligomers. Nevertheless, the fact that soluble tubulin dimers were able to bind MP *in vitro* suggests that polymer-specific structural forms of tubulin are not a prerequisite to MP binding, and furthermore, considering that the $–(H)_6$ tag was in close proximity to the affinity matrix, it is doubtful that the MP:tubulin interaction occurred solely via the extreme C-terminus of MP.

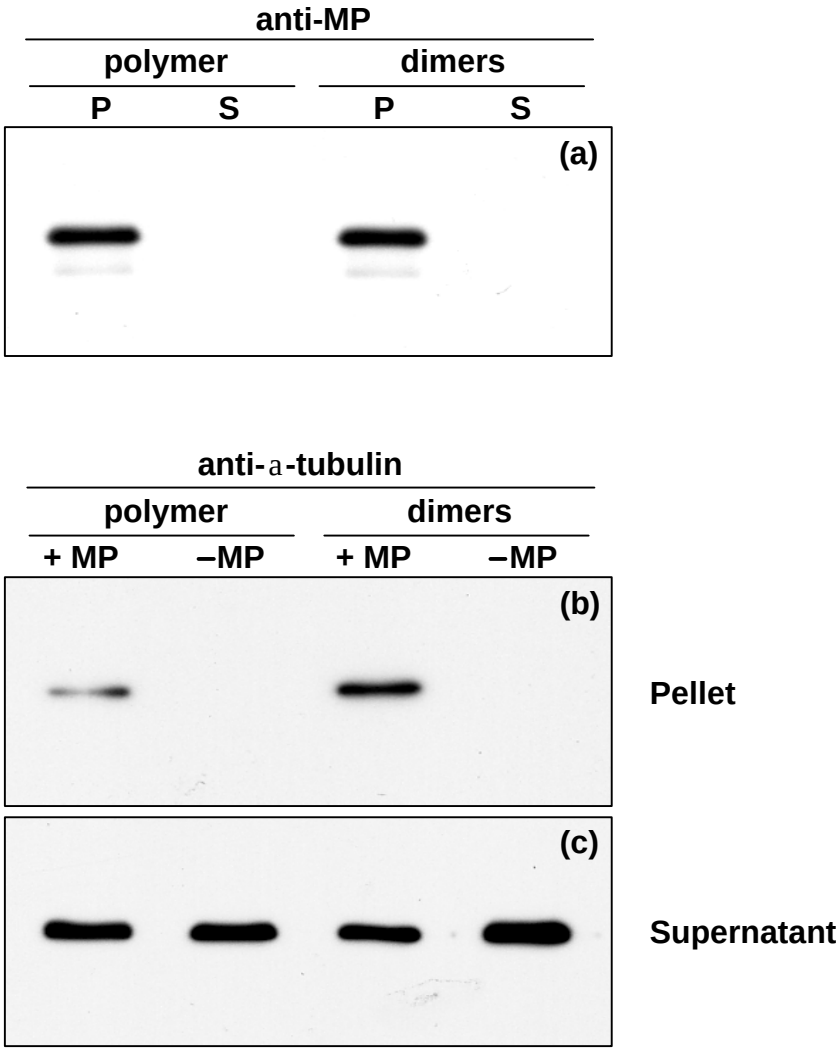

Figure 15 Co-precipitation of MTs and tubulin heterodimers *in vitro* using immobilized MP as an affinity bait. Ni^{2+}-NTA beads conjugated to MP (+ **MP**) or without MP (- **MP**) were incubated with *in vitro* polymerized MTs (**polymer**) or tubulin α/β dimers (**dimers**). Pellet (**P**) and supernatant (**S**) fractions were separated by centrifugation and analysed by SDS-PAGE and Western blotting using antibodies specific against MP or α-tubulin, respectively. As shown in (**a**), MP remained coupled to the Ni^{2+}-NTA beads throughout the course of the binding reaction. In pellet fractions containing MP, detectable amounts of both tubulin polymer and tubulin dimers were observed (**b**), although under the conditions used (Materials and Methods section 2.6.1), the MP:dimer interaction appeared to be favoured. In the absence of MP, no tubulin was detected in the pellets, indicating that tubulin co-sedimention with Ni^{2+}-NTA beads occurred due to an interaction with MP.

3.6.2 Co-precipitation of RNA and tubulin heterodimers *in vitro*

The putative role of RNA in the MP:tubulin interaction *in vitro* was investigated using an approach whereby MP (theoretical max. 3.25 μM) was immobilized on Ni^{2+}-NTA beads and used to co-precipitate combinations of tubulin dimers and RNA. Using a two-step approach, MP-conjugated beads were first incubated in the presence of tubulin heterodimers (1.63 μM) or the 6.7 kb *in vitro* transcribed TMV genomic RNA (50 nM or ~300 μM polymerized nucleotide). Subsequently, tubulin dimers, RNA or *pulldown buffer* were added to the reaction (as summarized in Fig. 16a) and incubated once again. To control for non-specific binding, RNA or tubulin were incubated with beads in the absence of MP. Pellet and supernatant fractions were separated by centrifugation before RNA was analyzed by non-denaturing agarose gel electrophoresis (Fig. 16c) and proteins were analyzed by SDS-PAGE and Western blotting (Fig. 16b). When incubated alone with MP-conjugated beads, both tubulin dimers (Fig. 16b1) and RNA (Fig. 16c4) appeared to co-precipitate with MP-conjugated beads. Although comparable amounts of MP were found exclusively in the pellet fractions, high levels of both tubulin and RNA could be detected in corresponding supernatant fractions (not shown), indicating that saturable binding had been achieved. At the MP:$tubulin_{monomer}$ ratio of 1:1, one would expect the majority of tubulin to be found in the pellet fraction (Results section 3.4.4). Since this was not the case, it was speculated that either MP was incompletely conjugated to the affinity matrix (i.e. << 3.25 μM) or that upon refolding, only a subset of MP had retained tubulin binding activity. Nevertheless, in control reactions where MP was absent, neither tubulin nor RNA (Fig. 16b5 and c6, respectively) was detected in pellet fractions, which confirmed that co-precipitation of either component had only occurred due to an interaction with MP. When MP-

conjugated beads were pre-incubated with tubulin before the addition of RNA, the amount of tubulin found in the pellet fraction was comparable to when tubulin was added alone (Fig. 16b2). However, the amount of detectable RNA in the pellet fraction was greatly reduced, which indicated that the MP:RNA interaction had been inhibited by the presence of tubulin (Fig. 16c2). Since RNA was able to bind MP in absence of tubulin, and indeed was present in a large molar excess over tubulin (when viewed in terms of nucleotides), it is likely that MP had a greater affinity for tubulin than RNA. In contrast, when RNA was incubated with MP-conjugated beads preceding the addition of tubulin, both components appeared to retain the capacity to interact with MP (Fig. 16c3 and b3, respectively), although to a lower level than when added alone. One possible explanation for this might be that tubulin out-competed RNA for an equivalent binding interface on the surface of MP. Although competitive effects cannot be ruled out, one might expect that at equilibrium, the level of pelleted material would be similar to when tubulin was added before RNA. Since both components were found in relatively high levels (and binding saturation had apparently occurred, not shown), it appeared that in fact a triple complex composed of MP, RNA and tubulin had formed. This being the case, it would suggest that although binding contacts essential for tubulin interactions were not entirely sequestered by the presence of RNA, there was a functional overlap between RNA and tubulin binding domains present within MP. Whether this putative molecular order of events would govern triple complex formation on the surface of polymerized tubulin, or indeed, whether such a complex would be viable *in planta* remains to be further analyzed.

(a)

Reaction	± MP	1st component	2nd component
1	+ MP	Tubulin	Buffer
2	+ MP	Tubulin	RNA
3	+ MP	RNA	Tubulin
4	+ MP	RNA	Buffer
5	- MP	Tubulin	Buffer
6	- MP	Tubulin	RNA

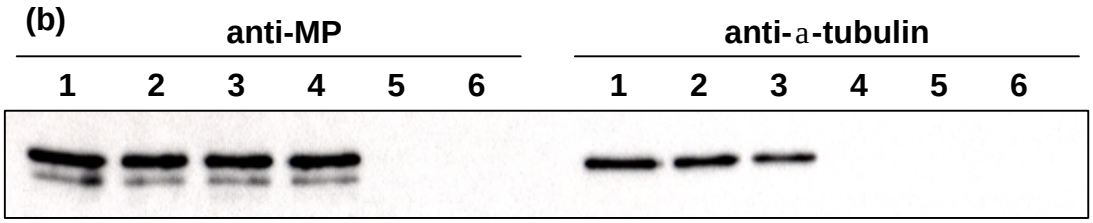

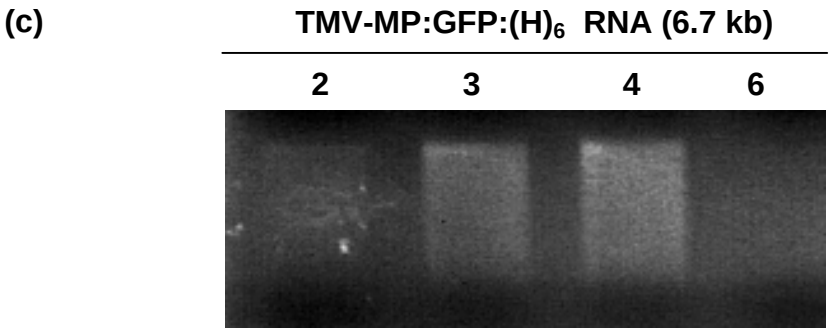

Figure 16 Co-precipitation of RNA and tubulin heterodimers *in vitro* using immobilized MP as an affinity bait. Using a two-step approach, Ni^{2+}-NTA beads conjugated to purified MP (theoretical max. 3.25 μM) were incubated in the presence of either a 6.7kb *in vitro* transcribed RNA (50 nM or ~300 μM polymerized nucleotide) or tubulin heterodimers (1.63 μM). Following this, tubulin, RNA or *pulldown buffer* were added to the beads, which were subsequently incubated and sedimented by centrifugation. Pelleted RNA was analyzed by 1 % non-denaturing agarose gel electrophoresis (**c**) and pelleted proteins were analyzed by SDS-PAGE and Western

blotting, using antibodies specific for MP and α-tubulin, respectively (**b**). The reaction combinations performed are summarized in Table (**a**) and correspond with the numbered lanes in (**b**) and (**c**). When added individually, both tubulin dimers (**b1**) and RNA (**c4**) appeared to co-sediment with MP, and in the corresponding supernatant fractions (not shown), detectable levels of both tubulin and RNA were observed which suggested that saturable binding had been achieved. In control reactions where MP was absent (reactions **5** and **6**), neither tubulin nor RNA appeared to interact with the sepharose beads, confirming a direct interaction with MP had occurred in both cases. When MP-conjugated beads were pre-incubated with tubulin preceding the addition of RNA, almost saturable binding of tubulin appeared to occur (**b2**), although under the conditions used, the capacity of RNA to interact with MP was severely impeded (**c2**). In contrast, when RNA was introduced before tubulin, both components appeared to bind MP (**b3** and **c3**), albeit to a lower level than when incubated alone with MP. Although inconclusive, these data suggest that at least in principle, an MP:RNA:MT triple complex is viable, and furthermore, residues within MP required for RNA binding may functionally overlap with those required to bind tubulin.

3.7 Apparent modulation of kinesin motor activity by MP

Since it has been described that microtubule association of MAP2 and tau proteins are inhibitory to molecular motor activity both *in vivo* (Ebneth *et al.*, 1998; Trinczek *et al.*, 1999; Stamer *et al.*, 2002) and *in vitro* (von Massow *et al.*, 1989; Lopez and Sheetz, 1993; Hagiwara *et al.*, 1994; Seitz *et al.*, 2002), we speculated that the interaction of MP with MTs may confer a similar effect. In order to test this hypothesis, we utilized the so-called 'MT gliding assay' whereby conventional human kinesin-1 was absorbed onto a glass surface before fluorescently labeled MTs were introduced in the presence or absence of purified MP (Materials and Methods section 2.5). Kinesin motor activity was then initiated with the addition of ATP and the rate of MT translocation was measured using digital fluorescence microscopy (Fig. 17a) by determining the relative position of at least 30 MT ends at known time intervals (150 velocity readings/experimental condition). In addition, the percentage of MTs undergoing any translocation was calculated for each respective experimental condition. In the absence of MP, the average velocity of kinesin-dependent MT translocation was found to be 0.20 ± 0.052 μm/sec (Fig. 17b), a value in agreement with previous reports (Seitz *et al.*, 2002). When 200 nM MP was added to the chamber prior to the initiation of kinesin motor activity, the average velocity of motile MTs was reduced to 0.16 ± 0.053 μm/sec (Fig. 17c), an interesting observation given that no discernible MP labeling on MTs was observed when equivalent MP:MT complexes were immunohistochemically labeled with an antibody specific for MP. Nevertheless, analysis of the mean values using a two-tailed unpaired *t*-test showed them to be statistically distinct ($P<0.001$, n = 150), which indicated that MP affected a weak inhibition on kinesin-dependent MT translocation. A more pronounced effect on the rate of MT translocation was observed

when 600 nM MP was used (0.14 ± 0.058 μm/sec), and although statistically different than the mean velocity resulting from 0 and 200 nM MP treatments, respectively (P<0.01, n = 150), it was apparent that the range of translocation speeds had deviated slightly from a normal distribution (Fig. 17d). Visual analysis of animated MT translocations recorded under the described conditions (supplementary data: www.fmi.ch/members/jamie.ashby) showed that, although the majority of MTs appeared to smoothly glide across the chamber surface, a number of motile MTs underwent intermittent stalling when ≥ 600 nM MP was used. Although stalling may account for the deviation from normally distributed data, it was apparent that due to this statistically irregular data spread at MP concentrations above 600 nM, reliable comparisons of average velocities could not be made. It should also be noted that, although not taken into account during velocity measurements, the percentage of motile MTs did appear to decrease concomitantly with increasing MP concentration (Fig. 17b-d). Moreover, when MP was used at either 850 nM or 1.0 μm, the percentage of motile MTs had decreased so dramatically (30.4 and 4.0 %, respectively) that the measurable sample population for determining velocity was below a reasonable statistical minimum. Interestingly, visual analysis of the few MTs actually translocating indicated that kinesin motor activity was largely unaffected in those isolated cases (www.fmi.ch/members/jamie.ashby). It is possible that these particular MTs represented a subset of the population which were only partially decorated with MP. Although the presence of MP did appear to modulate the overall rate of kinesin-dependent MT translocation, interpretation of these data with regard to the mechanism of inhibition remains somewhat tenuous. Under the experimental conditions applied, kinesin is predicted to be in a dimeric, processive form at a density of ~ 4000 molecules/μm^2 (Howard *et al.*, 1993; Moyer *et al.*, 1996). However, we have no

accurate knowledge of the polymerized tubulin concentration within the chamber. Visual comparisons before and after washing the chamber of unbound MTs showed that only a small percentage of introduced material actually adhered to the surface (not shown). Since each MT is therefore likely to be in favourable contact with several hundred kinesin molecules at any given time, one cannot determine whether inhibition arose due to a reduction in binding frequency between kinesin and tubulin, run length once bound or indeed modulation of kinesin motor activity itself. Current models for kinesin inhibition by microtubule-associated proteins favour a mechanism by which both proteins compete for equivalent binding contacts on β-tubulin, although once bound to the MT, kinesin is believed to translocate at normal rates (Lopez and Sheetz, 1993; Seitz *et al.*, 2002). It is unclear whether MP inhibits kinesin by a directly comparable mechanism, since if this were the case, one would not expect to observe a general decrease in MT translocation velocity at such a high density of kinesin. Although MP may indeed compete with kinesin for binding sites on tubulin, it remains plausible that the decreased rate of kinesin motor activity occurs by a more complex mechanism. In order for dimeric kinesins to translocate processively, one of the motor head domains must transiently dissociate from tubulin and move to the next available site in an ATP-dependent manner (Movie 6, www.fmi.ch/members/jamie.ashby). It could be speculated that the presence of MP on or in proximity to this second site imposes a steric constraint on such a kinesin motion, or moreover, directly impedes the so-called “power stroke” (Vale and Milligan, 2000). Intermittent stalling of MTs might then occur if one or more kinesin molecules are inhibited in this manner at a region of the MT which is decorated with particularly high levels of MP. Recovery from stalling might be orchestrated by the collective force of active kinesin motors which physically disrupt the non-motile kinesin:tubulin interaction or by displacement of the obstructive

MP. It was speculated that MP may directly bind to kinesin and inhibit motor activity by modulation of ATPase activity or steric hindrance. Although direct binding experiments are still required, preblocking of the perfusion chamber with 500 nM MP preceding the addition of MTs appeared to have a neglible effect on kinesin-dependent MT translocation, as determined visually (not shown). In addition, it was proposed that MP may bind non-specifically to the surface of the chamber, and at high concentrations, interact with MTs at stoichiometries sufficient to counteract kinesin force production i.e. anchor MTs to the surface. Non-specific effects of this nature cannot be discounted as the factor responsible for complete inhibition of motility at very high MP concentrations (> 600 nM), however, it is known that although MTs strongly adhere to plain glass surfaces, MT translocation can still be achieved if glass is preabsorbed with kinesin (von Massow *et al.*, 1989). Nevertheless, further experiments utilizing very low kinesin amounts or even single molecules (Howard *et al.*, 1989; Block *et al.*, 1990) at known MP:tubulin ratios are required in order to determine more precisely the mechanism by which MP apparently inhibits kinesin-1 motor activity *in vitro*.

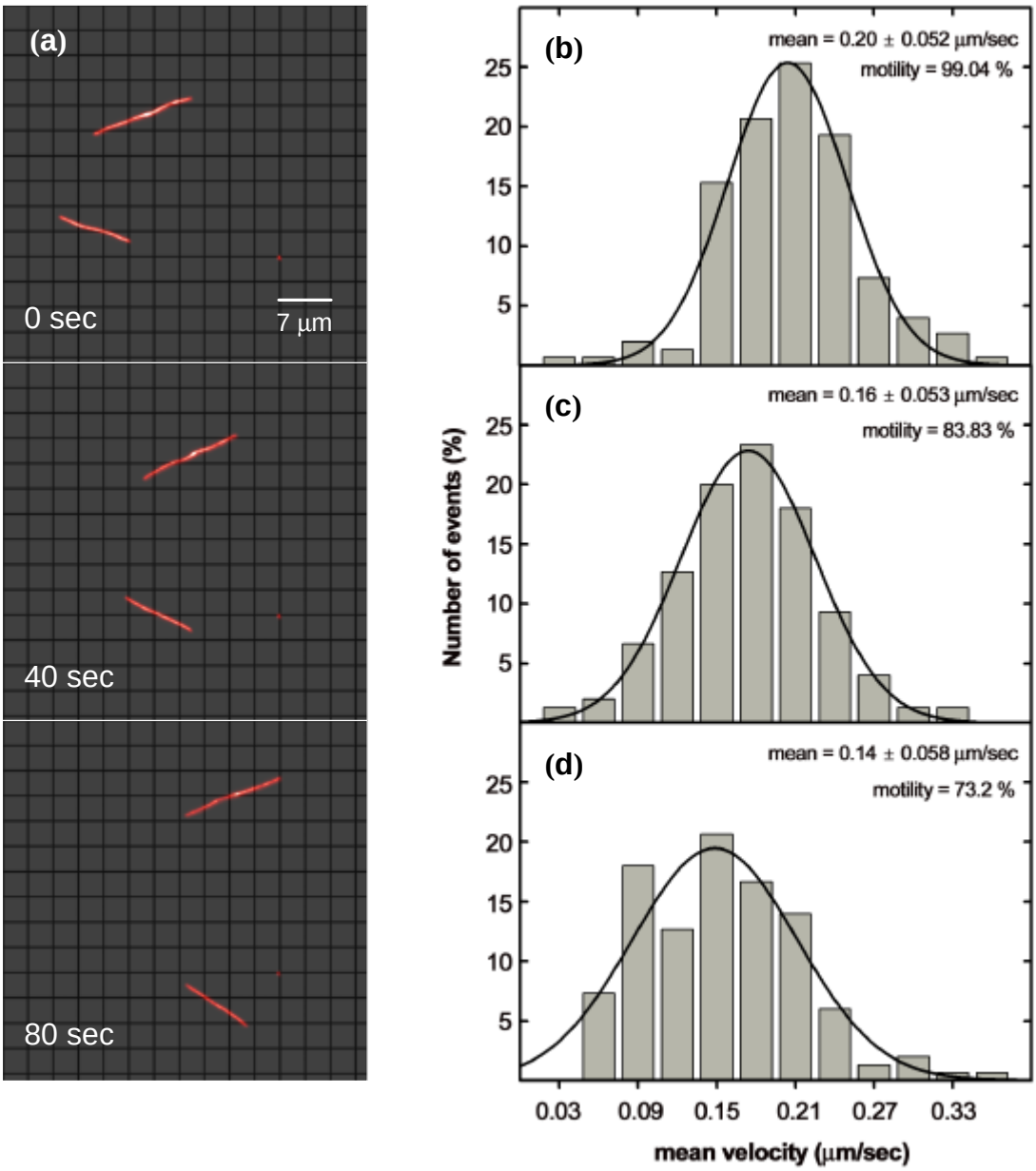

Figure 17 Apparent modulation of kinesin motor activity by MP *in vitro*. TRITC-labeled MTs (110 nM polymerized dimers) were absorbed to perfusion chambers precoated with GST-conjugated kinesin-1 and either buffer alone (**a** and **b**), 200 nM MP (**c**) or 600 nM MP (**d**) were perfused through the chamber and briefly incubated. Following the addition of *motility buffer*$^{+OS}$, images of "gliding" MTs were recorded by digital fluorescence microscopy, as illustrated in panel (**a**) and the velocity of MT translocation was determined by measuring the distance traveled by at least 30 individual MTs every 1.25 seconds for 2 minutes. Mean values (± S.D.) were determined from the pooled data (150 measurements per sample) and the percentage of MTs that underwent any translocation were also calculated for each respective

experimental condition. As can be seen in panels **b** and **c**, upon the introduction of 200 nM MP, the average velocity of kinesin-dependent MT translocation was reduced from 0.20 ± 0.052 μm/sec to 0.16 ± 0.053 μm/sec, respectively. Comparison of these means using an unpaired *t*-test showed that they were statistically unequal ($P<0.001$, n = 150), thereby suggesting that MP had a weak inhibitory effect on kinesin motor activity at this concentration. A further decrease in motility rate was found when 600 nM MP was used (0.14 ± 0.058 μm/sec), and although this figure was found to be statistically lower ($P<0.01$, n =150) than mean velocities resulting from 0 nM or 200 nM MP treatments, the data appeared to deviate slightly from a normal distribution. Irregularities in the data distribution became more pronounced when MP was employed at > 600 nM (not shown), and resulting mean values were not analyzed further. The percentage of MTs undergoing any motility also appeared to decrease with increasing concentrations of MP and at 1 μm MP, almost complete inhibition of MT motility was observed. Due to the high density of kinesin molecules (~ 4000 molecules/μm^2) and unknown tubulin concentration, it remains unclear as to the precise mechanism by which MP appeared to inhibit kinesin motor activity, however, these data may indicate that at low and high concentrations of MP, inhibition occurs via distinct modes of action.

4 Discussion

The experiments described in this thesis were performed in an attempt to further characterize the association of TMV movement protein (MP) with microtubules (MTs). At the onset of these studies, the available experimental evidence indicated that the MP:MT interaction was functionally required for vRNA trafficking. Briefly, MP was observed to redistribute from ER-derived replication sites onto MTs (Heinlein *et al.*, 1998; Gillespie *et al.*, 2002) and colocalize with vRNA at equivalent stages of infection (Más and Beachy, 1999). The appearance of MT-localized MP early during infection correlated with an increased rate of vRNA trafficking, and in cases where MP did not associate with MTs, intercellular vRNA spread was abolished (Kahn *et al.*, 1998; Boyko *et al.*, 2000a; Boyko *et al.*, 2000b). Although these observations provide a plausible argument for MT-dependent vRNA transport, it remains unclear whether MP:MT complexes directly engage in vRNA trafficking, or indeed, why the association of MP with MTs is usually observed relatively late during infection. Nevertheless, MP associates with MTs in a number of cell types, and based on the findings of this thesis, is proposed to function as a structural microtubule-associated protein (MAP). Possible mechanisms leading to the MP:MT association, and the potential consequences of such an interaction during TMV infection are discussed.

4.1 The MAP-like behaviour of MP

Upon ectopic expression, MP associates with MTs in tobacco leaf epidermal cells, BY-2 protoplasts, and COS-7 cells (Heinlein *et al.*, 1998; Boyko *et al.*, 2000a). The fact that viral replication and plant-encoded factors are dispensable for this association suggests that MP interacts with MTs in a specific manner, either by directly binding to tubulin, or via an accessory factor common to plants and animals. Furthermore, the

distribution of MP along MTs appears to be relatively uniform in most cases, which is consistent with the MT-localization of other MAPs known to directly interact with MTs, such as Tau in neurons or MAP65 in higher plants (Drewes *et al.*, 1998; Lloyd and Hussey, 2001). Following the identification of a region within MP sharing apparent homology to α- β- and γ-tubulins, it was proposed that MP may associate with MTs through a novel interaction involving 'dynamic coassembly' with polymerizing MTs (Boyko *et al.*, 2000a). Although tubulin mimicry cannot be discounted as a possible mechanism for mediating MP:MT interactions, the binding of MP to MTs *in vitro* is found to be independent of MT polymerization. Taken together with the localization data, it would seem that MP exhibits the basic characteristics of a structural MAP, and conceivably, might even modulate MT-dependent processes. A fundamental property of structural MAPs is their ability to stabilize MT dynamics (Wiche *et al.*, 1991). MTs initially form by the polymerization of tubulin dimers liganded to GTP. Through the hydrolytic activity of β-tubulin, GDP accumulates in the polymer structure and the resulting tubulin favors a curved configuration (Janosi *et al.*, 2002). MTs are thus rendered unstable and will rapidly depolymerize unless capped with GTP-tubulin or otherwise stabilized (Panda *et al.*, 2002; Caplow and Fee, 2003). Structural MAPs are thought to stabilize MTs by longitudinally crosslinking tubulin subunits and neutralizing the repulsive negative charges between dimers (Cassimeris and Spittle, 2001). The molecular mechanism by which MP stabilizes MTs is not understood, however, both *in vitro* and *in vivo*, the localization of MP to MTs appears to correlate with the inability of monoclonal antibodies to recognize C-terminal epitopes on α- or β-tubulin. Although MAPs have also been shown to bind the C-terminus of tubulin (Al-Bassam *et al.*, 2002), this apparent similarity to MP may be circumstantial given that MP shares no discernible sequence homology with any known MAP. Endogenous

MAPs interact with the acidic helices of tubulin by virtue of motifs rich in basic amino acids, and which are commonly arranged in tandem repeats (Olmsted, 1986; Downing, 2000). In MP, a single 42 residue basic domain has also been identified by computational analysis (Brill *et al.*, 2000). It has been demonstrated that deletion of this region leads to abolished MT association in TMV-infected plants (Boyko *et al.*, 2000c), and furthermore, this loss of MT binding corresponds with a change in the predicted net charge of MP:GFP from + 3.2 to – 2.8 at pH 7.5 (ProtParam, http://biobench.ph.chbs/aa/ProtParam/index.html). Although it is tempting to speculate that MP also binds MTs by ionic interactions, care should be taken when interpreting these findings, particularly as short N-terminal deletions and single point mutations outside of this basic region also confer a similar mislocalization of MP *in vivo* (Kahn *et al.*, 1998; Boyko *et al.*, 2000a; Boyko *et al.*, 2000c). During infection, the events leading up to the association of MP with MTs are not fully characterized. Therefore, it could be argued that not all MP mutants are equivalent with regard to dysfunction, as the observed loss of MT association *in vivo* could have arisen through the disruption of other upstream processes. By testing the ability of such mutant proteins to bind MTs *in vitro*, it may be possible to discriminate between domains and/or residues within MP that are essential for MT binding, and those which are involved other mechanisms, such as ER- or Pd-targeting. As mentioned above, MAPs are thought to stabilize MTs by traversing tubulin subunits and physically holding them together. Considering that MP only contains a single putative MT-binding domain, and is significantly smaller than most MAPs, what would explain the unusually high level of MT stability potentiated by MP? Perhaps the most attractive model involves the putative tubulin-mimicry domain of MP (Boyko *et al.*, 2000a). This region shares sequence similarity to the so-called tubulin ‘M-loop’, which is proposed to mediate lateral contacts between

tubulin protofilaments (Nogales *et al.*, 1999). Although rather speculative, MP may have the ability to emulate M-loop binding contacts, and by an unknown mechanism, strengthen the inter-protofilament interaction or perhaps counteract the curling forces imposed by GDP-β-tubulin. A similar stabilization mechanism is thought to occur in response to the anti-mitotic drug taxol, which binds in proximity to the nucleotide-binding domain of β-tubulin and makes interactions with the M-loop (Downing, 2000; Snyder *et al.*, 2001). However, because MP is larger than taxol by over an order of magnitude, one might expect that direct MP:tubulin binding contacts made at the protofilament interface would in fact be detrimental to the structural integrity of MTs. Certainly, one would expect to see aberrations within the microtubule lattice, but electron micrographs of MP:MT complexes assembled *in vitro* show filament structures to be relatively intact at low MP loads (not shown). Nevertheless, residues found within this mimicry domain of MP seem to be crucial for MP function, as disruption of this domain by point mutagenesis renders TMV temperature-sensitive with regard to cell-to-cell movement (Boyko *et al.*, 2000a). An alternative hypothesis to explain MP-induced MT stability might be the ability of MP to form stable oligomeric homocomplexes. It is known that *in vitro*, purified MP has a propensity to form aggregates unless conditions of low ionic strength are employed or micelle concentrations of detergent are present in the buffer (Waigmann and Zambryski, 1995; Brill *et al.*, 2000). Such oligomers were generally considered to have no functional relevance, however, it is conceivable that MP aggregation *in vitro* is simply a reflection of the chemical nature of this protein, and may represent a mode by which MP potentially 'overloads' MTs. Observations of MP:MT complexes *in situ* illustrate just how abundant MP is at the MT surface, and furthermore, immuno-gold labeling of MP:MT complexes formed *in vitro* has demonstrated that at high stoichiometries, MP

appears to form a sheath along the MT surface (not shown). Although further studies will be required to fully validate these findings, preliminary analyses indicate that these MP-derived structures are relatively uniform in size, and may be the result of a specific MP oligomer or at least an ordered, non-specific aggregate. Of course, the high levels of MP observed in association with MTs *in vitro* and *in vivo* may be the result of binding to sites other than the C-terminal helices. Supercomputer modeling of MTs using the Poisson-Boltzmann equation has revealed that much of the outer MT surface has a negative electrostatic potential and may be capable of interacting with the positively-charged MP (Baker *et al.*, 2001). Given that MP:MT complexes isolated from TMV-infected protoplasts or assembled *in vitro* remain stable under conditions of high ionic strength, a purely electrostatic interaction seems less likely. Unfortunately, results from the biochemical analysis of MP:MT interactions *in vitro* do not resolve the question of MP-induced MT stability further than suggesting that MP forms oligomers and/or binds multiple sites on the surface of MTs. In order to better characterize the mechanisms that govern this interaction, it may be necessary to image the complexes formed during infection at very high resolutions, a technically challenging endeavor.

4.2 MT-localization of MP in vivo

Although a functional relationship between the association of MP with MTs and intercellular spread of TMV infection is established (Boyko *et al.*, 2000a; Boyko *et al.*, 2000b), it remains unclear whether such MP:MT complexes can directly mediate vRNA transport. Furthermore, because MP exhibits the characteristics of a structural MAP, it has been suggested that late during infection, MP is involved in processes other than RNA trafficking. Nevertheless, vRNA transport appears to be *somehow* linked with the localization of MP to MTs, and therefore, further insight into the mechanism of MP-mediated RNA trafficking might be gained if one understands the

events which lead to formation of MP:MT complexes *in vivo*. During early stages of TMV infection, MP localizes to intersections of reticulated ER strands which subsequently aggregate to form large inclusion bodies. As infection proceeds into the mid stages, these large inclusions reduce in size and ER returns to a tubular form, concurrent with the appearance of MP in association with MTs (Heinlein *et al.*, 1998; Reichel and Beachy, 1998). Because the smaller aggregates appear to align with MTs, it has been proposed that MP is directly redistributed from ER onto neighbouring MTs (Heinlein, 2002b). Interestingly, biochemical fractionation experiments indicate that MP behaves as an integral ER-membrane protein, and consistent with this finding, two potential transmembrane helices have been identified in MP by computational analysis (Reichel *et al.*, 1999; Brill *et al.*, 2000). Furthermore, according to the model proposed by Brill *et al.* (2000), the putative MT binding region of MP is predicted to be accessible to the cytoplasm, which might suggest that ER-associated MP contacts the MT surface directly. Protein mediated interfaces between ER and MTs have been described in other systems (Terasaki *et al.*, 1986; Brandt *et al.*, 1995; Isenberg and Niggli, 1998; Maas *et al.*, 2000), and since MT-polymerization has been demonstrated to drive the modulation of tubulovesicular networks in *Xenopus* egg extracts (Waterman-Storer *et al.*, 1995), a similar mechanism has been proposed for the translocation of ER-associated TMV vRNPs. The results of this thesis indicate that polymerization is not required for the association of MP with MTs, and therefore, might suggest that a motor-dependent ER-gliding mechanism is more appropriate (Waterman-Storer and Salmon, 1998), if it indeed transpires that vRNP trafficking is a membrane-based process. Regardless, it still remains unclear how MP can apparently redistribute from small ER puncta onto the entire length of MTs without being observed in ER strands. Since evidence exists that TMV replication can occur on ER

without the formation of visible inclusion bodies (Boyko *et al.*, 2000c), it is conceivable that low levels of MP are actually transported through ER or translated proximal to MTs before accumulating on MTs to detectable amounts. Although ER-trafficking of MP has not been demonstrated, evidence does exist to support the concept of divergent MP transport pathways. For instance, when constitutively expressed in transgenic plants, MP fails to localize to MTs although Pd targeting appears to be largely unaffected (Reichel *et al.*, 1999). Although an interesting observation, Pd targeting alone is probably insufficient to support intercellular vRNA trafficking, since movement-deficient MP mutants unable to associate with MTs can still target and accumulate at Pd (Kahn *et al.*, 1998; Boyko *et al.*, 2000c). A possible link between the trafficking of vRNA and association of MP with MTs might be found when one looks at the mechanism by which other structural MAPs are deployed to MTs. In neurons, the axonal localization of Tau is dependent on 3' UTR *cis*-acting signals that direct *Tau* mRNA-containing granules to axonal MTs by a mechanism thought to involve the MT-dependent molecular motor protein KIF3a (Litman *et al.*, 1994; Behar *et al.*, 1995; Aranda-Abreu *et al.*, 1999; Aronov *et al.*, 2001; Aronov *et al.*, 2002). Other RNA-containing transport granules have been shown to contain several proteins, and in addition, translationally repressed ribosome:RNA complexes (Bassell *et al.*, 1998; Krichevsky and Kosik, 2001). In the case of *Tau* mRNA, it has been proposed that RNA movement and protein translation are interdependent mechanisms, although it is not clear whether Tau protein is synthesized by an axonal ribosome complex, or by co-transported factors (Aronov *et al.*, 2002). Nevertheless, it would seem that mRNA transport is a prerequisite to MT binding of Tau protein and it could be speculated that TMV MP is deployed to MTs using a similar mechanism. A common feature of RNA localization appears to be that transcripts are translationally

repressed during transit and derepressed when the final destination is reached (Jansen, 2001; Kloc *et al.*, 2002). Although it is conceivable that TMV would have little requirement for such a regulatory mechanism, MP:RNA complexes formed *in vitro* do not appear to support translation unless MP is phosphorylated (Karpova *et al.*, 1997; Karpova *et al.*, 1999). These sites of phosphorylation have not been identified, however, it is interesting to note that upon isolation of detergent-resistant MT fractions from TMV-infected protoplasts, MT-associated MP is focused in at least 4 spots of equivalent molecular weight on 2D-PAGE gels, which is consistent with protein phosphorylation (not shown). Furthermore, addition of unmodified MP to MT-enriched plant extracts results in rapid MP phosphorylation (not shown), thus supporting the concept that MP and TMV-specific might be co-transported along MTs in a translationally competent manner. How then might this complex arise? Since ectopically expressed MP also localizes to MTs, other viral components and specific *cis*-acting elements within genomic vRNA appear to be dispensable. It is plausible that sequences present within the MP ORF directly connect the RNP complex to a pre-existing transport complex, but because MP is translated from a subgenomic RNA, this would perhaps not fully explain the translocation of genomic vRNA. Alternatively, it may be possible that by virtue of cytoplasmically accessible domains, MP can directly interact with a motor protein and bud off from ER in the form of a ribosome-containing ER vesicle. A similar type of complex has been described to transport the dendrite localized developmental factor Purα (Ohashi et al., 2002), and may represent an analogous transport system to that proposed for TMV. Furthermore, preliminary observations of MP:GFP at very early stages of TMV-infection indicate that MP-containing granules move within the cytoplasm at rates consistent with motor-dependent trafficking. Although granule movement along microtubule filaments has

yet to be demonstrated, translocation does appear to occur in a saltatory, but directional fashion (Boyko *et al*., unpublished observations). If motor-based vesicular trafficking proves to be the mechanism responsible for vRNA movement, it would possibly clarify the apparently contradictory observations that MT is required for RNA transport, but the MP:MT complex is highly stable, and therefore, unlikely to support movement. It would be logical to propose that as vRNA is transported along MT networks in a granule, MP is constitutively translated, and due to its intrinsic ability to interact with MTs, accumulates on the MT surface. Preliminary evidence suggests that *in vitro*, MP does not directly compete with either Tau or MAP2 for equivalent binding sites, but can still apparently interact with MTs. Although it cannot be ruled out that MP actually bound these MAPs non-specifically, this result indicates that a direct interaction between MP and MTs *in vivo* may indeed be possible. Furthermore, the MAP-like distribution of MP *in vivo* may actually be a consequence of vRNA transport, but plays a specialized secondary role during mid to late stages of infection. Certainly, it will be imperative to distinguish between early and late MP:MT interactions in order to understand intracellular vRNA movement. A possible way to achieve this may be to determine the relative localization of TMV RNA and MP in relation to MT and ER compartments following silencing of the genes encoding kinesin and kinesin-like proteins. Although a loss of TMV movement and MP/RNA localization to MTs could result from indirect cytopathic effects, this approach may provide circumstantial evidence to support motor-dependent transport. Additionally, it may be possible to identify factors involved in such a transport complex by biochemical fractionation of MP-containing granules or by immunoprecipitation experiments.

4.3 Role of the MP:MT interaction

In most cases, MP can only be observed to associate with MTs in cells behind the leading edge of infection. Since the position of cells within the infection site indicates the temporal stage of viral infection, the MP:MT association is likely to take place following successful replication and cell-to-cell spread of the viral genome. Considering that MP may function as a MAP and that MP:MT interactions possibly represent a secondary feature of MT-based RNA transport, what possible role could the MP:MT complexes have during infection? Although rather open to interpretation, one suggestion is that MP provides a stable network of MTs along which viral trafficking can occur. Because MTs are highly dynamic, developmentally regulated organelles (Wasteneys, 2002; Shaw *et al.*, 2003), such stabilization may conceivably prolong the ability of TMV to traffic its genome. Sustained vRNA transport would not seem to be an essential process, since the viral genome would have probably entered neighbouring cells prior to this event, however, subtle effects on the efficiency of TMV spread cannot be discounted. An alternative proposal has been that MT-associated MP is actually part of a host-directed degradation pathway. It has been demonstrated that MP is polyubiquitinated in TMV-infected protoplasts, and furthermore, ubiquitination is enhanced following the addition of 26S proteasome inhibitors (Reichel and Beachy, 2000). Based on MP:GFP localization studies, inhibition of the 26S proteasome also leads to the apparent redistribution of MP from MTs to the ER-membranes of protoplasts and leaf epidermal cells during mid stages of infection (Reichel and Beachy, 2000; Gillespie *et al.*, 2002). While it is highly likely that a host plant would attempt to defend itself against viral invasion using such a degradation system, certain aspects regarding the involvement of MTs are unclear. The fact that proteins destined for proteasomal degradation localize to the perinucleus (Hellmann and Estelle, 2002;

Vierstra, 2003) may be incompatible with the organization of plant MTs. Following cytokinesis, MTs are certainly known to extend from the nucleus toward the cell cortex, however, throughout most of interphase, plant MTs are arranged cortically (Wasteneys, 2002). Furthermore, this cortical arrangement is commonly seen when MP is in association with MTs (Fig.14). It is claimed that because proteasome inhibition leads to MP distribution patterns consistent with a MP mutant enhanced in movement, ER-localized MP is indicative of protein that has evaded a MT-based degradation pathway (Gillespie *et al.*, 2002). However, it is also likely that proteasome inhibition would result in an overaccumulation of ubiquitinated proteins that were unable to *leave* the targeting pathway because the destination complex was inactive. This would then suggest that 26S proteasome targeting of MP is mediated by ER during infection, and not MTs. When overexpressed in CHO cells and neurons, the structural MAP Tau is known to inhibit the kinesin-dependent trafficking of vesicles, ER and mitochondria (Ebneth *et al.*, 1998; Stamer *et al.*, 2002). Experimental evidence described in this thesis supports the concept that when abundant on the surface of MTs, MP also has the ability to inhibit kinesin motor activity. What impact this putative action would have on viral infection is far from understood, however, it has been speculated that by inhibiting endogenous MT-dependent trafficking, MP is somehow affecting a counter-defense strategy. Sequence-specific RNA silencing has been proposed to function as a plant defense response against invading pathogens (Lindbo *et al.*, 1993; Covey *et al.*, 1997; Ratcliff *et al.*, 1997; Ratcliff *et al.*, 1999). Once activated by the recognition of foreign nucleic acids, sequence-specific signals can spread systemically and direct the targeting and degradation of these RNAs. TMV is an RNA virus which appears to avoid the effects of gene silencing during infection. It is not clear how TMV evades this potent defense mechanism, and it may in fact relate to modulation of Pd or simply

the speed of viral movement. However, one proposal is that MP decorated MTs cannot support the trafficking of silencing signals, and thus reduces the effectiveness of silencing against viral replication. Since the exact nature of silencing signals, and the mechanism by which they traffic is not fully understood, it must be conceded that this theory is largely speculative. Nevertheless, it would be interesting to determine whether silencing responses against infection could be elicited by the introduction of short dsRNAs with sequence homology to TMV RNA, and furthermore, whether these responses related in any way to the level of MP in association with MTs.

5 References

Ackmann, M., Wiech, H. and Mandelkow, E. (2000) Nonsaturable binding indicates clustering of tau on the microtubule surface in a paired helical filament-like conformation. *J Biol Chem* **275**: 30335-43.

Ainger, K., Avossa, D., Morgan, F., Hill, S. J., Barry, C., Barbarese, E. and Carson, J. H. (1993) Transport and localization of exogeneous myelin basic protein mRNA microinjected into oligodendrocytes. *J Cell Biol* **123**: 431-441.

Al-Bassam, J., Ozer, R. S., Safer, D., Halpain, S. and Milligan, R. A. (2002) MAP2 and tau bind longitudinally along the outer ridges of microtubule protofilaments. *J Cell Biol* **157**: 1187-96.

Allan, V. and Vale, R. (1994) Movement of membrane tubules along microtubules in vitro: evidence for specialised sites of motor attachment. *J Cell Sci* **107 (Pt 7)**: 1885-1897.

Aoki, S. and Takebe, I. (1975) Replication of tobacco mosaic virus RNA in tobacco mesophyll protoplasts *in vitro. Virology* **65**: 343-354.

Aranda-Abreu, G. E., Behar, L., Chung, S., Furneaux, H. and Ginzburg, I. (1999) Embryonic lethal abnormal vision-like RNA-binding proteins regulate neurite outgrowth and tau expression in PC12 cells. *J Neurosci* **19**: 6907-17.

Aronov, S., Aranda, G., Behar, L. and Ginzburg, I. (2001) Axonal tau mRNA localization coincides with tau protein in living neuronal cells and depends on axonal targeting signal. *J Neurosci* **21**: 6577-87.

Aronov, S., Aranda, G., Behar, L. and Ginzburg, I. (2002) Visualization of translated tau protein in the axons of neuronal P19 cells and characterization of tau RNP granules. *J Cell Sci* **115**: 3817-27.

Atkins, D., Hull, R., Wells, B., Roberts, K., Moore, P. and Beachy, R. N. (1991) The tobacco mosaic virus 30K movement protein in transgenic tobacco plants is localized to plasmodesmata. *J Gen Virol.* **72**: 209-211.

Baker, N. A., Sept, D., Joseph, S., Holst, M. J. and McCammon, J. A. (2001) Electrostatics of nanosystems: application to microtubules and the ribosome. *Proc Natl Acad Sci U S A* **98**: 10037-41.

Baron-Epel, O., Hernandez, D., Jiang, L. W., Meiners, S. and Schindler, M. (1988) Dynamic continuity of cytoplasmic and membrane compartments between plant cells. *J Cell Biol* **106**: 715-721.

Bass, B. L. (2000) Double-stranded RNA as a template for gene silencing. *Cell* **101**: 235-238.

Bassell, G. J., Zhang, H., Byrd, A. L., Femino, A. M., Singer, R. H., Taneja, K. L., Lifshitz, L. M., Herman, I. M. and Kosik, K. S. (1998) Sorting of beta-actin mRNA and protein to neurites and growth cones in culture. *J Neurosci* **18**: 251-265.

Beach, D. L., Salmon, E. D. and Bloom, K. (1999) Localization and anchoring of mRNA in budding yeast. *Curr Biol* **9**: 569-78.

Behar, L., Marx, R., Sadot, E., Barg, J. and Ginzburg, I. (1995) cis-acting signals and trans-acting proteins are involved in tau mRNA targeting into neurites of differentiating neuronal cells. *Int J Dev Neurosci* **13**: 113-27.

Bertrand, E., Chartrand, P., Schaefer, M., Shenoy, S. M., Singer, R. H. and Long, R. M. (1998) Localization of ASH1 mRNA particles in living yeast. *Mol Cell* **2**: 437-45.

Block, S. M., Goldstein, L. S. B. and Schnapp, B. J. (1990) Bead movement by single kinesin molecules studied with optical tweezers. *Nature* **348**: 348-352.

Bobola, N., Jansen, R. P., Shin, T. H. and Nasmyth, K. (1996) Asymmetric accumulation of Ash1p in postanaphase nuclei depends on a myosin and restricts yeast mating-type switching to mother cells. *Cell* **84**: 699-709.

Bohl, F., Kruse, C., Frank, A., Ferring, D. and Jansen, R. P. (2000) She2p, a novel RNA-binding protein tethers ASH1 mRNA to the Myo4p myosin motor via She3p. *EMBO J* **19**: 5514-24.

Bohm, K. J., Vater, W., Fenske, H. and Unger, E. (1984) Effect of microtubule-associated proteins on the protofilament number of microtubules assembled in vitro. *Biochim Biophys Acta* **800**: 119-26.

Bohrmann, J. and Biber, K. (1994) Cytoskeleton-dependent transport of cytoplasmic particles in previtellogenic to mid-vitellogenic ovarian follicles of Drosophila: time-lapse analysis using video-enhanced contrast microscopy. *J Cell Sci* **107 (Pt 4)**: 849-58.

Boyko, V., Ashby, J. A., Suslova, E., Ferralli, J., Sterthaus, O., Deom, C. M. and Heinlein, M. (2002) Intramolecular complementing mutations in *Tobacco mosaic virus* movement protein confirm a role for microtubule association in viral RNA transport. *J Virol* **76**: 3974-3980.

Boyko, V., Ferralli, J., Ashby, J., Schellenbaum, P. and Heinlein, M. (2000a) Function of microtubules in intercellular transport of plant virus RNA. *Nat Cell Biol* **2**: 826-832.

Boyko, V., Ferralli, J. and Heinlein, M. (2000b) Cell-to-cell movement of TMV RNA is temperature-dependent and corresponds to the association of movement protein with microtubules. *Plant J* **22**: 315-325.

Boyko, V., van der Laak, J., Ferralli, J., Suslova, E., Kwon, M.-O. and Heinlein, M. (2000c) Cellular targets of functional and dysfunctional mutants of tobacco mosaic virus movement protein fused to GFP. *J Virol* **74**: 11339-11346.

Bradford, M. M. (1976) A rapid and sensitive method for the quantification of microgram quantities of protein utilizing the principle of protein-dye binding. *Anal Biochem* **72**: 248-254.

Brandt, R., Leger, J. and Lee, G. (1995) Interaction of tau with the neural plasma membrane mediated by tau's amino-terminal projection domain. *J Cell Biol* **131**: 1327-40.

Braun, R. E., Behringer, R. R., Peschon, J. J., Brinster, R. L. and Palmiter, R. D. (1989) Genetically haploid spermatids are phenotypically diploid. *Nature* **337**: 373-6.

Brendza, R. P., Serbus, L. R., Duffy, J. B. and Saxton, W. M. (2000) A function for kinesin I in the posterior transport of *oskar* mRNA and Staufen protein. *Science* **289**: 2120-2122.

Brill, L. M., Nunn, R. S., Kahn, T. W., Yeager, M. and Beachy, R. N. (2000) Recombinant tobacco mosaic virus movement protein is an RNA-binding, alpha-helical membrane protein. *Proc Natl Acad Sci USA* **97**: 7112-7117.

Buck, K. W. (1999) Replication of tobacco mosaic virus RNA. *Philos Trans R Soc Lond B Biol Sci* **354**: 613-27.

Caldwell, K. A. and Handel, M. A. (1991) Protamine transcript sharing among postmeiotic spermatids. *Proc Natl Acad Sci U S A* **88**: 2407-11.

Caplow, M. and Fee, L. (2003) Concerning the chemical nature of tubulin subunits that cap and stabilize microtubules. *Biochemistry* **42**: 2122-6.

Carson, J. H., Worboys, K., Ainger, K. and Barbarese, E. (1997) Translocation of myelin basic protein mRNA in oligodendrocytes requires microtubules and kinesin. *Cell Motil Cytoskeleton* **38**: 318-28.

Carvalho, P., Tirnauer, J. S. and Pellman, D. (2003) Surfing on microtubule ends. *Trends Cell Biol* **13**: 229-37.

Cassimeris, L. and Spittle, C. (2001) Regulation of microtubule-associated proteins. *Int Rev Cytol* **210**: 163-226.

Chartrand, P., Singer, R. H. and Long, R. M. (2001) RNP localization and transport in yeast. *Annu Rev Cell Dev Biol* **17**: 297-310.

Chen, J. J., Janssen, B. J., Williams, A. and Sinha, N. (1997) A gene fusion at a homeobox locus: alterations in leaf shape and implications for morphological evolution. *Plant Cell* **9**: 1289-304.

Choi, S. B., Wang, C., Muench, D. G., Ozawa, K., Franceschi, V. R., Wu, Y. and Okita, T. W. (2000) Messenger RNA targeting of rice seed storage proteins to specific ER subdomains. *Nature* **407**: 765-7.

Chretien, D., Metoz, F., Verde, F., Karsenti, E. and Wade, R. H. (1992) Lattice defects in microtubules: protofilament numbers vary within individual microtubules. *J Cell Biol* **117**: 1031-40.

Citovsky, V., Knorr, D., Schuster, G. and Zambryski, P. (1990) The P30 movement protein of tobacco mosaic virus is a single-stranded nucleic acid binding protein. *Cell* **60**: 637-647.

Citovsky, V., Wong, M. L., Shaw, A. L., Venkataram Prasad, B. V. and Zambryski, P. (1992) Visualization and characterization of tobacco mosaic virus movement protein binding to single-starnded nucleic acids. *Plant Cell* **4**: 397-411.

Clark, I., Giniger, E., Ruohola-Baker, H., Jan, L. Y. and Jan, Y. N. (1994) Transient posterior localization of a kinesin fusion protein reflects anteroposterior polarity of the Drosophila oocyte. *Curr Biol* **4**: 289-300.

Clark, I. E., Jan, L. Y. and Jan, Y. N. (1997) Reciprocal localization of Nod and kinesin fusion proteins indicates microtubule polarity in the Drosophila oocyte, epithelium, neuron and muscle. *Development* **124**: 461-70.

Cooperstock, R. L. and Lipshitz, H. D. (2001) RNA localization and translational regulation during axis specification in the Drosophila oocyte. *Int Rev Cytol* **203**: 541-66.

Covey, S. N., Al-Kaff, N. S., Langara, A. and Turner, D. S. (1997) Plants combat infection by gene silencing. *Nature* **385**: 781-782.

Dabora, S. L. and Scheetz, M. P. (1988) The microtubule dependent formation of a tubulovascular network with characteristics of the endoplasmic reticulum from cultured cell extracts. *Cell* **54**: 27-35.

Davies, E., Fillingham, B. D., Oto, Y. and Abe, S. (1991) Evidence for the existence of cytoskeleton-bound polysomes in plants. *Cell Biol Int Rep* **15**: 973-81.

Dawson, W. O., Bubrick, P. and Grantham, G. L. (1988) Modifications of the tobacco mosaic virus coat protein gene affecting replication, movement, and symptomatology. *Phytopathology* **78**: 783-789.

Dawson, W. O., Schlegel, D. E. and Lung, M. C. Y. (1975) Synthesis of tobacco mosaic virus in intact tobacco leaves systemically inoculated by differential temperature treatment. *Virology* **65**: 565-573.

Deom, C. M., Oliver, M. J. and Beachy, R. N. (1987) The 30-kilodalton gene product of tobacco mosaic virus potentiates virus movement. *Science* **237**: 384-389.

Derry, W. B., Wilson, L. and Jordan, M. A. (1995) Substoichiometric binding of taxol suppresses microtubule dynamics. *Biochemistry* **34**: 2203-11.

Deshler, J. O., Highett, M. I. and Schnapp, B. J. (1997) Localization of Xenopus Vg1 mRNA by Vera protein and the endoplasmic reticulum. *Science* **276**: 1128-31.

Ding, B., Haudenshield, J. S., Hull, R. J., Wolf, S., Beachy, R. N. and Lucas, W. J. (1992) Secondary plasmodesmata are specific sites of localization of the tobacco mosaic virus movement protein in transgenic tobacco plants. *Plant Cell* **4**: 915-928.

Ding, B., Li, Q., Nguyen, L., Palukaitis, P. and Lucas, W. J. (1995) Cucumber mosaic virus 3a protein potentiates cell-to-cell trafficking of CMV RNA in tobacco plants. *Virology* **207**: 345-353.

Döhner, K., Wolfstein, A., Prank, U., Echeverri, C., Dujardin, D., Vallee, R. and Soseik, B. (2002) Function of dynein and dynactin in herpes simplex virus capsid transport. *Mol Biol Cell* **13**: 2795-2809.

Dorokhov, Y. L., Alexandrov, N. M., Miroshnichenko, N. A. and Atabekov, J. G. (1983) Isolation and analysis of virus-specific ribonucleoprotein of tobacco mosaic virus-infected tobacco. *Virology* **127**: 237-252.

Dorokhov, Y. L., Alexandrova, N. M., Miroshnichenko, N. A. and Atabekov, J. G. (1984) The informosome-like virus-specific ribonucleoprotein (vRNP) may be involved in the transport of tobacco mosaic virus infection. *Virology* **137**: 127-134.

Downing, K. H. (2000) Structural basis for the interaction of tubulin with proteins and drugs that affect microtubule dynamics. *Annu Rev Cell Dev Biol* **16**: 89-111.

Downing, K. H. and Nogales, E. (1998) Tubulin stucture: insights into microtubule properties and functions. *Curr Opin Struct Biol* **8**: 789-791.

Drewes, G., Ebneth, A. and Mandelkow, E. M. (1998) MAPs, MARKs and microtubule dynamics. *Trends Biochem Sci* **23**: 307-11.

Drygin, Y. F., Bordunova, O. A., Gallyamov, M. O. and Yaminsky, I. V. (1998) Atomic force microscopy examination of tobacco mosaic virus and virion RNA. *FEBS Lett* **425**: 217-21.

Duncan, J. E. and Warrior, R. (2002) The cytoplasmic dynein and kinesin motors have interdependent roles in patterning the Drosophila oocyte. *Curr Biol* **12**: 1982-91.

Ebneth, A., Godemann, R., Stamer, K., Illenberger, S., Trinczek, B., Mandelkow, E.-M. and Mandelkow, E. (1998) Overexpression of Tau protein inhibits kinesin-dependent trafficking of vesicles, mitochondria and endoplasmic reticulum: implications for Alzheimer's disease. *J Cell Biol* **143**: 777-794.

Echeverri, C. J., Paschal, B. M., Vaughan, K. T. and Vallee, R. B. (1996) Molecular characterization of the 50-kD subunit of dynactin reveals function for the

complex in chromosome alignment and spindle organization during mitosis. *J Cell Biol* **132**: 617-33.

Edgar, B. A., Kiehle, C. P. and Schubiger, G. (1986) Cell cycle control by the nucleo-cytoplasmic ratio in early Drosophila development. *Cell* **44**: 365-72.

Edgar, B. A., Odell, G. M. and Schubiger, G. (1987) Cytoarchitecture and the patterning of fushi tarazu expression in the Drosophila blastoderm. *Genes Dev* **1**: 1226-37.

Elbashir, S. M., Harborth, J., Lendeckel, W., Yalcin, A., Weber, K. and Tuschl, T. (2001) Duplexes of 21-nucleotide RNAs mediate RNA interference in cultured mammalian cells. *Nature* **411**: 494-8.

Elisha, Z., Havin, L., Ringel, I. and Yisraeli, J. K. (1995) Vg1 RNA binding protein mediates the association of Vg1 RNA with microtubules in Xenopus oocytes. *EMBO J* **14**: 5109-14.

Enquist, L. W. (2002) Break ins and break outs: Viral interactions with the cytoskeleton of mammalian cells. *Annu Rev Cell Dev Biol* **18**: 135-161.

Epel, B. L., Padgett, H. S., Heinlein, M. and Beachy, R. N. (1996) Plant virus movement protein dynamics probed with a GFP-protein fusion. *Gene* **173**: 75-79.

Farrell, K. W., Jordan, M. A., Miller, H. P. and Wilson, L. (1987) Phase dynamics at microtubule ends: the coexistence of microtubule length changes and treadmilling. *J Cell Biol* **104**: 1035-46.

Ferguson, H. A. and Goodrich, J. A. (2001) Expression and purification of recombinant human c-Fos/c-Jun that is highly active in DNA binding and transcriptional activation in vitro. *Nucleic Acids Res* **29**: E98.

Ferrandon, D., Elphick, L., Nüsslein-Volhard, C. and St Johnston, D. (1994) Staufen protein associates with the 3'UTR of *bicoid* mRNA to form particles that move in a microtubule-dependent manner. *Cell* **79**: 1221-1232.

Forristall, C., Pondel, M., Chen, L. and King, M. L. (1995) Patterns of localization and cytoskeletal association of two vegetally localized RNAs, Vg1 and Xcat-2. *Development* **121**: 201-8.

Fujiwara, T., Giesman-Cookmeyer, D., Ding, B., Lommel, S. A. and Lucas, W. J. (1993) Cell-to-cell trafficking of macromolecules through plasmodesmata potentiated by the red clover necrotic mosaic virus movement protein. *Plant Cell* **5**: 1783-1794.

Fukata, Y., Itoh, T. J., Kimura, T., Menager, C., Nishimura, T., Shiromizu, T., Watanabe, H., Inagaki, N., Iwamatsu, A., Hotani, H. et al. (2002) CRMP-2 binds to tubulin heterodimers to promote microtubule assembly. *Nat Cell Biol* **4**: 583-91.

Fullilove, S. L. and Jacobson, A. G. (1971) Nuclear elongation and cytokinesis in Drosophila montana. *Dev Biol* **26**: 560-77.

Gillespie, T., Boevink, P., Haupt, S., Roberts, A. G., Toth, R., Vantine, T., Chapman, S. and Oparka, K. J. (2002) Functional analysis of a DNA shuffled movement protein reveals that microtubules are dispensable for the cell-to-cell movement of tobacco mosaic virus. *Plant Cell* **14**: 1207-1222.

Glotzer, J. B., Saffrich, R., Glotzer, M. and Ephrussi, A. (1997) Cytoplasmic flows localize injected oskar RNA in Drosophila oocytes. *Curr Biol* **7**: 326-37.

Goelet, P., Lomonossoff, G. P., Butler, P. J., Akam, M. E., Gait, M. J. and Karn, J. (1982) Nucleotide sequence of tobacco mosaic virus RNA. *Proc Natl Acad Sci U S A* **79**: 5818-22.

Gutzeit, H. O. (1986) The role of microfilaments in cytoplasmic streaming in Drosophila follicles. *J Cell Sci* **80**: 159-69.

Haarer, B. K., Petzold, A., Lillie, S. H. and Brown, S. S. (1994) Identification of MYO4, a second class V myosin gene in yeast. *J Cell Sci* **107 (Pt 4)**: 1055-64.

Hafen, E., Kuroiwa, A. and Gehring, W. J. (1984) Spatial distribution of transcripts from the segmentation gene fushi tarazu during Drosophila embryonic development. *Cell* **37**: 833-41.

Hagiwara, H., Yorifuji, H., Sato-Yoshitake, R. and Hirokawa, N. (1994) Competition between motor molecules (kinesin and cytoplasmic dynein) and fibrous microtubule-associated proteins in binding to microtubules. *J Biol Chem* **269**: 3581-3589.

Hamilton, A., Voinnet, O., Chappel, L. and Baulcombe, D. (2002) Two classes of short interfering RNA in RNA silencing. *EMBO J* **21**: 4671-4679.

Hamilton, A. J. and Baulcombe, D. C. (1999) A species of small antisense RNA in posttranscriptional gene silencing in plants. *Science* **286**: 950-952.

Han, J. R., Yiu, G. K. and Hecht, N. B. (1995) Testis/brain RNA-binding protein attaches translationally repressed and transported mRNAs to microtubules. *Proc Natl Acad Sci U S A* **92**: 9550-4.

Haywood, V., Kragler, F. and Lucas, W. J. (2002) Plasmodesmata: pathways for protein and ribonucleoprotein signaling. *Plant Cell* **Supplement**: S303-S325.

Heinlein, M. (2002a) Plasmodesmata:dynamic regulation and role in macromolecular cell-to-cell signalling. *Curr Opin Plant Biol* **5**: 543-552.

Heinlein, M. (2002b) The spread of Tobacco mosaic virus infection: insights into the cellular mechanism of RNA transport. *Cell Mol Life Sci* **59**: 58-82.

Heinlein, M., Epel, B. L., Padgett, H. S. and Beachy, R. N. (1995) Interaction of tobamovirus movement proteins with the plant cytoskeleton. *Science* **270**: 1983-1985.

Heinlein, M., Padgett, H. S., Gens, J. S., Pickard, B. G., Casper, S. J., Epel, B. L. and Beachy, R. N. (1998) Changing patterns of localization of the tobacco mosaic virus movement protein and replicase to the endoplasmic reticulum and microtubules during infection. *Plant Cell* **10**: 1107-1120.

Hellmann, H. and Estelle, M. (2002) Plant development: regulation by protein degradation. *Science* **297**: 793-797.

Hills, G. J., Plaskitt, K. A., Young, N. D., Dunigan, D. D., Watts, J. W., Wilson, T. M. A. and Zaitlin, M. (1987) Immunogold localization of the intracellular sites of structural and nonstructural tobacco mosaic virus proteins. *Virology* **161**: 488-496.

Hollinshead, M., Rodger, G., Van Eijl, H., Law, M., Hollinshead, R., Vaux, D. J. T. and Smith, G. L. (2001) Vaccinia virus utilizes microtubules for movement to the cell surface. *J Cell Biol* **154**: 389-402.

Holt, C. A. and Beachy, R. N. (1991) In vivo complementation of infectious transcripts from mutant tobacco mosaic virus cDNAs in transgenic plants. *Virology* **181**: 109-117.

Howard, J., Hudspeth, A. J. and Vale, R. D. (1989) Movement of microtubules by single kinesin molecules. *Nature* **342**: 154-158.

Howard, J., Hunt, A. J. and Baek, S. (1993) Assay of microtubule movement driven by single kinesin molecules. *In 'Methods in Cell Biology'* **39**: 137-147.

Howard, J. and Hyman, A. A. (2003) Dynamics and mechanics of the microtubule plus end. *Nature* **422**: 753-8.

Hulme, E. C. and Birdsall, N. J. M. (1991). Strategy and tactics in receptor-binding studies. In *Receptor-ligand interactions: a practical approach*, pp. 63-174. Oxford: Oxford University Press.

Isenberg, G. and Niggli, V. (1998) Interaction of cytoskeletal proteins with membrane lipids. *Int Rev Cytol* **178**: 73-125.

Ishikawa, M., Meshi, T., Ohno, T. and Okada, Y. (1991) Specific cessation of minus-strand RNA accumulation at an early stage of tobacco mosaic virus infection. *J Virol* **65**: 861-868.

Jackson, A. O., Mitchell, D. M. and Siegel, A. (1971) Replication of tobacco mosaic virus. I. Isolation and characterization of double-stranded forms of ribonucleic acid. *Virology* **45**: 182-91.

Jackson, D. and Hake, S. (1997) Morphogenesis on the move: cell-to-cell trafficking of plant regulatory proteins. *Curr Opin Genet Devel* **7**: 495-500.

Janosi, I. M., Chretien, D. and Flyvbjerg, H. (2002) Structural microtubule cap: stability, catastrophe, rescue, and third state. *Biophys J* **83**: 1317-30.

Jansen, R.-P. (2001) mRNA localization: message on the move. *Nat Rev Mol Cell Biol* **2**: 1-10.

Jansen, R. P., Dowzer, C., Michaelis, C., Galova, M. and Nasmyth, K. (1996) Mother cell-specific HO expression in budding yeast depends on the unconventional myosin myo4p and other cytoplasmic proteins. *Cell* **84**: 687-97.

Januschke, J., Gervais, L., Dass, S., Kaltschmidt, J. A., Lopez-Schier, H., St Johnston, D., Brand, A. H., Roth, S. and Guichet, A. (2002) Polar transport in the Drosophila oocyte requires Dynein and Kinesin I cooperation. *Curr Biol* **12**: 1971-81.

Johnstone, O. and Lasko, P. (2001) Translational regulation and RNA localization in Drosophila oocytes and embryos. *Annu Rev Genet* **35**: 365-406.

Kahn, T. W., Lapidot, M., Heinlein, M., Reichel, C., Cooper, B., Gafny, R. and Beachy, R. N. (1998) Domains of the TMV movement protein involved in subcellular localization. *Plant J* **15**: 15-25.

Karpova, O. V., Ivanov, K. I., Rodionova, P., Dorokhov, Y. L. and Atabekov, J. G. (1997) Nontranslatability and dissimilar behavior in plants and protoplasts of viral RNA and movement protein complexes formed *in vitro. Virology* **230**: 11-21.

Karpova, O. V., Rodionova, N. P., Ivanov, K. I., Kozlovsky, S. V., Dorokhov, Y. L. and Atabekov, J. G. (1999) Phosphorylation of tobacco mosaic virus movement protein abolishes its translation repressing ability. *Virology* **261**: 20-24.

Kim, J. Y., Yan, Z., Cilia, M., Khalfan-Jagani, Z. and Jackson, D. (2002) Intercellular trafficking of a *KNOTTED1* green fluorescent protein fusion in the leaf and shoot meristem of *Arabidopsis. Proc Natl Acad Sci USA* **99**: 4103-4108.

Kim, M., Canio, W., Kessler, S. and Sinha, N. (2001) Developmental changes due to long-distance movement of a homeobox fusion transcript in tomato. *Science* **293**: 287-289.

Kim, W., Li, X. and Okita, T. (1993) Expression of storage protein multigene families in developing rice endosperm. *Plant Cell Physiol* **34**: 595-603.

Kimura, T., Hashimoto, I., Nishikawa, M. and Fujisawa, J. I. (1996) A role for Rev in the association of HIV-1 gag mRNA with cytoskeletal beta-actin and viral protein expression. *Biochimie* **78**: 1075-80.

Kiselyova, O. I., Yaminsky, I. V., Karger, E. M., Frolova, O. Y., Dorokhov, Y. I. and Atabekov, J. G. (2001) Visualization by atomic force microscopy if tobacco mosaic virus movement protein-RNA complexes formed in vitro. *J Gen Virol* **82**: 1503-1508.

Klahre, U., Crete, P., Leuenberger, S. A., Iglesias, V. A. and Meins, F. J. (2002) High molecular weight RNAs and small interfering RNAs induce systemic posttranscriptional gene silencing in plants. *Proc Natl Acad Sci USA* **99**: 11981-11986.

Kloc, M., Bilinski, S., Chan, A. P., Allen, L. H., Zearfoss, N. R. and Etkin, L. D. (2001) RNA localization and germ cell determination in Xenopus. *Int Rev Cytol* **203**: 63-91.

Kloc, M., Zearfoss, N. R. and Etkin, L. D. (2002) Mechanisms of subcellular mRNA localization. *Cell* **108**: 533-44.

Klotz, I. M. (1946) The application of the law of mass action to binding by proteins: interactions with calcium. *Arch Biochem* **9**: 109-117.

Knowles, R. B., Sabry, J. H., Martone, M. E., Deerinck, T. J., Ellisman, M. H., Bassell, G. J. and Kosik, K. S. (1996) Translocation of RNA granules in living neurons. *J Neurosci* **16**: 7812-20.

Kotlizky, G., Katz, A., van der Laak, J., Boyko, V., Lapidot, M., Beachy, R. N., Heinlein, M. and Epel, B. L. (2001) A dysfunctional movement protein of *Tobacco mosaic virus* interferes with targeting of wild type movement protein to microtubules. *Mol Plant Microbe Interact* **7**: 895-904.

Krichevsky, A. M. and Kosik, K. S. (2001) Neuronal RNA granules: a link between RNA localization and stimulation-dependent translation. *Neuron* **32**: 683-96.

Krishnan, H. B., Franceschi, V. R. and Okita, T. W. (1986) Immunochemical studies on the role of the golgo complex in protein-body formation in rice seeds. *Planta* **169**: 471-480.

Kristensson, K., Holmes, K. V., Duchala, C. S., Zeller, N. K., Lazzarini, R. A. and Dubois-Dalcq, M. (1986) Increased levels of myelin basic protein transcripts in virus-induced demyelination. *Nature* **322**: 544-7.

Kühn, C., Franceschi, V. R., Schulz, A., Lemoine, R. and Frommer, W. B. (1997) Macromolecular trafficking indicated by localization and turnover of sucrose transporters in enucleate sieve elements. *Science* **275**: 1298-1300.

Kuhn, C., Quick, W. P., Schultz, A., Sonnewald, U. and Frommer, W. B. (1996) Companion cell-specific inhibition of the potato sucrose transporter SUT1. *Plant Cell & Envir* **19**: 1115-1123.

Lall, S., Francis-Lang, H., Flament, A., Norvell, A., Schupbach, T. and Ish-Horowicz, D. (1999) Squid hnRNP protein promotes apical cytoplasmic transport and localization of Drosophila pair-rule transcripts. *Cell* **98**: 171-80.

Lebeurier, G. and Hirth, L. (1966) Effect of elevated temperatures on the development of two strains of tobacco mosaic virus. *Virology* **29**: 385-395.

Lee, C. and Chen, L. B. (1988) Dynamic behavior of endoplasmic reticulum in living cells. *Cell* **54**: 37-46.

Lee, J. C. and Timasheff, S. N. (1977) In vitro reconstitution of calf brain microtubules: effects of solution variables. *Biochemistry* **16**: 1754-64.

Lehto, K., Bubrick, P. and Dawson, W. O. (1990) Time course of TMV 30k protein accumulation in intact leaves. *Virology* **174**: 290-293.

Lewandowski, D. J. and Dawson, W. O. (2000) Functions of the 126- and 183-kDa proteins of tobacco mosaic virus. *Virology* **271**: 90-8.

Li, Q. and Palukaitis, P. (1996) Comparison of the nucleic acid- and NTP-binding properties of the movement protein of cucumber mosaic cucumovirus and tobacco mosaic tobamovirus. *Virology* **216**: 71-79.

Li, X., Franceschi, V. R. and Okita, T. W. (1993) Segregation of storage protein mRNAs on the rough endoplasmic reticulum membranes of rice endosperm cells. *Cell* **72**: 869-79.

Lindbo, J. A., Silva-Rosales, L., Proebsting, W. M. and Dougherty, W. G. (1993) Induction of a highly specific antiviral state in transgenic plants: implications for regulation of gene expression and virus resistance. *Plant Cell* **5**: 1749-1759.

Litman, P., Barg, J. and Ginzburg, I. (1994) Microtubules are involved in the localization of tau mRNA in primary neuronal cell cultures. *Neuron* **13**: 1463-74.

Liu, B., Dai, R., Tian, C. J., Dawson, L., Gorelick, R. and Yu, X. F. (1999) Interaction of the human immunodeficiency virus type 1 nucleocapsid with actin. *J Virol* **73**: 2901-8.

Lloyd, C. and Hussey, P. (2001) Microtubule-associated proteins in plants--why we need a MAP. *Nat Rev Mol Cell Biol* **2**: 40-7.

Long, R. M., Gu, W., Lorimer, E., Singer, R. H. and Chartrand, P. (2000) She2p is a novel RNA-binding protein that recruits the Myo4p-She3p complex to ASH1 mRNA. *EMBO J* **19**: 6592-601.

Long, R. M., Singer, R. H., Meng, X., Gonzalez, I., Nasmyth, K. and Jansen, R. P. (1997) Mating type switching in yeast controlled by asymmetric localization of ASH1 mRNA. *Science* **277**: 383-7.

Lopez, L. A. and Sheetz, M. P. (1993) Steric inhibition of cytoplasmic dynein and kinesin motility by MAP2. *Cell Motil Cytoskeleton* **24**: 1-16.

Lucas, W. J., Bouche-Pillon, S., Jackson, D. P., Nguyen, L., Baker, L., Ding, B. and Hake, S. (1995) Selective trafficking of KNOTTED1 homeodomain protein and its RNA through plasmodesmata. *Science* **270**: 1980-1983.

Lucas, W. J. and van der Schoot, C. (1993) Plasmodesmata and the supracellular nature of plants. *New Phytol* **125**: 435-476.

Lucas, W. J., Yoo, B.-C. and Kragler, F. (2001) RNA as a long-distance information macromolecule in plants. *Nat Rev Mol Cell Biol* **2**: 849-857.

Maas, T., Eidenmuller, J. and Brandt, R. (2000) Interaction of tau with the neural membrane cortex is regulated by phosphorylation at sites that are modified in paired helical filaments. *J Biol Chem* **275**: 15733-40.

Mabit, H., Nakano, M. Y., Prank, U., Saam, B., Döhner, K., Sodeik, B. and Greber, U. F. (2002) Intact microtubules support adenovirus and herpes simplex virus infections. *J Virol* **76**: 9962-9971.

Mallardo, M., Schleich, S. and Krijnse Locker, J. (2001) Microtubule-dependent organization of vaccinia virus core-derived early mRNAs into distinct cytoplasmic structures. *Mol Biol Cell* **12**: 3875-91.

Martelli, G. P. and Russo, M. (1977) Plant virus inclusion bodies. *Adv Virus Res* **21**: 175-266.

Martin, A., O'Hare, P., McLauchlan, J. and Elliott, G. (2002) Herpes simplex virus tegument protein VP22 contains overlapping domains for cytoplasmic localization, microtubule interaction, and chromatin binding. *J Virol* **76**: 4961-70.

Martin, S. G., Leclerc, V., Smith-Litiere, K. and Johnston, D. S. (2003) The identification of novel genes required for Drosophila anteroposterior axis formation in a germline clone screen using GFP-Staufen. *Development* **130**: 4201-15.

Más, P. and Beachy, R. N. (1998) Distribution of TMV movement protein in single living protoplasts immobilized in agarose. *Plant J* **15**: 835-842.

Más, P. and Beachy, R. N. (1999) Replication of tobacco mosaic virus on endoplasmic reticulum and role of the cytoskeleton and virus movement in intracellular distribution of viral RNA. *J Cell Biol* **147**: 945-958.

McLean, B. G., Zupan, J. and Zambryski, P. C. (1995) Tobacco mosaic virus movement protein associates with the cytoskeleton in tobacco plants. *Plant Cell* **7**: 2101-2114.

Melton, D. A. (1987) Translocation of a localized maternal mRNA to the vegetal pole of Xenopus oocytes. *Nature* **328**: 80-2.

Meshi, T., Watanabe, Y., Saito, T., Sugimoto, A., Maeda, T. and Okada, Y. (1987) Function of the 30 kd protein of tobacco mosaic virus: involvement in cell-to-cell movement and dispensability for replication. *EMBO J* **6**: 2557-2563.

Mlotshwa, S., Voinnet, O., Mette, M. F., Matzke, M., Vaucheret, H., Ding, S. W., Pruss, G. and Vance, V. B. (2002) RNA silencing and the mobile silencing signal. *Plant Cell* **Supplement**: S289-S301.

Moore, P., Frenczik, C. A., Deom, C. M. and Beachy, R. N. (1992) Developmental changes in plasmodesmata in transgenic tobacco expressing the movement protein of tobacco mosaic virus. *Protoplasma* **170**: 115-127.

Morales, C. R., Lefrancois, S., Chennathukuzhi, V., El-Alfy, M., Wu, X., Yang, J., Gerton, G. L. and Hecht, N. B. (2002) A TB-RBP and Ter ATPase complex accompanies specific mRNAs from nuclei through the nuclear pores and into intercellular bridges in mouse male germ cells. *Dev Biol* **246**: 480-94.

Motulsky, H. and Christopoulos, A. (2003). Fitting models to data using linear and non-linear regression: a practical guide to curve fitting: Oxford University Press.

Mouland, A. J., Mercier, J., Luo, M., Bernier, L., DesGroseillers, L. and Cohen, E. A. (2000) The double-stranded RNA-binding protein Staufen is incorporated in human immunodeficiency virus type 1: evidence for a role in genomic RNA encapsidation. *J Virol* **74**: 5441-51.

Mouland, A. J., Xu, H., Cui, H., Krueger, W., Munro, T. P., Prasol, M., Mercier, J., Rekosh, D., Smith, R., Barbarese, E. et al. (2001) RNA trafficking signals in human immunodeficiency virus type 1. *Mol Cell Biol* **21**: 2133-43.

Moyer, M. L., Gilbert, S. P. and Johnson, K. A. (1996) Purification and characterization of two monomeric kinesin constructs. *Biochemistry* **35**: 6321-6329.

Muench, D. G., Wu, Y., Coughlan, S. J. and Okita, T. W. (1998) Evidence for a Cytoskeleton-Associated Binding Site Involved in Prolamine mRNA Localization to the Protein Bodies in Rice Endosperm Tissue. *Plant Physiol* **116**: 559-69.

Munchow, S., Sauter, C. and Jansen, R. P. (1999) Association of the class V myosin Myo4p with a localised messenger RNA in budding yeast depends on She proteins. *J Cell Sci* **112 (Pt 10)**: 1511-8.

Mundry, K. W., Watkins, P. A. C., Ashfield, T., Plaskitt, K. A., Eisele-Walter, S. and Wilson, T. M. A. (1991) Complete uncoating of the 5' leader sequence of tobacco mosaic virus RNA occurs rapidly and is required to initiate cotranslational virus disassembly *in vitro*. *J Gen Virol* **72**: 769-777.

Nilsson-Tillgren, T. (1970) Studies on the biosynthesis of TMV. 3. Isolation and characterization of the replicative form and the replicative intermediate RNA. *Mol Gen Genet* **109**: 246-56.

Nilsson-Tillgren, T., Kielland-Brandt, M. C. and Bekke, B. (1974) Studies on the biosynthesis of tobacco mosaic virus. VI. On the subcellular localization of double-stranded viral RNA. *Mol Gen Genet* **128**: 157-169.

Nogales, E., Whittaker, M., Milligan, R. A. and Downing, K. H. (1999) High-resolution model of the microtubule. *Cell* **96**: 70-88.

Norby, J. G., Ottolenghi, P. and Jensen, J. (1980) Scatchard plot: common misinterpretation of binding experiments. *Anal Biochem* **102**: 318-320.

Noueiry, A. O., Lucas, W. J. and Gilbertson, R. L. (1994) Two proteins of a plant virus coordinate nuclear and plasmodesmal transport. *Cell* **76**: 925-932.

Nunez, E., Wei, X., Delgado, C., Rodriguez-Crespo, I., Yelamos, B., Gomez-Gutierrez, J., Peterson, D. L. and Gavilanes, F. (2001) Cloning, expression, and purification of histidine-tagged preS domains of hepatitis B virus. *Protein Expr Purif* **21**: 183-91.

Ohashi, S., Koike, K., Omori, A., Ichinose, S., Ohara, S., Kobayashi, S., Sato, T. A. and Anzai, K. (2002) Identification of mRNA/protein (mRNP) complexes containing Purα, mStaufen, fragile X protein, and myosin Va and their association with rough endoplasmic reticulum equipped with a kinesin motor. *J Biol Chem* **277**: 37804-10.

Okita, T. W. and Choi, S. B. (2002) mRNA localization in plants: targeting to the cell's cortical region and beyond. *Curr Opin Plant Biol* **5**: 553-9.

Okita, T. W., Li, X. and Roberts, M. W. (1994) Targeting of mRNAs to domains of the endoplasmic reticulum. *Trends Cell Biol* **4**: 91-96.

Okita, T. W. and Rogers, J. C. (1996) Compartmentation of proteins in the endomembrane system of plant cells. *Annu Rev Plant Physiol Plant Mol Biol* **47**: 327-350.

Olmsted, J. (1986) Microtubule-associated proteins. *Annu Rev Cell Biol* **2**: 421-457.

Ooshika, I., Watanabe, Y., Meshi, T., Okada, Y., Igano, K., Inouye, K. and Yoshida, N. (1984) Identification of the 30 k protein of TMV by immunoprecipitation with antibodies directed against a synthetic peptide. *Virology* **132**: 71-78.

Oparka, K. J., Prior, D. A. M., Santa Cruz, S., Padgett, H. S. and Beachy, R. N. (1997) Gating of epidermal plasmodesmata is restricted to the leading edge of expanding infection sites of tobacco mosaic virus. *Plant J* **12**: 781-789.

Ori, N., Juarez, M. T., Jackson, D., Yamaguchi, J., Banowetz, G. M. and Hake, S. (1999) Leaf senescence is delayed in tobacco plants expressing the maize homeobox gene knotted1 under the control of a senescence-activated promoter. *Plant Cell* **11**: 1073-80.

Osman, T. A. and Buck, K. W. (1996) Complete replication in vitro of tobacco mosaic virus RNA by a template-dependent, membrane-bound RNA polymerase. *J Virol* **70**: 6227-6234.

Palacios, I. M. and St Johnston, D. (2001) Getting the message across: the intracellular localization of mRNAs in higher eukaryotes. *Annu Rev Cell Dev Biol* **17**: 569-614.

Palacios, I. M. and St Johnston, D. (2002) Kinesin light chain-independent function of the Kinesin heavy chain in cytoplasmic streaming and posterior localisation in the Drosophila oocyte. *Development* **129**: 5473-85.

Palauqui, J.-C., Elmayan, T., Pollien, J.-M. and Vaucheret, H. (1997) Systemic aquired silencing: transgene-specific post-transcriptional silencing is transmitted by grafting from silenced stocks to non-silenced scions. *EMBO J* **16**: 4738-4745.

Palukaitis, P., Garcia-Arenal, F., Sulzinski, M. A. and Zaitlin, M. (1983) Replication of tobacco mosaic virus. VII. Further characterization of single- and double-stranded virus-related RNAs from TMV-infected plants. *Virology* **131**: 533-545.

Panda, D., Miller, H. P. and Wilson, L. (2002) Determination of the size and chemical nature of the stabilizing "cap" at microtubule ends using modulators of polymerization dynamics. *Biochemistry* **41**: 1609-17.

Pedrotti, B., Soffientini, A. and Islam, K. (1993) Sulphonate buffers affect the recovery of microtubule-associated proteins MAP1 and MAP2: evidence that MAP1A promotes microtubule assembly. *Cell Motil Cytoskeleton* **25**: 234-42.

Pfeiffer, D. C. and Gard, D. L. (1999) Microtubules in Xenopus oocytes are oriented with their minus-ends towards the cortex. *Cell Motil Cytoskeleton* **44**: 34-43.

Pokrywka, N. J. and Stephenson, E. C. (1991) Microtubules mediate the localization of bicoid RNA during Drosophila oogenesis. *Development* **113**: 55-66.

Pokrywka, N. J. and Stephenson, E. C. (1995) Microtubules are a general component of mRNA localization systems in *Drosophila* oocytes. *Dev Biol* **167**: 363-370.

Porath, J., Carlsson, J., Olsson, I. and Belfrage, G. (1975) Metal chelate affinity chromatography, a new approach to protein fractionation. *Nature* **258**: 598-9.

Ralph, R. K., Bullivant, S. and Wojcik, S. J. (1971) Cytoplasmic membranes as a possible site of tobacco mosaic virus RNA replication. *Virology* **43**: 713-716.

Ratcliff, F., Harrison, B. D. and Baulcombe, D. C. (1997) A similarity between viral defense and gene silencing in plants. *Science* **276**: 1558-1560.

Ratcliff, F. G., MacFarlane, S. A. and Baulcombe, D. C. (1999) Gene silencing without DNA: RNA-mediated cross-protection between viruses. *Plant Cell* **11**: 1207-1215.

Reichel, C. and Beachy, R. N. (1998) Tobacco mosaic virus infection induces severe morphological changes of the endoplasmatic reticulum. *Proc Natl Acad Sci USA* **95**: 11169-11174.

Reichel, C. and Beachy, R. N. (2000) Degradation of the tobacco mosaic virus movement protein by the 26S proteasome. *J Virol* **74**: 3330-3337.

Reichel, C., Más, P. and Beachy, R. N. (1999) The role of the ER and cytoskeleton in plant viral trafficking. *Trends Plant Sci* **4**: 458-463.

Rickoll, W. L. (1976) Cytoplasmic continuity between embryonic cells and the primitive yolk sac during early gastrulation in Drosophila melanogaster. *Dev Biol* **49**: 304-10.

Riechmann, V. and Ephrussi, A. (2001) Axis formation during Drosophila oogenesis. *Curr Opin Genet Dev* **11**: 374-83.

Rietdorf, J., Ploubidou, A., Reckmann, I., Holmström, A., Frischknecht, F., Zettl, M., Zimmermann, T. and Way, M. (2001) Kinesin-dependent movement on microtubules precedes actin-based motility of vaccinia virus. *Nature Cell Biol* **3**: 992-1000.

Robards, A. W. and Lucas, W. J. (1990) Plasmodesmata. *Annu. Rev. Plant Physiol. Plant Mol Biol* **41**: 369-419.

Rosenthal, H. E. (1967) A graphic method for the determination and presentation of binding parameters in a complex system. *Anal Biochem* **20**: 525-532.

Ruiz-Medrano, R., Xoconostle0Cazares, B. and Lucas, W. J. (1999) Phloem long-distance transport of CmNACP mRNA: implications for supracellular regulation in plants. *Development* **126**: 4405-4409.

Saito, T., Meshi, T., Takamatsu, N. and Okada, Y. (1987) Coat protein gene sequence of tobacco mosaic virus encodes a host response determinant. *Proc Natl Acad Sci USA* **84**: 6074-6077.

Sambrook, J. and Russell, D. W. (2001). Molecular cloning: a laboratory manual: Cold Spring Harbour Laboratory Press.

Sami-Subbu, R., Choi, S. B., Wu, Y., Wang, C. and Okita, T. W. (2001) Identification of a cytoskeleton-associated 120 kDa RNA-binding protein in developing rice seeds. *Plant Mol Biol* **46**: 79-88.

Scatchard, G. (1949) The attraction of proteins for small molecules and ions. *Ann N.Y. Acad Sci* **51**: 660-662.

Schmies, G., Chizhov, I. and Engelhard, M. (2000) Functional expression of His-tagged sensory rhodopsin I in Escherichia coli. *FEBS Lett* **466**: 67-9.

Schnorrer, F., Bohmann, K. and Nüsslein-Volhard, C. (2000) The molecular motor dynein is involved in targeting swallow and bicoid RNA to the anterior pole of Drosophila oocytes. *Nat Cell Biol* **2**: 185-190.

Schwartz, S. P., Aisenthal, L., Elisha, Z., Oberman, F. and Yisraeli, J. K. (1992) A 69-kDa RNA-binding protein from Xenopus oocytes recognizes a common motif in two vegetally localized maternal mRNAs. *Proc Natl Acad Sci U S A* **89**: 11895-9.

Seitz, A., Kojima, H., Oiwa, K., Mandelkow, E.-M., Song, Y.-H. and Mandelkow, E. (2002) Single-molecule investigation of the interference between kinesin, tau and MAP2c. *EMBO J* **21**: 4896-4905.

Shaw, J. G. (1999) Tobacco mosaic virus and the study of early events in virus infections. *Phil Trans R Soc Lond B* **354**: 603-611.

Shaw, S. L., Kamyar, R. and Ehrhardt, D. W. (2003) Sustained microtubule treadmilling in Arabidopsis cortical arrays. *Science* **300**: 1715-8.

Shevchenko, A., Wilm, M., Vorm, O. and Mann, M. (1996) Mass spectrometric sequencing of proteins silver-stained polyacrylamide gels. *Anal Chem* **68**: 850-8.

Siegel, A., Hari, V. and Kolacz, K. (1978) The effect of tobacco mosaic virus infection on host and virus-specific protein synthesis in protoplasts. *Virology* **85**: 494-503.

Sil, A. and Herskowitz, I. (1996) Identification of asymmetrically localized determinant, Ash1p, required for lineage-specific transcription of the yeast HO gene. *Cell* **84**: 711-22.

Sinha, N. (1999) Leaf development in angiosperms. *Annu Rev Plant Physiol Plant Mol Biol* **50**: 419-446.

Snyder, J. P., Nettles, J. H., Cornett, B., Downing, K. H. and Nogales, E. (2001) The binding conformation of Taxol in beta-tubulin: a model based on electron crystallographic density. *Proc Natl Acad Sci U S A* **98**: 5312-6.

Sodeik, B. (2000) Mechanisms of viral transport in the cytoplasm. *Trends Microbiol* **8**: 465-472.

Spittle, C. S. and Cassimeris, L. (1996) Mechanisms blocking microtubule minus end assembly: evidence for a tubulin dimer-binding protein. *Cell Motil Cytoskeleton* **34**: 324-35.

St Johnston, D., Driever, W., Berleth, T., Richstein, S. and Nusslein-Volhard, C. (1989) Multiple steps in the localization of bicoid RNA to the anterior pole of the Drosophila oocyte. *Development* **107 Suppl**: 13-9.

Stamer, K., Vogel, R., Thies, E., Mandelkow, E. and Mandelkow, E.-M. (2002) Tau blocks traffic of organelles, neurofilaments and APP vesicles in neurons and enhances oxidative stress. *J Cell Biol* **156**: 1051-1063.

Steeves, T. A. and Sussex, I. M. (1989). Patterns in plant development. Cambridge: Cambridge University Press.

Stern, D. B. and Gruissem, W. (1987) Control of plastid gene expression: 3' inverted repeats act as mRNA processing and stabilizing elements, but do not terminate transcription. *Cell* **51**: 1145-1157.

Strathern, J. N. and Herskowitz, I. (1979) Asymmetry and directionality in production of new cell types during clonal growth: the switching pattern of homothallic yeast. *Cell* **17**: 371-81.

Takizawa, P. A., Sil, A., Swedlow, J. R., Herskowitz, I. and Vale, R. D. (1997) Actin-dependent localization of an RNA encoding a cell-fate determinant in yeast. *Nature* **389**: 90-3.

Takizawa, P. A. and Vale, R. D. (2000) The myosin motor, Myo4p, binds Ash1 mRNA via the adapter protein, She3p. *Proc Natl Acad Sci U S A* **97**: 5273-8.

Tang, G., Reinhart, B. J., Bartel, D. P. and Zamore, P. D. (2003) A biochemical framework for RNA silencing in plants. *Genes Dev* **17**: 49-63.

Terasaki, M., Chen, L. B. and Fujiwara, K. (1986) Microtubules and the endoplasmic reticulum are highly interdependent structures. *J Cell Biol* **103**: 1557-1568.

Theurkauf, W. E., Smiley, S., Wong, M. L. and Alberts, B. M. (1992) Reorganization of the cytoskeleton during Drosophila oogenesis: implications for axis specification and intercellular transport. *Development* **115**: 923-36.

Timasheff, S. N. (2002) Protein-solvent preferential interactions, protein hydration, and the modulation of biochemical reactions by solvent components. *Proc Natl Acad Sci U S A* **99**: 9721-6.

Tomenius, K., Clapham, D. and Meshi, T. (1987) Localization by immunogold cytochemistry of the virus-coded 30K protein in plasmodesmata of leaves infected with tobacco mosaic virus. *Virology* **160**: 363-371.

Trinczek, B., Ebneth, A., Mandelkow, E.-M. and Mandelkow, E. (1999) Tau regulates the attachment/detachment but not the speed of motors in microtubule-dependent transport of single vesicles and organelles. *J. Cell Sci.* **112**: 2355-2367.
Tsiantis, M. (2001) Control of shoot cell fate: beyond homeoboxes. *Plant Cell* **13**: 733-8.

Turner, F. R. and Mahowald, A. P. (1976) Scanning electron microscopy of Drosophila embryogenesis. 1. The structure of the egg envelopes and the formation of the cellular blastoderm. *Dev Biol* **50**: 95-108.

Vale, R. D. and Milligan, R. A. (2000) The way things move: looking under the hood of molecular motor proteins. *Science* **288**: 88-95.

Van den Berg, C., Willemsen, V., Hage, W. and Scheres, B. (1995) Cell fate in the *Arabidopsis* root meristem determined by directional signaling. *Nature* **378**: 62-65.

van Eeden, F. J., Palacios, I. M., Petronczki, M., Weston, M. J. and St Johnston, D. (2001) Barentsz is essential for the posterior localization of oskar mRNA and colocalizes with it to the posterior pole. *J Cell Biol* **154**: 511-23.

Vanitharani, R., Chellappan, P. and Fauquet, C. M. (2003) Short interfering RNA-mediated interference of gene expression and viral DNA accumulation in cultured plant cells. *Proc Natl Acad Sci U S A* **100**: 9632-6.

Verity, A. N. and Campagnoni, A. T. (1988) Regional expression of myelin protein genes in the developing mouse brain: in situ hybridization studies. *J Neurosci Res* **21**: 238-48.

Vierstra, R. D. (2003) The ubiquitin/26S proteasome pathway, the complex last chapter in the life of many plant proteins. *Trends Plant Sci* **8**: 135-42.

Voinnet, O. and Baulcombe, D. C. (1997) Systemic signaling in gene silencing. *Nature* **389**: 553.

von Massow, A., Mandelkow, E.-M. and Mandelkow, E. (1989) Interaction between kinesin, microtubules and microtubule-associated protein 2. *Cell Motil Cytoskeleton* **14**: 562-571.

Waigmann, E., Lucas, W., Citovsky, V. and Zambryski, P. (1994) Direct functional assay for tobacco mosaic virus cell-to-cell movement protein and identification of a domain involved in increasing plasmodesmal permeability. *Proc Natl Acad Sci USA* **91**: 1433-1437.

Waigmann, E. and Zambryski, P. (1995) Tobacco mosaic virus movement protein-mediated protein transport between trichome cells. *Plant Cell* **7**: 2069-2079.

Wasteneys, G. O. (2002) Microtubule organization in the green kingdom: chaos or self-order? *J Cell Sci* **115**: 1345-54.

Watanabe, Y., Emori, Y., ooshika, I., Meshi, T., Ohno, T. and Okada, Y. (1984) Synthesis of TMV-specific RNAs and proteins at the early stage of infection in tobacoo protoplasts: transient expression of 30k protein and its mRNA. *Virology* **133**: 18-24.

Watanabe, Y. and Okada, Y. (1986) *In vitro* viral RNA synthesis by a subcellular fraction of TMV-inoculated tobacco protoplasts. *Virology* **149**: 73-74.

Waterhouse, P. M., Wang, M.-B. and Finnegan, E. J. (2001) Role of short RNAs in gene silencing. *Trends Plant Sci* **6**: 297-301.

Waterman-Storer, C. and Salmon, E. D. (1998) Endoplasmic reticulum membrane tubules are distributed by microtubules in living cells using three distinct mechanisms. *Curr Biol* **8**: 798-806.

Waterman-Storer, C. M., Gregory, J., Parsons, S. F. and Salmon, E. D. (1995) Membrane/microtubule tip attachment complexes (TACs) allow the assembly dynamics of plus ends to push and pull membranes into tubulovesicular networks in interphase Xenopus egg extracts. *J Cell Biol* **130**: 1161-9.

Waxman, P. G., del Campo, A. A., Lowe, M. C. and Hamel, E. (1981) Induction of polymerization of purified tubulin by sulfonate buffers. Marked differences between 4-morpholineethanesulfonate (Mes) and 1,4-piperazineethanesulfonate (Pipes). *Eur J Biochem* **120**: 129-36.

Wiche, G., Oberkanins, C. and Himmler, A. (1991) Molecular structure and function of microtubule-associated proteins. *Int Rev Cytol* **124**: 217-273.

Wilkie, G. S. and Davis, I. (2001) Drosophila wingless and pair-rule transcripts localize apically by dynein-mediated transport of RNA particles. *Cell* **105**: 209-19.

Wilsch-Brauninger, M., Schwarz, H. and Nusslein-Volhard, C. (1997) A sponge-like structure involved in the association and transport of maternal products during Drosophila oogenesis. *J Cell Biol* **139**: 817-29.

Wilson, L., Miller, H. P., Farrell, K. W., Snyder, K. B., Thompson, W. C. and Purich, D. L. (1985) Taxol stabilization of microtubules in vitro: dynamics of tubulin addition and loss at opposite microtubule ends. *Biochemistry* **24**: 5254-62.

Wilson, T. M. A. (1984) Cotranslational disassembly of tobacco mosaic virus *in vitro. Virology* **137**: 255-265.

Wilson, T. M. A. (1985) Nucleocapsid disassembly and early gene expression by positive-strand RNA viruses. *J Gen Virol* **66**: 1201-1207.

Wolf, S., Deom, C. M., Beachy, R. N. and Lucas, W. J. (1989) Movement protein of tobacco mosaic virus modifies plasmodesmatal size exclusion limit. *Science* **246**: 377-379.

Xoconostle-Cazares, B., Xiang, Y., Ruiz-Medrano, R., Wang, H. L., Monzer, J., Yoo, B. C., McFarland, K. C., Franceschi, V. R. and Lucas, W. J. (1999) Plant paralog to viral movement protein that potentiates transport of mRNA into the phloem. *Science* **283**: 94-98.

Yamagata, H., Tamura, K., Tanaka, K. and Kasai, Z. (1986) Cell-free synthesis of rice prolamin. *Plant Cell Physiol* **27**: 1419-1422.

Yamagata, H. and Tanaka, K. (1986) The site of synthesis and accumulation of rice storage proteins. *Plant Cell Physiol* **27**: 135-145.

Yisraeli, J. K., Sokol, S. and Melton, D. A. (1990) A two-step model for the localization of maternal mRNA in Xenopus oocytes: involvement of microtubules and microfilaments in the translocation and anchoring of Vg1 mRNA. *Development* **108**: 289-98.

Young, N. D., Forney, J. and Zaitlin, M. (1987) Tobacco mosaic virus replicase and replicative structures synthesized in vitro. *J Cell Sci* **7 (Suppl.)**: 277-285.

Young, N. D. and Zaitlin, M. (1986) An analysis of tobacco mosaic virus replicative structures synthesized *in vitro. Plant Mol Biol* **6**: 455-465.

Zambryski, P. and Crawford, K. (2000) Plasmodesmata: gatekeepers for cell-to-cell transport of developmental signals in plants. *Annu Rev Cell Dev Biol* **16**: 393-421.

Zierler, K. (1989) Misuse of nonlinear Scatchard plots. *Trends Biochem Sci* **14**: 314-317.

Appendix I Media and solutions

Bacterial Media

2 X YT bacterial growth media

16 mg/mL tryptone

10 mg/mL Bacto Yeast Extract

5 mg/mL NaCl

Luria Bertani (LB) Agar for bacterial plates

10 mg/mL tryptone

5 mg/mL Bacto Yeast Extract

10 mg/mL NaCl

15 mg/mL Agar

Buffers used for Inclusion Body Isolation and Ni^{2+}-NTA affinity chromatography

Lysis Buffer

20 mM Tris-CL, pH 8.0

30 U DNase I (Ambion Inc.)

10 μg/mL RNase A (Promega)

2 X working strength Protease Inhibitor Cocktail, minus EDTA (Boehringer Mannheim)

Inclusion Body Wash Buffer

20 mM Tris-CL, pH 8.0

2 M Urea

500 mM NaCl

10 μg/mL RNase A

2 % (v/v) Triton X-100

1 X working strength Protease Inhibitor Cocktail, minus EDTA

Solubilization buffer (SB5, 20 and 500)

100 mM NaH_2PO_4, pH 7.5

1 M NaCl

10 mM Tris base (Used to reduce methionine carbomylation due to Urea)

8 M Urea

10 % (v/v) Glycerol

Note: numbers denote the concentration of Imidazole (mM).

Buffers used for binding and visualization of MP:MT complexes

BRB80 (Brinkley Reaction Buffer)

80 mM Pipes-OH, pH 6.8

1 mM $MgCl_2$

1 mM EGTA

Kinesin binding buffer

BRB80 containing:

1 mM DTT

10 μM Taxol

0.25 mg/mL casein

Kinesin wash buffer

BRB80 containing:

1 mM DTT

10 μM Taxol

0.1 % (w/v) BSA

MAP binding buffer

12 mM Pipes-OH, pH 6.85

0.5 mM $MgCl_2$

10 % (v/v) Glycerol

0.01 % (v/v) Tween-20

10 μM Taxol

Pulldown buffer

40 mM Pipes-OH, pH 6.85

0.5 mM $MgCl_2$

10 % (v/v) Glycerol

0.01 % (v/v) Tween-20

5 mM Imidazole

Buffers used for kinesin motility assays

Motility Buffer

50 mM Pipes-OH, pH 6.85

1 mM EGTA

1 mM $MgCl_2$,

2 mM ATP

10 μM Taxol

150 mM KCl

Minimal buffer

50 mM Pipes-OH, pH 6.85

1 mM $MgCl_2$

10 μM Taxol

Oxygen Scavenger System

Motility buffer containing:

18 μg/mL catalase

0.1 mg/mL glucose oxidase

2.25 mg/mL D-glucose

10 mM DTT

Appendix II Primers

Primers for PCR amplication of the MP gene from plasmid pTf5-NX2

Forward primer: 5’ gtttcgcgagcgctctagttgtt 3’

Reverse primer: 5’ cgaggtcaaggatccagcggcc 3’

Primers used for insertion of –$(H)_6$ tags into plasmid pTf5-NX2

TMV-MP:$(H)_6$:GFP

Sense strand: 5’ tcgacggttcccatcaccatcaccatcac 3’

Antisense strand: 3’ gccaagggtagtggtagtggtagtggatc 5’

TMV-MP:GFP:$(H)_6$

Sense strand: 5’ ggccgctcatcaccatcaccatcactaa 3’

Antisense strand: 3’ cgagtagtggtagtggtagtgattagct 5’

Appendix III Mathematical and statistical models

Saturation binding curve equations

Assuming no chemical catalysis and the law of mass action, a simple bimolecular binding reaction can be described in the following way

$$[\mathrm{R}]\,[\mathrm{L}] \underset{k_2}{\overset{k_1}{\rightleftharpoons}} [\mathrm{RL}] \qquad (1)$$

where [R] is the concentration of receptor (tubulin), [L] is the concentration of ligand (MP) and [RL] is the concentration of receptor:ligand complex. The probability of [RL] formation is proportional to k_1[R] [L], where k_1 is the association *rate* constant, and the probability of [RL] breakdown is proportional to k_2[RL], where k_2 is the dissociation *rate* constant, respectively.

Thus, the rate of change of [RL] formation is proportional to the difference in rate constants.

$$\frac{\Delta[\mathrm{RL}]}{\Delta \mathrm{t}} = \left(k_1\,[\mathrm{R}][\mathrm{L}]\right) - \left(k_2\,[\mathrm{RL}]\right) \qquad (2)$$

This relates to the free energy of binding in the usual way.

$$\Delta \mathrm{G}^{\circ} = -\,\mathrm{RT}\,ln\left(\frac{\text{product}}{\text{substrate}}\right) \qquad (3a)$$

$$\Delta \mathrm{G}^{\circ} = -\,\mathrm{RT}\,ln\left(\frac{[\mathrm{RL}]}{[\mathrm{R}][\mathrm{L}]}\right) \qquad (3b)$$

However, at chemical equilibrium, there is no change in the rate of [RL] formation.

$$\frac{\Delta[\mathrm{RL}]}{\Delta \mathrm{t}} = 0 = \left(k_1\,[\mathrm{R}][\mathrm{L}]\right) - \left(k_2\,[\mathrm{RL}]\right)$$

$$\left(k_1\,[\mathrm{R}][\mathrm{L}]\right) = \left(k_2\,[\mathrm{RL}]\right) \qquad (4)$$

Therefore, according to $\Delta G^{o} = -RT\,ln(K_a)$

$$\frac{[RL]}{[R][L]} = K_a = \frac{1}{K_d} \tag{5}$$

$$[RL] = [R][L]\,K_a \tag{6}$$

Where K_a is the association constant and K_d is the dissociation constant.

At equilibrium, the amount of receptor *fractionally* bound by ligand (Y) is defined in the following way, where R_t is the total concentration of receptor and the law of mass action is assumed.

$$Y = \frac{[RL]}{[R_t]}$$

$$Y = \frac{[RL]}{[R]+[RL]} \tag{7}$$

Substituting [RL] for (eq. 6):

$$Y = \frac{[R][L]K_a}{[R]+[R][L]K_a} \tag{8}$$

Which simplifies to the Langmuir form (Scatchard, 1949):

$$Y = \frac{[L]K_a}{1+[L]K_a}$$

And when written in terms of the dissociation constant:

$$Y = \frac{([L]/K_d)}{1+([L]/K_d)}$$

Which can be solved for K_d:

$$Y = \frac{[L]}{K_d + [L]} \tag{9}$$

This takes the line form of y = ax/b+x. Plotting Y versus [L] yields a rectangular hyperbole where K_d is equal to [L] at half saturation.

$$\frac{1}{2} = \frac{[L]_{1/2}}{K_d + [L]_{1/2}}$$

$$(K_d + [L]_{1/2}) = 2[L]_{1/2}$$

$$K_d = [L]_{1/2} \tag{10}$$

In the case of a macromolecule, there may be multiple *equivalent* binding sites. Y is then substituted for $\bar{\nu}$, which is the fraction of all receptors that are bound, assuming the intrinsic binding affinity for ligand is the same in all cases and the receptor sites do not interact with each other.

$$\bar{\nu} = \frac{n[L]}{K_d + [L]} \tag{11}$$

In practical terms, one can plot $\bar{\nu}$ ($[MP]_{bound}$) versus [L] ($[MP]_{free}$), yielding a curve with the same shape as (eq. 8) and an equal value for K_d. Saturation occurs in this case at n, the number of equivalent binding sites.

To determine whether non-equivalent, non-interacting binding sites exist on a macromolecule, eq. 10 can be expanded to a two-site model.

$$\bar{v} = \frac{n_1 [L]}{K_{d1} + [L]} + \frac{n_2 [L]}{K_{d2} + [L]} \qquad (12)$$

Plots of $[L]_{bound}$ versus $[L]_{free}$ are hyperbolic, but yield K_d and n values for each respective type of site. Binding data fit to a multiple-site model must be statistically compared to lower order models by analysis of variance (ANOVA) to ensure the strength of fit is not simply due to an increase in inflexion points.

Linearization of equilibrium binding data

The Scatchard-Rosenthal plot (Scatchard, 1949; Rosenthal, 1967) can be used as a visual aid in the interpretation of equilibrium binding data. Deviations from the predicted straight line give intuitive clues as to the mechanism of binding, e.g. whether multiple non-equivalent binding sites exist or whether equivalent binding sites display allosteric effects on subsequent ligand binding (cooperativity).

The one-site equilibrium binding equation (eq. 11) can be manipulated in the following way to obtain the Scatchard form.

$$\frac{\bar{v}}{n} = \frac{[L]}{K_d + [L]}$$

$$\bar{v}(K_d + [L]) = n [L]$$

$$\bar{v} K_d = - \bar{v} [L] + n [L] = (-\bar{v} + n) [L]$$

$$\frac{\bar{v}}{[L]} = \frac{(-\bar{v} + n)}{K_d} = \frac{- \bar{v}}{K_d} + \frac{n}{K_d}$$

$$\frac{\bar{v}}{[L]} = \frac{-1}{K_d} \bar{v} + \frac{n}{K_d} \qquad (13)$$

Plots of $[L]_{bound}/[L]_{free}$ versus $[L]_{bound}$ give a straight line (y = mx + b) when the criteria for a single equivalent, non-interacting binding site are met. The slope equals $-1/K_d$ and x-intercept equals n. Following transformation, data points (x-axis) do not conform to the Gaussian distribution, therefore, values for n and K_d are rendered unreliable. Bi- and multiphasic binding curves are indicative of multiple types of binding site and/or cooperativity of binding, although multivalent ligands or non-specific binding cannot be firmly discounted without further experimentation (Norby et al., 1980; Zierler, 1989).

Comparison of binding models by analysis of variance (ANOVA)

One-way ANOVA is a statistical method which allows two or more groups of data to be compared according to the difference in the mean value between the groups and the degree of variability within the groups themselves. Since both equilibrium binding models (eq. 11 and 12) are related, it is possible to directly compare the strength of curve fit by calculating the F *ratio* in the following way, where SS is the residual sum-of-squares (the difference between the observed and predicted curves) and df is the residual degrees of freedom or difference between the total number of samples and total number of adjustable parameters within the model (Motulsky and Christopoulos, 2003):

Null hypothesis (null): The simpler model is most appropriate

Alternative hypothesis (alt): The more complex model is more appropriate

$$\text{F } ratio = \frac{(SS_{null} - SS_{alt})/(df_{null} - df_{alt})}{SS_{alt}/df_{alt}}$$

In basic terms, this equation answers the question whether a perceived improved fit using a complex model is ‘worth’ the additional variables within the modeled term (decrease in degrees of freedom). F *ratio* values above 1 indicate that the complex model is statistically distinct from the simple model and fits the data more strongly. To determine the probability that random scatter within the data led to the complex model to fit better, one can calculate the *P*-value using the an automated algorithm (e.g. function =FDIST in Microsoft Excel 2000). *P*-values less than 0.05 (5%) confirm that the null hypothesis can be reasonably rejected.

Non-linear regression outputs (SigmaPlot 2001, SPSS inc.)

One-site model

Nonlinear Regression

[Variables]
x = col(1)
y = col(2)
[Parameters]
a = max(y)
b = x50(x,y)
[Equation]
f= a*x/(b+x)
fit f to y
tolerance=0.000001
stepsize=100
iterations=100

R = 0.98341850 Rsqr = 0.967 Adj Rsqr = 0.963

Standard Error of Estimate = 0.4553

Analysis of Variance:

	DF	SS	MS	F
Regression	1	54.8617	54.8617	264.6556
Residual	9	1.8657	0.2073	
Total	10	56.7274		

Two-site model

Nonlinear Regression

[Variables]
x = col(1)
y = col(2)
'Automatic Initial Parameter Estimate Functions
[Parameters]
a = max(y)/2
b = .5*x50(x,y)
c = max(y)/2
d = 1.5*x50(x,y)
[Equation]
f= a*x/(b+x)+c*x/(d+x)
fit f to y
tolerance=0.000001
stepsize=100
iterations=100

R = 0.99297596 Rsqr = 0.986 Adj Rsqr = 0.980

Standard Error of Estimate = 0.3368

Analysis of Variance:

	DF	SS	MS	F
Regression	3	55.9333	18.6444	164.3483
Residual	7	0.7941	0.1134	
Total	10	56.7274		

Comparison of kinesin motility rates using the two-tailed unpaired students *t*-test

When different groups of data conform to a Gaussian (normal) distribution and the variance of each group is the same (homoscedastic) , the *t*-test can be employed in order to determine whether each respective group has a significantly different mean (μ) value. In principle, this is achieved by determining the probability that observed differences between the means are simply due to a high standard deviation (σ), i.e. the result of variability within one or both groups, or actually arose due to a significant measurable difference. In the case of apparent kinesin motility rates, velocity data were

obtained from reactions performed at different times and with different batches of reagent. Therefore, the data groups can be considered to be independent and a two-tailed unpaired *t*-test can be used with the null hypothesis (null) that the mean MT velocity of two groups is the same, and an alternative hypothesis (alt) that the means are different. The *t*-statistic was manually calculated as described below and when it was greater than the corresponding value obtained from a *t*-distribution with the same degrees of freedom, the null hypothesis was reasonably rejected.

If both groups have the same sample number (n), one calculates the *pooled* standard deviation (S), where σ is the standard deviation.

$$S = \sqrt{\frac{(\sigma_{null}^2 + \sigma_{alt}^2)}{2}} \qquad \text{(eq. 14)}$$

From this, the standard error (S.E.) of the difference between the means $(\mu_{null} - \mu_{alt})$ is calculated.

$$S.E.D. = S\sqrt{\frac{1}{n_{null}} + \frac{1}{n_{alt}}} \qquad \text{(eq.15)}$$

And finally the t-statistic is calculated thus.

$$t = \frac{(\mu_{null} - \mu_{alt})}{S.E.D.} \qquad \text{(eq. 16)}$$

The degrees of freedom equal (n_{null} + n_{alt}) –2 and the corresponding critical *t*-values are read from a *t*-distribution table at 5, 1 and 0.1% confidence intervals, respectively.

Calculated *t*-statistic values

	Buffer	200nM MP	600 nM MP
Mean velocity (μ), μm/s	0.195	0.157	0.139
Standard deviation (σ)	0.052	0.053	0.058
Variance*	2.7×10^{-4}	2.8×10^{-4}	3.4×10^{-4}
Sample size (n)	150	150	150

Buffer versus 200 nM MP

Null hypothesis: μ (buffer) = μ (200)

t-statistic = 6.27

$t_{critical}$ (P = 0.05) = 1.96

$t_{critical}$ (P = 0.01) = 2.576

$t_{critical}$ (P = 0.001) = 3.291

Conclusion: reject null hypothesis at 99.9% confidence level

200 nM MP versus 600 nM MP

Null hypothesis: μ (200) = μ (600)

t-statistic = 2.81

$t_{critical}$ (*P* = 0.05) = 1.96

$t_{critical}$ (*P* = 0.01) = 2.576

$t_{critical}$ (*P* = 0.001) = 3.291

Conclusion: reject null hypothesis at 99 % confidence level

* To verify that variance values were sufficiently similar, an heteroscedastic (unequal variance) *t*-test was employed using Microsoft Excel 2000 software. The results of this analysis were fully consistent with the above *t*-statistic values, indicating that a pooled variance *t*-test was indeed the most appropriate for these data.

Appendix IV Publication